DEPARTMENT OF PHYSICS,
UNIVERSITY OF JYVÄSKYLÄ
RESEARCH REPORT No. 6/2006

MODIFIED MULTIPOLE STRUCTURE FOR ELECTRON CYCLOTRON RESONANCE ION SOURCES

BY
PEKKA SUOMINEN

Academic Dissertation
for the Degree of
Doctor of Philosophy

To be presented, by permission of the
Faculty of Mathematics and Science
of the University of Jyväskylä,
for public examination in Auditorium FYS-1 of the
University of Jyväskylä on June 16, 2006
at 12 o'clock noon

Jyväskylä, Finland
June 2006

ISBN 978-951-39-3171-1
URN:ISBN:978-951-39-3171-1

Preface

This thesis work was carried out in 2003 – 2006 at the Department of Physics in the University of Jyväskylä.

Being a member of the ion source group has been very memorable time and a privilege, therefore I would first of all like to thank my supervisor Dr. Hannu Koivisto. His guidance and support in the course of this work has been truly invaluable. I want to express my sincere gratitude also to Dr. Olli Tarvainen with whom I enjoyed to work several years, sharing glorious working hours, lunch breaks, amusing (but educative) conferences and cheerful free time. Working with both Hannu and Olli usually did not even feel like work but more like fun.

Whenever help was needed all the people at the Department of Physics were very kind. Warmest thanks to you all. As I'm more technically than theoretically orientated I wish to express special thanks to all technical staff of the Accelerator Laboratory and all the "työpajan äijät", mechanical and electronics. My thesis work would not have been so successful without them and particularly Mr. Veikko Nieminen who helped me in the mechanical design. I also want to thank the whole RADEF-team for interesting challenges and support.

Of course "*hard"* work needs a counterbalance. For that I would like to thank all my friends, especially Mr. Jarno Latvala and Mr. Eemeli Hytönen for their genuine friendship. Finally I want to thank my family: mother, father and brother for their encouragement at any time or concerning any subject when it was needed.

Jyväskylä, June 2006

Pekka Suominen

Abstract

Highly-charged heavy-ion beams are usually produced with Electron Cyclotron Resonance Ion Sources (ECRIS) where the microwave heated plasma is confined in a strong magnetic field. The magnetic field is divided into an axial part (produced by solenoid magnets) and to a radial part (produced by multipole magnet). Experiments have shown that the radial magnetic field component plays a crucial role in the production of highly-charged ions. However, in several modern ECRIS the radial magnetic field strength is below the optimum value, mainly due to the limits in permanent magnet technology. Unfortunately, methods to increase the radial magnetic field strength while still using permanent magnets are often limited.

In this thesis work new techniques to improve the radial magnetic field have been studied by simulations and experiments. Due to the computer simulations performed a remarkable radial magnetic field improvement was reached with a relatively simple and cost-effective idea called the Modified MultiPole Structure (MMPS). The MMPS differs strongly from former studies as here the magnetic field is increased only locally without affecting the plasma size. It was not known how this would affect the properties of the plasma and production of highly-charged heavy ions. Consequently, the idea had to be studied experimentally and a new MMPS plasma chamber prototype was designed and constructed for the JYFL 6.4 GHz ECRIS. The new construction is versatile and made it possible to perform several new types of measurements. These showed that the MMPS works well and is especially applicable to increase very high charge-state ion production. Typically the ion current increases by a factor of 2 – 3 in the case of highly charged ions such as Ar^{16+}.

Contents

1. Introduction

Ion beams are used in numerous applications. In industry, they are for example used in surface treatment or in integrated chip technology to modify the semiconductor properties. In the future, ion beam lithography can probably be applied in fabrication of smaller and faster microprocessors. Medical technology uses ion beams for example to produce radioisotopes or in ion beam therapy, where an ion beam is used to destroy cancerous cells. Ion beams also play an important role in nuclear and material physics research.

The ion beam is produced in an ion source, where neutral particles are ionized. In a negative ion source neutral atoms receive an extra electron and in positive ion sources one or several electrons are removed. The charge-state of the ion corresponds to the number of removed electrons. From the ion source the ions are extracted into the beam line with a high voltage.

Accelerators are used to increase the ion beam energy so that it meets the requirement set by the application. In accelerators the ion energy is increased in an electric field. The maximum achievable energy of a linear accelerator increases with the ion charge-state, q. In cyclic accelerators, such as a cyclotron or a synchrotron, maximum energy is proportional to q^2. The use of higher charge-state ions can reduce the accelerator size and the facility costs. This gives a strong motivation to use a powerful ion source, which is capable of producing intense beams of highly-charged ions. There are numerous types of ion source but highly-charged heavy ions are mainly produced either with an Electron Beam Ion Source (EBIS) or with an Electron Cyclotron Resonance Ion Source (ECRIS).

Cyclotrons are the most common accelerators for heavy ions and are often equipped with an ECRIS. This is mainly because the ECRIS produces a continuous ion beam, which with a cyclotron can be used more effectively than pulsed EBIS beams. An ECRIS is also relatively simple to operate and can even be operated for months without maintenance. The magnetic confinement is one of the key parameters when producing highly-charged ions with an ECRIS. In this thesis a new magnetic field structure called Modified MultiPole Structure (JYFL-MMPS) has been developed. It is a cost-effective technique to increase the multipole magnetic field and improve the magnetic confinement. The author has designed the first MMPS prototype plasma chamber for the JYFL 6.4 GHz ECRIS.

The MMPS-technique can be used in plasma ion sources where a homogenous magnetic field is not necessary (as it is in accelerator magnets). The MMPS is applicable for quadrupole, sextupole, octupole, and high order multipole magnets. However, this work focuses mainly on sextupoles (a.k.a. hexapoles) used in electron cyclotron resonance ion sources. The experimental part of this thesis also includes testing of the new concept. In the course of this work it was

confirmed that the MMPS can be used to improve the performance of ECR ion sources.

2. Electron cyclotron resonance ion source

The history of the ECRIS starts in the late 1960s, when Electron Cyclotron Resonance Heating (ECRH) was used to generate plasmas for fusion research [Gel96]. In fact, the first ECRIS was originally a device for plasma fusion research until R. Geller transformed it to an ion source. After the first ECRIS prototype several hundred ECRIS's have been constructed for industry and research. In 1987 Geller and co-workers published semi-empirical "scaling laws" [Gel87], which predict the dependence of some parameters on the performance of an ECRIS. The most important scaling law is perhaps for the microwave frequency. Geller proposed that the extracted ion beam intensity (of charge-state *q*) increases with the square of the injected microwave frequency, i.e. $I_q \propto f^2$. This behavior gives strong motivation to use microwave frequencies as high as possible. However, a limit is set by the magnetic field, which has to be strong enough for the electron resonance with the microwaves and for sufficient magnetic confinement of the plasma. This thesis work focuses especially on the effect of the ECRIS magnetic field configuration on highly-charged ion production. The next chapter presents the operating principle of an ECRIS.

2.1. Operating principle

Magnetic confinement of the plasma plays a crucial role in the production of highly-charged ions. In addition, the ionization process needs excellent vacuum conditions to make ion production and ion beam transport possible. The material which is to be ionized is fed into the plasma chamber together with microwaves. Under the correct magnetic field conditions microwaves can heat the electrons, which cause the so-called step-by-step ionization in collisions with the gas atoms. As a result, a magnetically confined plasma is formed. The ions are extracted from the plasma into the beam line via a proper extraction system. The operating principle of an ECRIS is presented in figure 2.1.

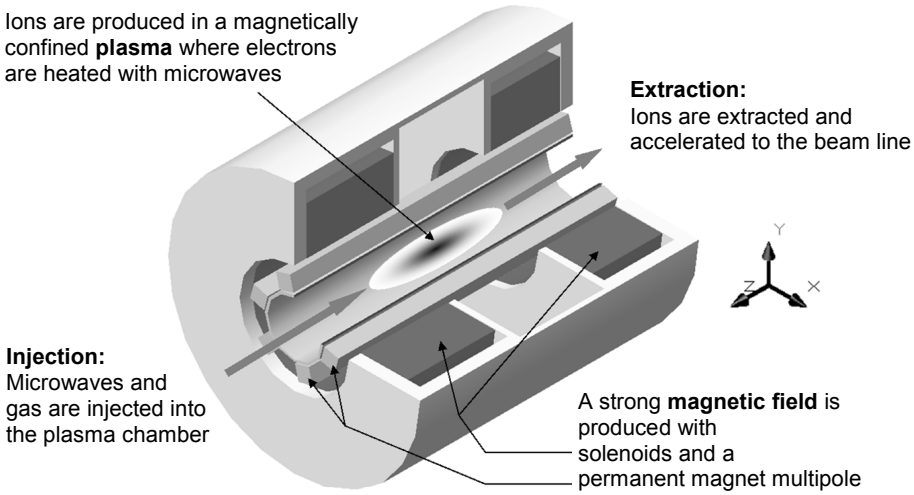

Figure 2.1. Operating principle of an ECRIS.

2.1.1. Vacuum conditions

The mean free path is the average distance an atom, molecule or ion travels between collisions. In an ECRIS vacuum the mean free path between the ion and neutral has to be long in order to prevent charge-exchange processes, where the highly-charged ion captures an electron (usually from neutral atom). As a result of the process, the charge-state of the highly charged ion decreases. Together with step-by-step ionization an equilibrium conditions will be reached and a specific charge-state distribution in the plasma will be formed. The probability for charge-exchange increases with ion charge-state and neutral pressure inside the ECRIS (see for example [Knu81]). To minimize the charge-exchange process, excellent vacuum conditions are required (< 10^{-7} mbar). Usually the cross-section for charge-exchange is several orders of magnitude higher than the cross-section of ionization. For example, for Ar^{8+} the charge-exchange cross-section is 2000 times higher than the maximum cross-section for ionization to Ar^{9+} ($1.6 \cdot 10^{-19}$ m^2 / $\sim 7 \cdot 10^{-23}$ m^2 [Taw87]). In addition, this applies only in the optimum case in which the electron impact energy for ionization is about 1 keV. For other impact energies the ratio is even higher. As a consequence, the production of highly charged ions requires high vacuum conditions.

Another important vacuum and plasma related parameter is the electron density (usually called the plasma density, n_e). In order to achieve good ionization conditions the plasma electron density has to be high enough. In an ECRIS it is in the range of 10^{11} – 10^{12} cm^{-3} [Gel96]. The electron density can be increased by adding more gas, but after the optimum value is reached the neutral pressure becomes too high for highly-charged ion production. Some extra electrons can be gained using a plasma chamber wall material which has a high secondary electron emission coefficient [Lyn87].

2.1.2. Magnetic field

In an ECRIS the charged particles are confined in a strong magnetic trap, known as a magnetic bottle, where the ions and electrons forming the plasma bounce back and forth. Most modern ECRISs for highly-charged heavy-ion production utilize a so-called minimum magnetic field structure (Min-B). This structure contains a multipolar magnetic field in addition to solenoids ("simple mirror" - structure). In a Min-B structure the magnetic field minimum is located at the center of the plasma chamber and the magnetic field increases in all directions from the location of Min-B (at the centre of the plasma chamber). This structure makes it possible to have a closed surface (ECR surface) where efficient heating of electrons by microwaves takes place. The magnetic field of the JYFL 6.4 GHz ECRIS shown in figure 2.2. represents a typical Min-B structure. The ECRIS magnetic field structure is presented in detail in chapter 3.

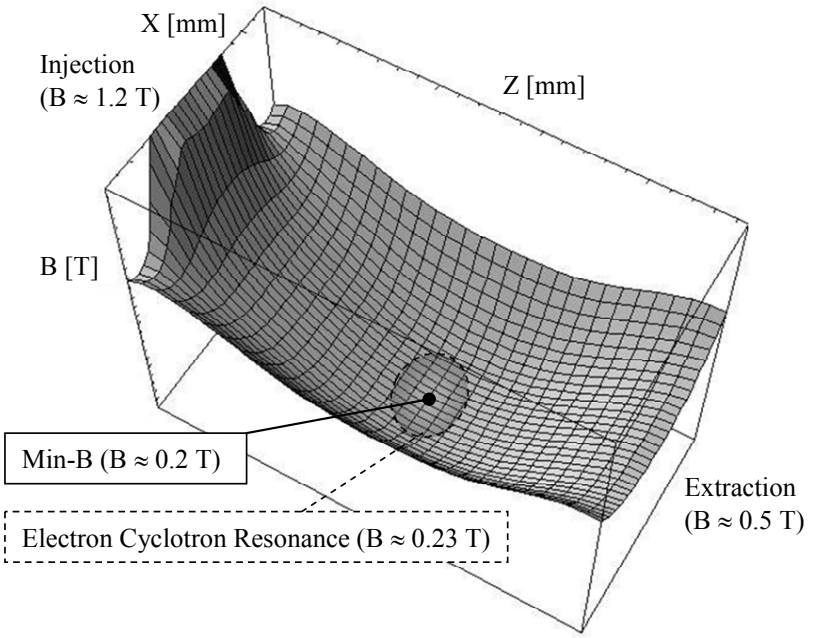

Figure 2.2. Typical (Min-B) magnetic field structure of the 6.4 GHz ECRIS.

2.1.3. Electron heating with microwaves

In a magnetic field, electrons circulate around the magnetic field lines with a frequency given by equation: $f = eB/(2\pi\, m_e)$, where B is magnetic field flux density, e (= 1.602×10^{-19} coulombs) and m_e (= 9.11×10^{-31} kilograms) are the electron charge and mass, respectively. When microwaves which have the

same frequency as the circulating electrons are launched into the plasma chamber, Electron Cyclotron Resonance (ECR) heating can occur (see for example [Gel96]).

The ECRIS magnetic field is designed so that there are closed, constant strength magnetic field surfaces surrounding the plasma chamber centre (Min-B, see figure 2.2). At a certain surface the magnetic field is correct to set up a resonance between the electron and (right hand circularly polarized) microwave. This surface is called the ECR (or resonance) surface. If the electric field of the microwave is in same phase as the electron rotation, the microwave energy can be efficiently transferred to kinetic energy of the electron. After sufficient electron heating the atoms can be ionized through collisions. According to the afore-mentioned scaling law the use of as high a microwave frequency as possible is desirable. The effect of the frequency on the intensities can be seen in figure 2.3, which shows an overview of the performances of different ECRISs.

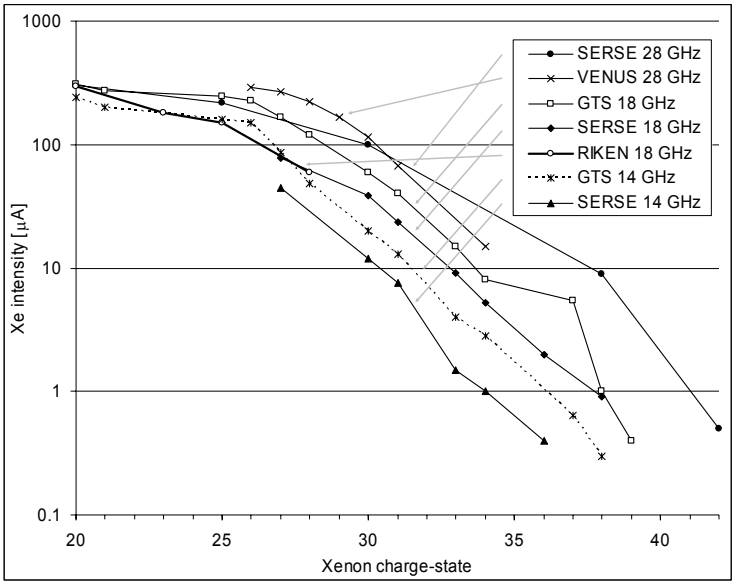

Figure 2.3. Xenon ion beam intensities of different ECRISs as a function of charge-state [Hit04], [Gam00], [Gam99], [Lei06], [Nak04], [Gam01].

2.1.4. Ionized material

An ECRIS can be used to produce highly charged ions from various elements. The most easily produced ions are from gases. Neutral gas is allowed to diffuse into the plasma where collisions with the energetic electrons cause the ionization of the gas. When the gas atom becomes ionized it interacts with the electric and magnetic fields and becomes trapped. Molecules can be also ionized with an ECRIS but they tend to be broken up easily in the plasma.

Frequently two different mass gases are injected into the ECRIS at the same time. This is known as the gas-mixing-method [Dre85]. As a consequence of ion-ion collisions the lighter mixing-gas carries out part of the kinetic energy of the heavier ions improving their confinement. This process increases the production of highly-charged ions from the heavier gas.

Solid material has to be vaporized before ionization. This can be done for example with an oven (see for example [Cla89], [Hit93] and [Lan02]), which is located in the plasma chamber. The oven is usually heated resistively using a direct current (DC). Recently, good results with inductively heated (AC or RF) ovens for ECRIS usage have been reported (see for example [Cav04] and [Zav06]). The operating temperature of the oven depends on the material which must be vaporized. For some elements a temperature higher than 2000°C is needed, which exceeds the operating temperatures of available ECRIS-oven technology.

Ions from volatile compounds can be produced using the so-called MIVOC method (Metallic Ions from VOlatile Compounds) [Koi94]. In this method, the volatile material is in a small evacuated chamber where the material vaporizes and diffuses into the plasma. The gas flow can be controlled with a leak valve. The method is especially applicable to produce high intensity metal ion beams from non-volatile elements (for example for iron from $Fe(C_5H_5)_2$ or nickel from $Ni(C_5H_5)_2$). In most cases the compound used contains carbon, which accumulates on the plasma chamber walls reducing the secondary electron emission, the plasma electron density and thus the ECRIS performance.

The sputtering technique [Har95, Von02] is an efficient method for refractory elements. In this method the sputtering sample is located in the plasma chamber at a negative voltage with respect to the plasma chamber. The plasma is ignited mainly with a mixing-gas. The negative voltage (few kV) applied to the sputtering sample attracts ions from the plasma causing the sputtering of material. The sputtered material goes into the plasma and is ionized.

One rarely used method is laser ablation [Har94], where a high energy laser pulse is focused on the sample and instantaneously explodes the surface into vapor. With a proper setup the vapor goes to the plasma and gets ionized. The insertion technique introduces a solid material directly into contact with the plasma (see for example [Gel86] and [Nak90]). In this method the “heating efficiency” strongly depends on the gas pressure, magnetic field settings and so on, making the source sensitive for tunings.

2.1.5. Ion extraction

Plasma losses from the magnetic bottle are concentrated at locations where the magnetic field goes through the plasma chamber walls and especially where the field is low. The ECRIS magnetic field is designed such that the lowest magnetic field, where ions can escape the magnetic bottle, is at the extraction

side of the plasma chamber (see figure 2.2). An accelerating electric field at the extraction forms the ion beam from the plasma and accelerates the ions to the beam line. For practical reasons the beam line is at ground potential meaning that the plasma chamber, where the ions are produced, must be at high voltage (see figure 2.4). The acceleration voltage is usually between 10 and 50 kV. More detailed information about the ion extraction of an ECRIS can be found, for example, from [Bro89] and [Gel96].

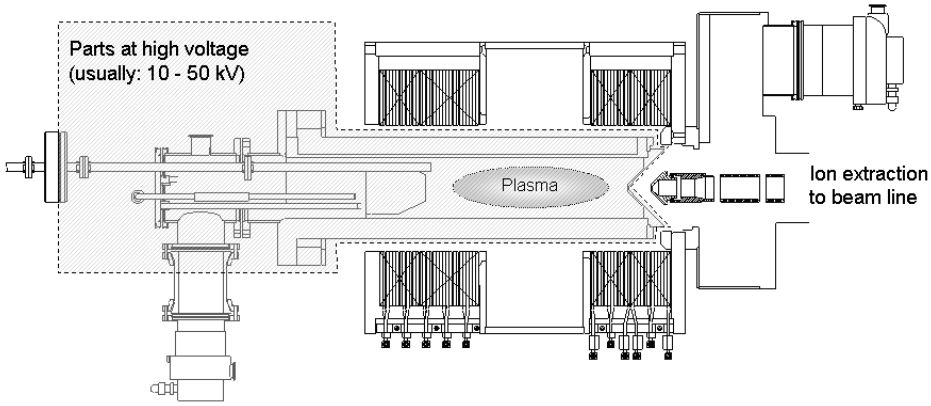

Figure 2.4. Schematic picture of parts of the ECRIS which are at high voltage.

2.2. Charged particle in the ECRIS magnetic field

The plasma physics of the ECRIS is beyond the scope of the present work. However, this chapter gives a short introduction by studying the motion of a single particle in a magnetic field. This is a good starting point to understand the ECRIS related plasma physics. A better overview of general plasma physics can be found for example from [Gol95] and a more detailed review of ECRIS plasma physics from [Gel96] and [Tar05].

2.2.1. Single-particle motion

The motion of a charged particle in electric and magnetic fields is defined by the Lorenz force

$$\vec{F} = q(\vec{E} + \vec{v} \times \vec{B}) \quad \left(= m\vec{a} = m\frac{v_\perp^2}{r} \right), \tag{1}$$

where *q* is the charge, $\vec{E}$ the electric field, $\vec{v}$ the velocity, $\vec{B}$ the magnetic field flux density, m the particle mass, $\vec{a}$ the acceleration, $v_\perp$ the velocity perpendicular with respect to the magnetic field and r the orbit radius of the circulating particle. In a simple case where $\vec{E}$ = 0 the particle moves a helical

orbit around the magnetic field line (see figure 2.5a). The radius of the motion of a particle having velocity $v_\perp$ can be derived from equation (1), as

$$r = \frac{m\ v_\perp}{q\ B}. \tag{2}$$

The relativistic mass increase has to be taken into account in the case of electrons, whose energy can be up to ~1 MeV. Ion energies in ECRIS plasma are much lower (up to around 100 eV) and a relativistic treatment is not needed. Table 2.1 lists some radii for different particles in an ECRIS plasma.

Table 2.1. Some examples of electron and ion radii (in millimeters) in an ECRIS (B = 0.23 T).

	1 eV	10 eV	100 eV	1 keV	10 keV	100 keV
Electron	0.015 mm	0.046	0.147	0.464	1.473	4.858

	1 eV	20 eV	40 eV	60 eV	80 eV	100 eV
Proton	0.6 mm	2.8	4.0	4.9	5.6	6.3
$^{40}Ar^{+}$	4.0	18	25	31	36	40
$^{40}Ar^{8+}$	0.5	2.2	3.1	3.8	4.4	5.0
$^{40}Ar^{16+}$	0.2	1.1	1.6	1.9	2.2	2.5

The gyro (or cyclotron) frequency for a particle circulating the magnetic field line can be derived from equation (2) as

$$f = \frac{q\ B}{2\pi\ m}. \tag{3}$$

The frequency **for ions** is (note: MHz)

$$f = \frac{Q\ B}{A} 15.25\ \ MHz \tag{4}$$

where *Q* is the ion charge-state and *A* ion mass [amu]. The frequency **for** (cold) **electrons** is (note: GHz)

$$f = B\ 28\ \ GHz. \tag{5}$$

The last equation is very important as it defines the Electron Cyclotron Resonance (ECR) frequency. For example, if the plasma (electron) heating is required to occur in a 1 T magnetic field, the microwave frequency has to be 28 GHz. In practice, the ECRIS magnetic field has to be designed for a fixed frequency set by the available transmitter. Typical frequencies for commercially available transmitters are 2.45, 6.4, 8, 14, 18 and 28 GHz.

Equation (3) shows that the magnetic field has to increase with the relativistic mass in order to maintain the resonance conditions. For example, an electron

with an energy of about 100 keV has a relativistic “mass increase” of about 20 % (= 100 keV / 511 keV). In the JYFL 6.4 GHz ECRIS magnetic field structure (typical Min-B shown in figure 2.2) this means that the 100 keV electron resonance surface (0.27 T) is separated by about 5 mm from the 0 keV surface (0.23 T). The electron cyclotron resonance magnetic field (B_{ecr}) values for some frequencies and electron energies are listed in table 2.2.

Table 2.2. Resonance magnetic field values for different frequencies and electron energies.

Frequency [GHz]	B_{ecr} [T] (0 keV)	B_{ecr} [T] (1 keV)	B_{ecr} [T] (10 keV)	B_{ecr} [T] (100 keV)	B_{ecr} [T] (1 MeV)
2.45	0.088	0.088	0.089	0.105	0.259
6.4	0.23	0.23	0.23	0.27	0.68
8	0.29	0.29	0.29	0.34	0.84
10	0.36	0.36	0.36	0.43	1.06
14	0.50	0.50	0.51	0.60	1.48
18	0.64	0.64	0.66	0.77	1.90
28	1.00	1.00	1.02	1.20	2.96

2.2.2. Magnetic mirror, magnetic bottle and loss cone

Previously, simple cases with uniform magnetic field were studied. This must to be extended for the ECRIS where the magnetic field is non-homogenous (but time independent). A parameter related to the rotation energy and the magnetic field strength, the magnetic moment (μ), has to be defined

$$\mu = \frac{1}{2} m \frac{v_\perp^2}{B} = \frac{E_\perp}{B} = const. \qquad \text{i.e.} \quad \frac{d\mu}{dt} = 0 \tag{6}$$

where $E_\perp$ is the kinetic energy related to the velocity component perpendicular to the magnetic field. It can be also derived that the magnetic moment is time independent (if the particle energy remains constant). Assuming that the particle starts its motion from magnetic field B_1 and moves towards the higher magnetic field B_2 (> B_1), equation (6) gives

$$\frac{E_{\perp,1}}{B_1} = \frac{E_{\perp,2}}{B_2} . \tag{7}$$

As the magnetic moment is constant, the rotational energy $E_\perp$ has to increase with the magnetic field. Due to the conservation of energy ($E_{tot} = E_\perp + E_\parallel$) the “parallel” kinetic energy has to simultaneously decrease, i.e. $E_{\parallel,2} < E_{\parallel,1}$. Consequently, the velocity parallel to the magnetic field decreases and finally the particle is reflected back to direction of lower magnetic field. This motion is depicted in figures 2.5(b) and 2.6.

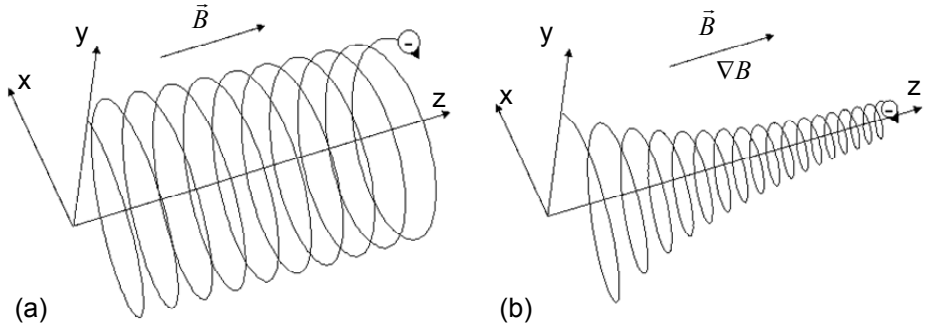

Figure 2.5. Electron trajectory in (a) homogenous and (b) increasing magnetic field.

The increasing magnetic field acts as a mirror for charged particles. Two magnetic mirrors can be used to form a magnetic bottle as shown in figure 2.6.

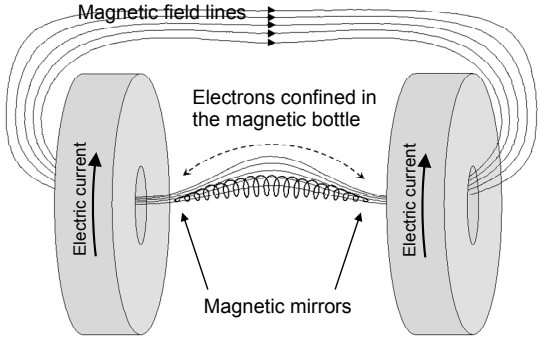

Figure 2.6. Trajectory of the charged particle confined in the magnetic bottle formed by two solenoids.

However, the magnetic mirror cannot reflect every charged particle. Only particles with a large enough $\vec{v}_{\perp} / \vec{v}_{\parallel}$ ratio will be reflected. This ratio is often referred to as the pitch-angle (α) defined in figure 2.7. Particles having a smaller pitch angle than the critical pitch-angle (α_0) can go through the magnetic mirror.

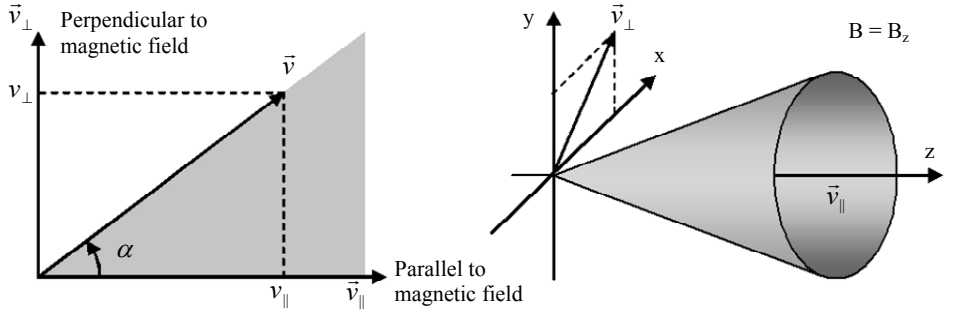

Figure 2.7. Definitions of the pitch-angle and loss cone in 2D and 3D.

In order to derive the critical pitch-angle α_0, it is assumed that the magnetic field of the starting point is B_0, the maximum magnetic field is B_m and $v_\perp$ is set to be $v \sin\alpha$. The critical pitch-angle is then given by equation

$$\frac{\sin^2\alpha_0}{B_0} = \frac{\sin^2\alpha_m}{B_m} \quad \Rightarrow \quad \alpha_0 = \arcsin\left(\frac{B_0}{B_m}\right)^{1/2}. \tag{8}$$

At the mirror point, $v_\parallel$ is zero and the pitch-angle $\alpha_m = 90°$. The equation shows that the critical pitch-angle is smaller when the magnetic field maximum (B_m) increases. Consequently, the magnetic field maxima should be as high as possible to achieve better confinement of the particles in the magnetic bottle. In three dimensions (3D) the critical pitch-angle defines the loss cone as shown in grey in figure 2.7. Fortunately, in the electron cyclotron resonance the microwave accelerates the $v_\perp$ component of the velocity. Consequently, the pitch-angle of the electrons increases and improves their confinement in the magnetic bottle.

The “mirror strength” of the magnetic bottle is commonly expressed by the so-called mirror ratio. It is the ratio of the magnetic field strengths at the maximum and at the starting point. The mirror ratio can be defined as

$$R = \frac{B_m}{B_0} = \frac{B_m}{B_{ECR}}, \tag{9}$$

where B_{ECR} is usually taken as the denominator because it is a fixed value set by the injected microwave frequency. Often three different mirror ratios are defined: for injection, extraction and the radial confinement, i.e. R_{inj}, R_{ext} and R_{rad}. The importance of these values is discussed in more detail in the next chapter.

3. Magnetic fields in an ECRIS

Most of the laboratory plasmas are confined in a magnetic bottle, which in the simplest case can be formed with two solenoid magnets. However, ECRISs constructed in that manner are not capable of producing very high charge-state ions. Better magnetic confinement can be achieved with a Min-B structure, which is a combination of a solenoidal magnetic field and a multipolar magnetic field. The multipolar magnetic field is sometimes known as the radial magnetic field and solenoidal magnetic field the axial magnetic field. Figure 3.1 shows two dimensional (2D) sketches of the solenoidal and multipolar magnetic field structures and the magnetic field lines in an ECRIS. A combined structural sketch showing the positions of the solenoids and permanent magnets is presented in figure 2.1.

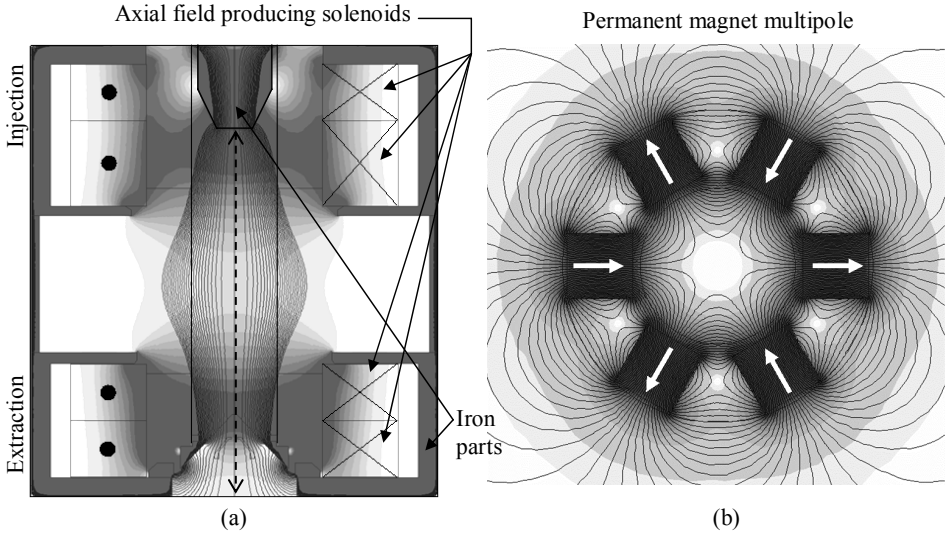

Figure 3.1. a) Solenoidal magnetic field structure b) multipolar magnetic field structure. Note that the pictures are not to scale (see figure 2.1 for comparison).

3.1. Solenoidal magnetic field

The typical solenoidal magnetic field of an ECRIS is produced with two or more electromagnets (DC-coils), which are known as an injection and extraction coils (or solenoids). A typical magnetic profile of this type of setup is shown in figure 3.2. The continuous line shows the magnetic field profile at the symmetry axis of the plasma chamber (denoted with a dashed arrow in figure 3.1). The magnetic field at the extraction is usually lower than at the injection in order to increase the ion extraction from the plasma chamber.

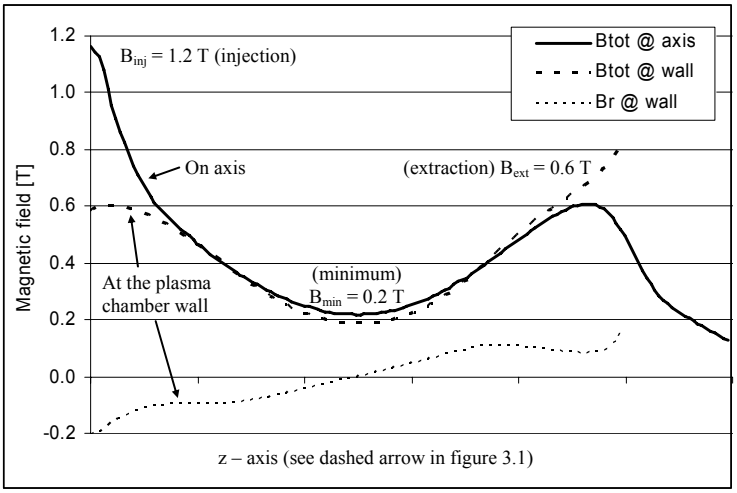

Figure 3.2. Solenoidal magnetic field profile of the JYFL 6.4 GHz ECRIS.

The solenoidal magnetic field is often known as the axial magnetic field because the magnetic field vector is mainly axial (B_z). This is somewhat misleading because at the plasma chamber wall the radial component (B_r) of the solenoid field can be quite high. For example, in figure 3.2 at injection B_r and B_{tot} are -0.2 T and 0.6 T, respectively. Due to the shape of the solenoid field, B_r has an opposite direction at the injection and extraction (see magnetic field lines in figures 3.1 and 3.4). At the symmetry axis of the plasma chamber the radial component is zero.

Because the magnetic field shape and the strength are critical parameters affecting the production of highly charged ions, in some ECRIS's an extra solenoid is added between the injection and extraction solenoids (see for example [Cia94], [Hit02] and [Nak06]). This solenoid is used to adjust the minimum magnetic field strength (Min-B) and is sometimes polarized opposite to decrease the value of B_{min}. The optimum magnetic field values are discussed in more detail in chapter 3.4.

The magnetic field strength is often increased with iron (see figure 3.1). When the ECRIS is covered with an "iron yoke", the stray field decreases and the magnetic field inside the ECRIS increases. The maximum magnetic field at the injection can be further increased by adding an iron-plug (see figure 3.1). The maximum magnetic field that can be achieved using normal conducting (Room Temperature; RT or "conventional") coils is typically about 2.5 T. This is mainly limited by the iron saturation magnetic field, which is about 2.3 T. Conventional ECRISs can operate at a maximum microwave frequency of about 18 GHz (see for example: [Nak00] and [Hit02b].

In order to use higher frequencies the magnetic field has to be stronger. Consequently, some ECRIS's have been constructed using a superconducting magnet system (see for example [Cia96], [Nak02], [Lyn04], [Zha04]). A value of

over 4 T is reached in the ECRIS VENUS [Lyn04] at LBNL (Berkeley, USA). Superconductors allow very high current densities in the coils and needs cooling only to keep the conductor temperature below $T_{critical}$ (4 K with liquid helium, LHe, and 77 K with liquid nitrogen, LN_2).

The “solenoidal” magnetic field can also be produced with permanent magnets (see figure 3.3). The maximum magnetic field reached is about 2 T, which allows a maximum microwave frequency of about 10 - 14 GHz (for example: [Hit05]). Usually the ECRIS magnetic field has to be tuned for maximum ion current. Tuning with a permanent magnet structure is complicated, but can be arranged by using movable iron or permanent magnet parts (see for example [Hit05]). In figure 3.3 the central permanent magnet ring can be moved to adjust B_{min}. Another option is to let the magnetic field stay constant and tune the frequency of a wide-band microwave amplifier, such as the traveling wave tube amplifier (see for example [Sor95]). The benefit of using permanent magnets to produce axial magnetic field is the compact size and easy high voltage insulation. When the ECRIS magnetic field is fully produced by permanent magnets there is no power consumption to maintain the magnetic field. In superconducting ECRISs the power consumption is some kilowatts, which is mainly used for cooling (to keep the superconductor temperature below $T_{critical}$). RT coil power consumption can be several tens of kilowatts or even hundreds of kilowatts. One has to make a compromise between the price of the magnet, magnetic field strength and the operating costs caused by the high power need.

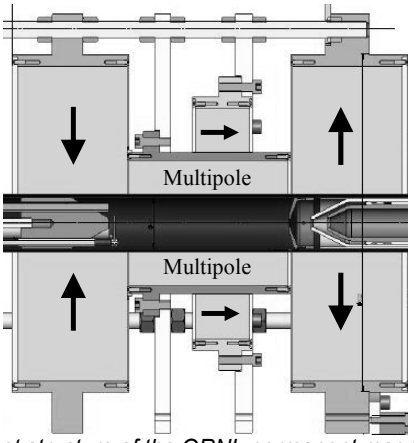

Figure 3.3. Magnet structure of the ORNL permanent magnet ECRIS [Hit05].

The white region in figure 3.4 (a close-up of figure 3.1a) shows where the magnetic field is lower than 0.23 T (6.4 GHz / 0 keV electron resonance field) and dark gray where the magnetic field is higher than 0.27 T (6.4 GHz / 100 keV electron resonance field). The grayscale between is related to the resonance area. In a simple mirror solenoid structure it collides with the plasma chamber walls meaning that there is resonance at the plasma chamber walls. It has been observed that such a structure cannot be used for highly-charged ion production. However, it has high production efficiency for singly-charged ions.

To produce highly-charged ions, a closed resonance volume is needed. Such a magnetic field structure (Min-B) includes a multipolar magnetic field.

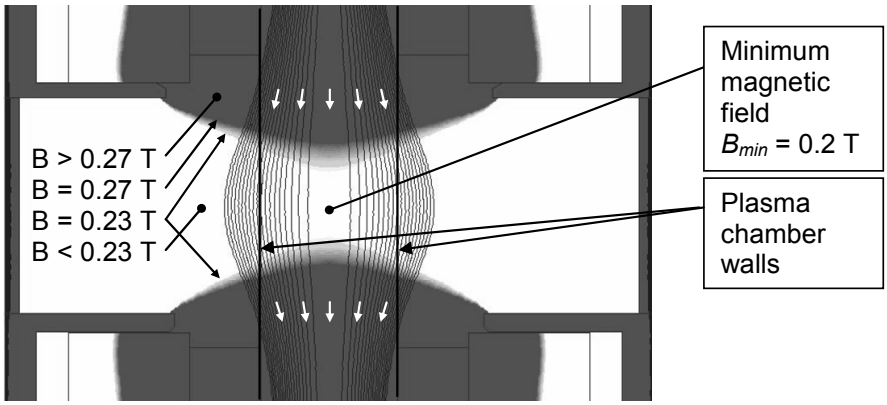

Figure 3.4. A close-up of figure 3.1a showing the ECR heating area of a typical 6.4 GHz ECRIS solenoid structure.

3.2. Multipolar magnetic field

The multipole introduces the magnetic mirror effect also in the radial direction (cylindrical coordinate system). The multipolar field is therefore often called a radial magnetic field. For the magnetic mirror effect the multipolar magnetic field strength has to increase as a function of radius.

A multipole can have 2, 4, 6, 8, and so on, magnetic poles. Figure 3.1(b) shows an example of 6 pole multipole – a hexapole. In the figure, it is formed with six permanent magnets. A typical permanent magnet multipole is cylindrical and is made of several slices as shown in figure 3.5. Such a structure is called a Halbach-type multipole by its inventor K. Halbach [Hal80]. Figure 3.5 also shows how a 24-segment multipole can have a different number of poles (note that only the symmetric, 90 degree, part of the multipole is shown).

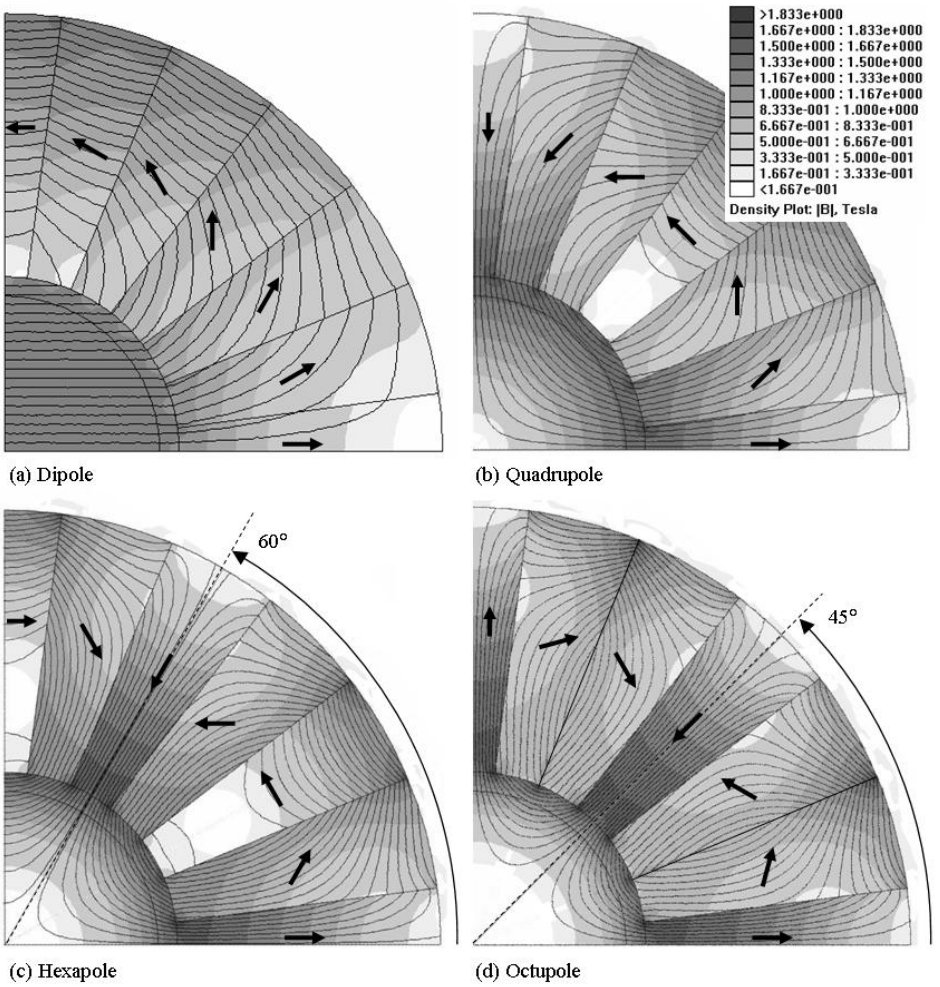

Figure 3.5. Construction of Halbach-type multipoles of different order.

Figure 3.6 shows a comparison between the magnetic field strengths of the multipoles shown above, which all have the same dimensions (plasma chamber inner radius 40 mm, $R_{magnet} \in \{45\text{ mm}, 113\text{ mm}\}$).

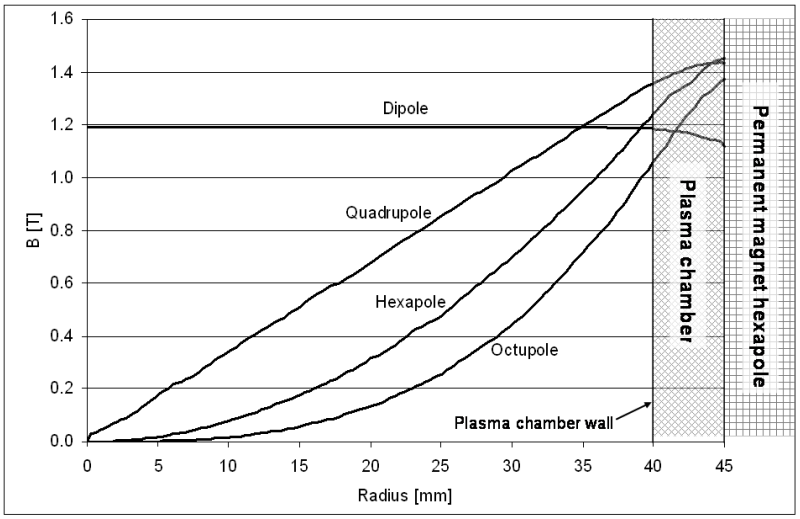

Figure 3.6. Magnetic field profile of the multipoles shown in figure 3.5.

A dipole has a homogenous magnetic field, which is often used for beam bending and separating ions with a different mass/charge (M/Q) -ratio. The dipole field is not suitable for use as an ECRIS multipole because its magnetic field strength is constant as a function of radius and therefore charged particles do not feel the magnetic mirror effect.

A quadrupole is a magnetic field structure often used for beam focusing. As shown in figure 3.6 it has the highest magnetic field strength at the plasma chamber wall and an increasing magnetic field would cause the magnetic mirror effect. Consequently, it would work as an ECRIS multipole. However, the ion extraction from an ECRIS with a quadrupole would not be very efficient due to the plasma shape at the extraction area. In a quadrupole the magnetic field strength increases linearly with radius.

A sextupole (hexapole) is a magnetic field structure, which is used typically for chromaticity correction [Cas94] in synchrotrons and storage rings. Consequently, to maintain high beam quality, sextupoles are designed to be as homogenous as possible. This means that the total magnetic field strength at a given radius is constant and increases as r^2 as a function of the radius.

An octupole is practically the highest order multipole used in accelerators. It is used for example to introduce Landau damping [Cas94] in storage rings. The octupole field increases as r^3.

The most common multipole in an ECRIS is a sextupole (hexapole). The reason can be seen from figure 3.8 where the plasma flux intersects with the plasma electrode forming a triangular shape. This shape concentrates plasma flux close to the central axis and allows one to efficiently extract ions through a round aperture. The corresponding shape in a quadrupole field would be just a thin line. In the case of an octupole the plasma concentration at the axis would

be good but the magnetic field strength at the plasma chamber walls would be smaller. This would increase the plasma losses at the walls and decrease the intensity of the extracted ion beam. ECRISs with octupoles have been constructed (for example [Dup90]) but all modern ECRISs are equipped with a sextupole. The multipole structure investigated in this work is also focused on sextupoles.

3.3. Plasma in the ECRIS magnetic field

Electrons are efficiently trapped in the magnetic field because their velocity component is mainly perpendicular with the magnetic field (due to the ECR heating mechanism). Electrons rotate around the magnetic field lines following them very closely. In a hexapole magnetic field there are six locations where the magnetic field lines are perpendicular to the plasma chamber wall (see figure 3.7).

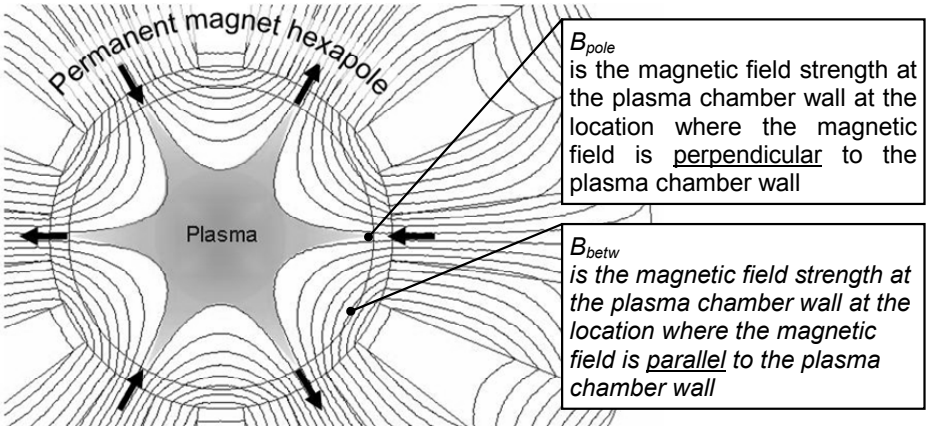

Figure 3.7. Plasma in a hexapole magnetic field.

Figure 3.8 shows a photograph at the inside of an ECRIS plasma chamber. As mentioned previously, the solenoid magnetic field is mainly axial but has a radial component at the plasma chamber wall. Due to the curvature shown in figure 3.4 the radial component is opposite at the injection and at the extraction side. Consequently, its effect to the multipolar magnetic field varies from pole to pole at injection and extraction. For example, at the odd numbered poles (1, 3 and 5) in figure 3.8, the radial component of the solenoid field has decreased the hexapole field at the injection and increased it at the extraction. For this reason at the odd numbered poles the plasma can radially escape the magnetic bottle mainly at the injection but not at the extraction. At the even numbered poles (2, 4 and 6) the effect is opposite. The figure 3.8 shows also the triangular plasma pattern burned on the plasma electrode (round shape in the lower part). At the center of the plasma electrode there is an 8 mm round hole for ion extraction out from the ECRIS. It can be seen that the area of the "usable" plasma flux is very small compared to the area of the plasma flux lost to the plasma chamber walls.

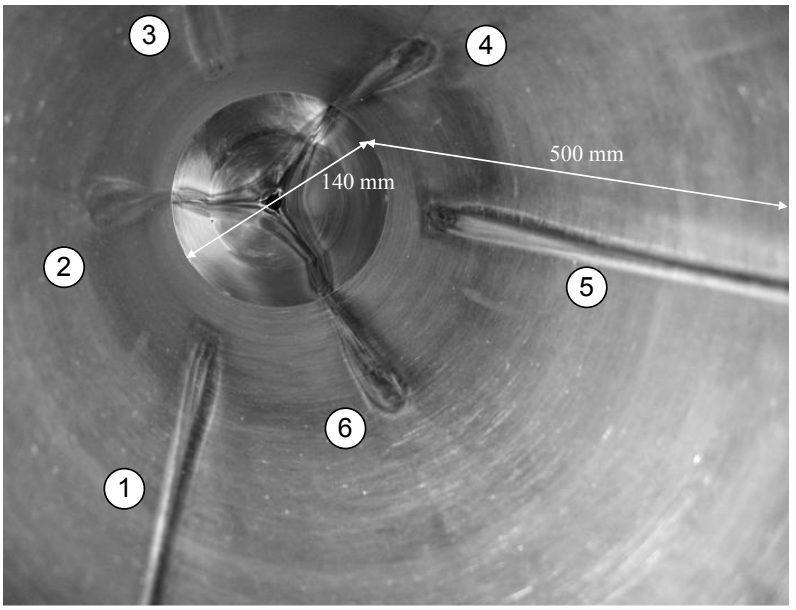

Figure 3.8. Plasma flux patterns burned on the plasma chamber wall of the JYFL 6.4 GHz ECRIS (view from the injection side).

3.4. Experimental scaling laws for the magnetic field

The optimum magnetic field configuration for maximum performance has been studied using fully superconducting ECRIS's in which both the solenoid and the multipole fields are adjustable. Measurements were carried out using 2.45 GHz [Sri96], 6.4 GHz [Ant94], 14 GHz [Lud98] and 18 GHz [Gam99] frequencies using the SC-ECRIS (MSU/NSCL, Michigan, USA) and SERSE (INFN-Catania, Italy). Preliminary experiments were also performed using 28 GHz [Gam01] in SERSE but in this experiment the optimum magnetic field conditions were not reached (because SERSE was originally designed for 18 GHz). Based on these tests, the so-called "magnetic field scaling laws" for the optimum magnetic field configuration were summarized as follows [Hit02]:

$$B_{inj} = 4 \; B_{ECR} \tag{10}$$

$$B_{rad} = 2 \; B_{ECR} \tag{11}$$

$$B_{\min} = 0.4 \; B_{rad} \qquad \left(= 0.8 \; B_{ECR}\right) \tag{12}$$

$$B_{ext} = 0.9 \; B_{rad} \qquad \left(= 1.8 \; B_{ECR}\right) \tag{13}$$

The last two scaling laws were originally calculated with B_{rad} but in this thesis the notation in brackets will be used. This gives the following mirror ratios $R_{inj} \approx 4$, $R_{rad} \approx 2$, $R_{ext} \approx 1.8$. In addition, it was found that the value of B_{min} should be about $0.8 \times B_{ECR}$. These values are widely accepted in the ECRIS community and recent experiments with the fully superconducting 28 GHz ECRIS VENUS [Lei05] have shown their validity. Several experiments have shown that it is especially important that the radial mirror ratio is at least 2. This can be seen from figure 3.9 where the measured xenon intensities are plotted as a function of the radial mirror ratio. Also shown in the figure is the effect of the frequency on the intensities.

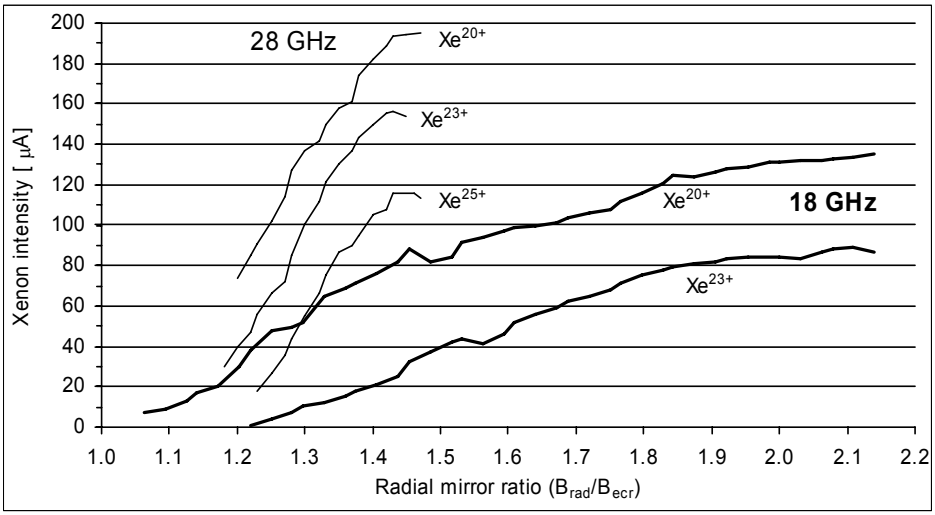

Figure 3.9. Xenon ion intensities as a function of radial mirror ratio [Gam01].

Table 3.1 shows some coil and hexapole combinations for various ECRIS's. The so-called conventional structure includes room temperature operating (RT) solenoids and a permanent magnet (PM) multipole. In a hybrid-ECRIS the solenoids are superconducting and the multipole is made of permanent magnets.

Table 3.1. Magnetic field structures, strengths and mirror ratios of some ECRISs. The coils and hexapole can be either: room temperature (RT), high temperature superconducting (HT-SC), low temperature superconducting (SC) or permanent magnet (PM).

ECRIS	Coils / Hexapole		Freq. [GHz]	Maximum available values for						
				Magnetic field [T]				Mirror ratio		
				B_{inj}	B_{ext}	B_{min}	B_{rad}	R_{inj}	R_{ext}	R_{rad}
JYFL 6.4 GHz MMPS-ECRIS [Ärj90], [Suo06]	RT	PM	6.4	1.2	0.6	0.2	0.55 0.85 (1)	5.3	2.6	2.4 3.4
JYFL 14 GHz ECRIS [Koi01]	RT	PM	14	2.0	1.0	0.4	0.85	4.0	2.0	1.7
Grenoble Test Source – "GTS" [Hit02b]	RT	PM	14	2.5	1.2	0.43	1.15	5.0	2.4	2.3
			18					3.9	1.9	1.8
Riken LHeFree-ECRIS "RAMSES" [Nak02]	SC	PM	18	3.0	2.0	0.5	1.2	4.7	3.1	1.9
INFN-Catania "SERSE" [Gam99], [Gam01]	SC	SC	14	2.7	1.6	0.9	1.45 (3)	5.4	3.2	2.9
			18					4.2	2.5	2.3
			(28) (2)					2.7	1.6	1.5
LBNL Berkeley "VENUS" [Lyn04]	SC	SC	18	4.0	3.0	1.0	2.2 (3)	6.2	4.7	3.4
			28					4.0	3.0	2.2
PM-ECRIS at ORNL [Hit05]	PM	PM	12 (4)	1.8	0.9	0.43	1.05	4.2	2.1	2.5
			14					3.6	1.8	2.1
A-PHOENIX (5) [Thu04]	HT-SC	PM	28	3.0	3.0	1.0	1.5 2.3 (6)	3.0	3.0	1.5 2.3

(1) The MMPS makes it possible to boost the radial magnetic field locally up to 0.85 T.
(2) Scaling laws are not fully satisfied when using 28 GHz in SERSE
(3) Superconducting hexapole - strength can be adjusted
(4) Equipped with 12 -14 GHz Traveling Wave Tube Amplifier (TWTA)
(5) The source is under construction.
(6) 3D magnetic field simulations show that the MMPS makes it possible to boost the radial magnetic field up to 2.3 T [Thu06].

3.5. Different hexapole structures

A hexapole magnet for an ECRIS can be constructed in several ways. A conventional method is to use six rectangular permanent magnet blocks, which are magnetized radially (see figure 3.1b). Such a structure can be used to reach a maximum field of about 0.5 T, which is only adequate for an ECRIS operating at frequencies up to 10 GHz.

3.5.1. Halbach-type hexapoles

In modern ECRISs the hexapole is usually cylindrical, Halbach-type. This kind of hexapole is typically built from 12, 24 or 36 permanent magnet segments. The 12-segment structure often has six gaps between the segments (see figure 3.10). These gaps are used to get radial access to the plasma chamber, for example to improve vacuum pumping. This structure is therefore known as

"open hexapole". The radial ports reduce the total amount of permanent magnet material which can be used, decreasing the hexapole field. This structure is used in the AECR-U type [Xie97] ECRIS. At present, the strongest AECR-U type hexapole has a radial magnetic field of about 1 T [Von04]. The 24- and 36- segment structures are usually "closed" to have the maximum amount of permanent magnet material and maximize the magnetic field strength. The 36-segment structure has a few percent higher and more homogenous magnetic field than the 24-segment structure. Each permanent magnet segment has the magnetization direction optimized. The design shown in figure 3.11 includes the strongest ECRIS permanent magnet hexapole reported so far (in 2005), which is a 36-segment Halbach type hexapole with extremely large outer diameter. The maximum radial magnetic field at the plasma chamber wall (B_{pole}) will be about 1.5 T [Thu04]. In addition, it is made of three different permanent magnet layers in order to avoid any demagnetization effects. The hexapole outer diameter under the solenoids (see figure 3.11) is closer to "typical" values meaning that the radial magnetic field strength there is about 1.2 T. An improvement of 10 % [Thu06] was reached here by using an optimized Offset-Halbach structure which was developed in the course of this thesis work and is described later in chapter 3.6.2.

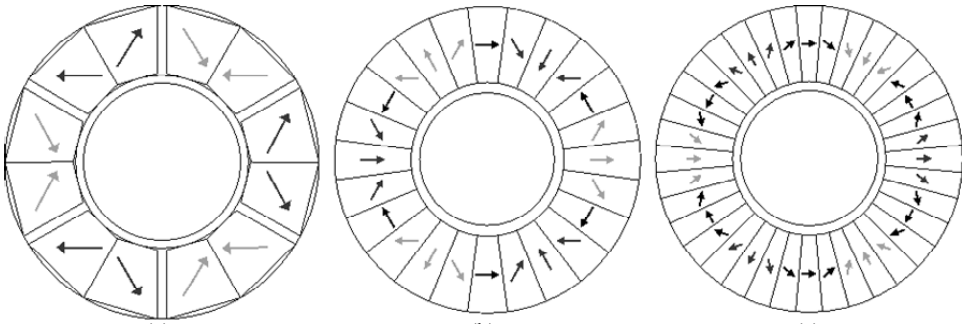

Figure 3.10. Halbach-type hexapole: (a) 12-segment, (b) 24-segment, (c) 36-segment.

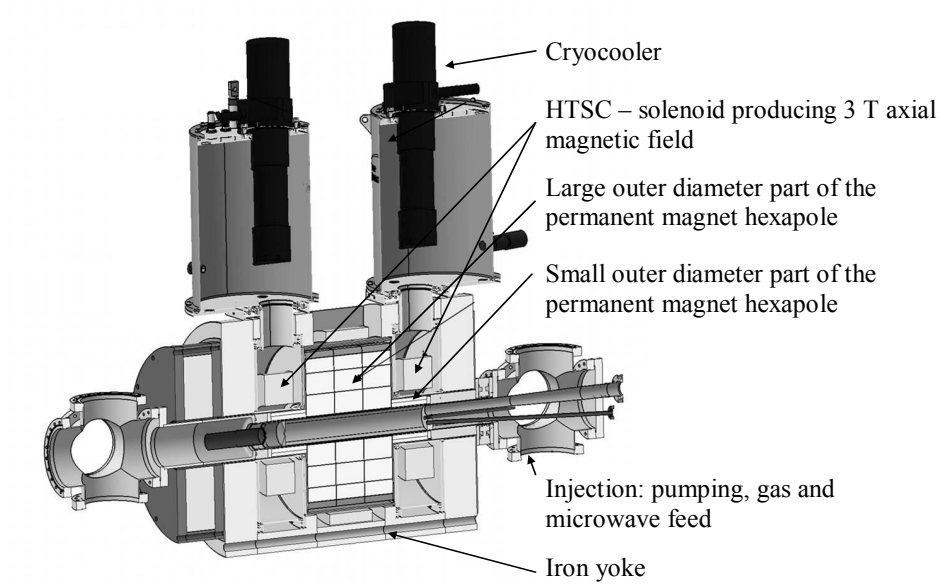

Figure 3.11. A design of A-PHOENIX [Thu06].

3.5.2. Superconducting hexapoles

A superconducting (SC) hexapole is usually constructed using six so-called "race-track" magnets as shown in figure 3.12. The machining of such magnets requires very high tolerances and good clamping. If the superconducting wire can move even slightly it can cause heat by mechanical friction and the whole magnet might quench. All superconducting ECRIS hexapoles are constructed using low-temperature (LHe at 4 K) superconducting wire. This is because small radius race-track magnets are necessary in order to have a compact ECRIS hexapole. Today's high temperature superconductors (LN_2) cannot be used for such small wire radii. In addition, LHe-superconductors require a very good thermal insulation and liquid nitrogen for a thermal shield. The inner bore of the SC hexapole has to be at room temperature because of the plasma. Between the plasma and SC hexapole some radiation shielding is necessary in order to prevent x-ray radiation heating the superconductors. Consequently, a superconducting ECRIS hexapole has a complex design and is very expensive.

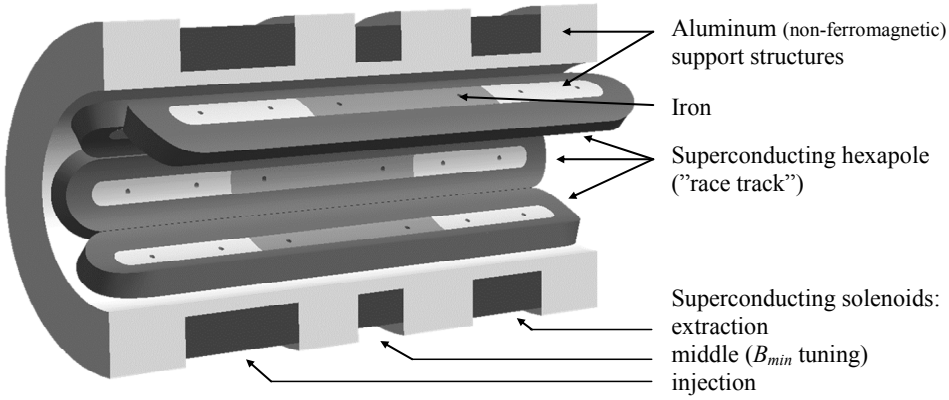

Figure 3.12. Schematic picture of fully superconducting ECRIS: VENUS [Lei99].

There are only a few ECRISs in the world which have a SC hexapole. The best performing fully SC ECRISs are (in order of year of construction): SC-ECRIS [Ant94] at NSCL-MSU, USA; SERSE [Cia94] at INFN-Catania, Italy and VENUS [Lyn04] in LBNL, Berkeley, USA. The most powerful SC-hexapole is in VENUS, where a maximum radial field of 2.4 T is available. A schematic picture of the VENUS magnetic field structure is shown in figure 3.12. A comparison between comparative radii PM and SC hexapoles is shown in figure 3.13 where, in part (b), one of the race-track magnets is highlighted. Note that there is no iron included in the simulations. The current density in the superconducting hexapole has to be very high (73.5 A/mm^2) in order to reach the same B_{pole} value (1.25 T) in both structures. In fact, it has to be even higher because the cryostat needs more space and the plasma chamber wall must be thicker.

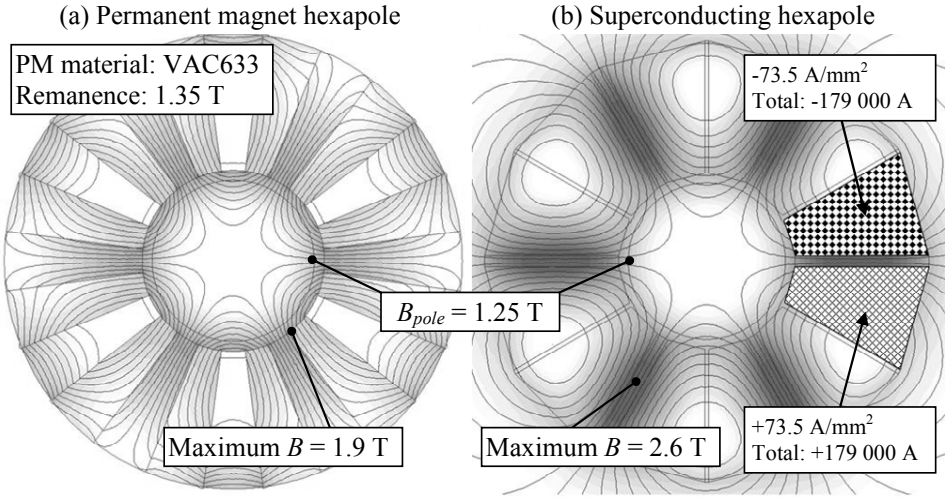

Figure 3.13. Comparison between (a) permanent magnet and (b) superconducting hexapoles.

A new superconducting ECRIS called SECRAL [Zha04] is being finished in 2006 in Lanzhou, China. SECRAL has a unique feature whereby the SC hexapole is located outside the SC solenoids. In this structure the forces between the superconductors are lower making the design easier. The source is also very compact, only 1 m in length and in diameter. However, if the hexapole field strength at the plasma chamber wall (r = 63 mm) is 2 T and the hexapole field r^2-dependence is assumed, the hexapole field is 6.1 T on the inner surface of the SC hexapole (r = 110 mm). For comparison, in VENUS the hexapole strength is higher (2.4 T) at the plasma chamber wall (r = 70 mm) whilst still being lower (4.9 T) on the inner surface of the SC hexapole (r = 100 mm).

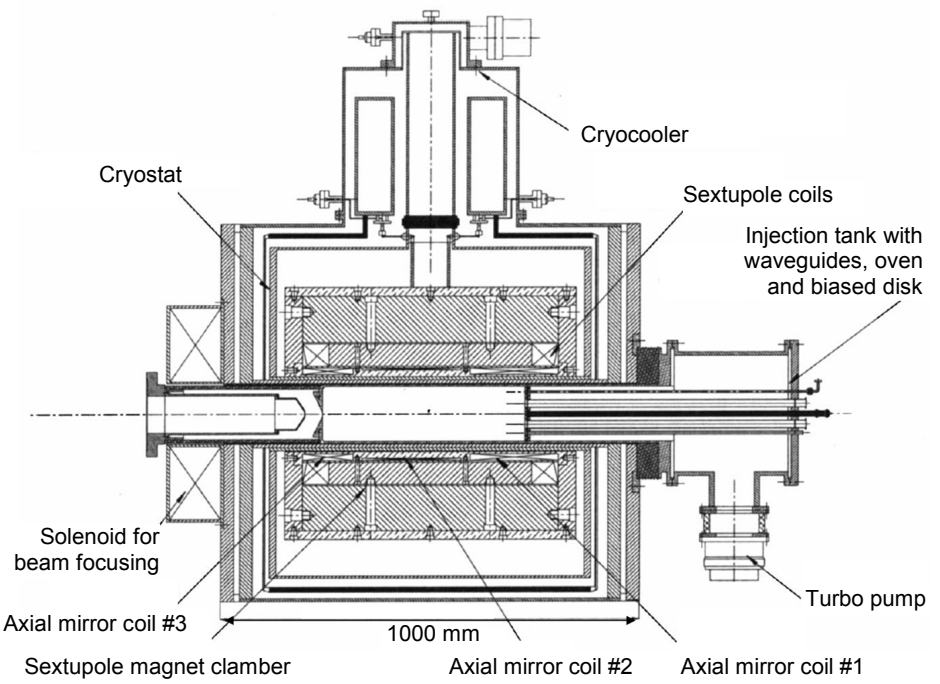

Figure 3.14. Superconducting ECRIS: SECRAL at Lanzhou, China [Zha04].

The next generation fully superconducting ECRIS will be called MS-ECRIS (Multipurpose Superconducting ECRIS). The design is being made within a collaboration called “Ion Source for Intense Beams of Heavy Ions” (ISIBHI) with 11 European nuclear physics laboratories. The first prototype will be built in GSI, Germany, and should be completed in 2008. This ECRIS will have the strongest magnetic confinement built so far: B_{inj} = 4.5 T, B_{ext} = 3.2 T, B_{rad} = 2.7 T [Cia06].

3.6. Design of permanent magnet hexapoles for ECRISs

As the superconducting technique is expensive and technically challenging several ECRIS projects prefer to use more conventional techniques; permanent magnet hexapoles and room temperature operating (copper) solenoids. The limits of this RT technique are already in sight and therefore permanent magnet hexapole design becomes more and more difficult. Consequently, the design has to be made very carefully taking all the relevant aspects into account.

3.6.1. Magnetic field simulation codes

Permanent magnet hexapoles are usually designed using computer codes, which can utilize two-dimensional Cartesian (2D), two-dimensional axial-symmetry cylindrical (AS) or three-dimensional Cartesian coordinates (3D). The preliminary models are usually made with 2D or AS codes, which use much less memory and computer time than pure 3D codes. In this thesis work a desktop computer was used and the typical time needed to solve 2D models was around one minute, while for 3D models it was up to several hours.

There are only few free codes as most codes are only available commercially. However, these often include several usable modules for solving electric field, high frequency, heat transfer, structural mechanics, chemical reactions, and so on. Some of the most well known and used codes are listed in table 3.2. In this work three free codes were used: *Poisson Superfish* and Finite Element Method Magnetics (*FEMM*) for 2D and *RADIA* for 3D magnetic field simulations.

Table 3.2. Examples of magnetic field simulation codes.

Free	2D	AS	3D	Code	Available from (in Feb 2006)
	x	x	x	ANSYS® Emag™	http://www.ansys.com/
	x	x	x	FEMLAB	http://www.femlab.com/
x	x	x		FEMM	http://femm.foster-miller.net/
	x	x	x	VF Opera / Tosca	http://www.vectorfields.com/
x	x	x		Poisson Superfish	http://laacg1.lanl.gov/laacg/services/download_sf.phtml
(1)	x	x	x	ANSOFT Maxwell	http://www.ansoft.com/
	x	x	x	Integrated software magneto / amperes	http://www.integratedsoft.com/
x			x	RADIA (2)	http://www.esrf.fr/Accelerators/Groups/InsertionDevices/Software/Radia/

(1) Maxwell 2D student version is available free
(2) User interface is based on *Mathematica* program (Wolfram Research, Inc., http://www.wolfram.com/)

Poisson Superfish is a collection of programs for calculating static magnetic and electric fields and radio-frequency electromagnetic fields in either 2D or axially-symmetric cylindrical coordinates. It uses the Finite Element Method

(FEM) in which the problem geometry is covered by a mesh of triangles. The code calculates the magnetic vector potential inside these elements and solves a system of equations, which is found by assuming the magnetic vector potential to be continuous in the whole mesh geometry. The correct solution is found when the total energy of all the elements is minimized. The solution becomes more accurate with a dense mesh, i.e. with a higher number of triangles in the model. Because *Poisson Superfish* is a 2D code computer memory consumption is not a problem and it can be used to obtain very accurate results.

FEMM works somewhat like *Poisson Superfish* but the user interface is much more convenient. In this thesis FEMM results were verified with *Poisson Superfish* and found to be practically identical. Consequently, FEMM was used in most of the simulations.

In RADIA a different method is used, whereby a number of 3D-objects are created in which the material magnetic properties are assumed to be constant. This is called a Boundary Element Method (BEM). Because the state of the material magnetization depends on the external magnetic field, the solver uses an iterative process, which is called relaxation. A more accurate result can be found by increasing the number of objects in the model, i.e. by cutting big objects into smaller pieces. This also enables the magnetization distribution inside the magnetic material to be retrieved. The magnetic field at any point can be calculated as a vector sum of all the objects in the model. Consequently, in a very big model calculating the magnetic field values can take a lot of computing time.

In order to reduce this computing time, some boundary conditions can be utilized. The hexapole geometry has six identical 60 degree sectors, which can be divided into two identical, but mirrored 30 degree sectors. Consequently, the least memory consumptive model is a 30 degree “slice” of the hexapole. The boundary line at $\theta = 0^\circ$ has to be determined with the Dirichlet boundary condition, meaning that the magnetic flux cannot pass the boundary line. The boundary line at $\theta = 30^\circ$ has to be determined with Neumann’s boundary condition, where the magnetic flux passes the boundary line perpendicularly. The computing time for such a 30 degree slice is only 1/12 of that for the whole 360 degree hexapole model. The results obtained are, however, identical to these from the “complete model”.

3.6.2. Offset-Halbach hexapoles

Typically Halbach-type hexapoles are constructed as shown in figure 3.15, where six segments are magnetized radially (i.e. blocks 1, 5, etc.). As mentioned in chapter 3.2, hexapoles are usually designed to be as homogenous as possible. However, in an ECRIS this is not needed. The hexapole magnetic field is divided into the radial and azimuthal components. The radial component provides the radial mirror field and should be high

enough for the adequate confinement of the plasma. The azimuthal component can be lower than the radial component but still sufficient in order to ensure the closed ECR surface. Figure 3.7 defines two magnetic field values at the plasma chamber wall; B_{betw} and B_{pole}. The maximum radial magnetic field strength is described by B_{pole} ($\vec{B}$ perpendicular to the plasma chamber wall), while the maximum azimuthal magnetic field strength is described by B_{betw} ($\vec{B}$ parallel to the plasma chamber wall). As was shown in figure 3.7 the plasma flux hits the plasma chamber wall at the location where the magnetic field vector is perpendicular to the plasma chamber wall. At this point the magnetic field, B_{pole}, should have the highest value possible in order to improve the confinement of the plasma. The values of B_{pole} and B_{betw} can be varied by differing the magnetization angles.

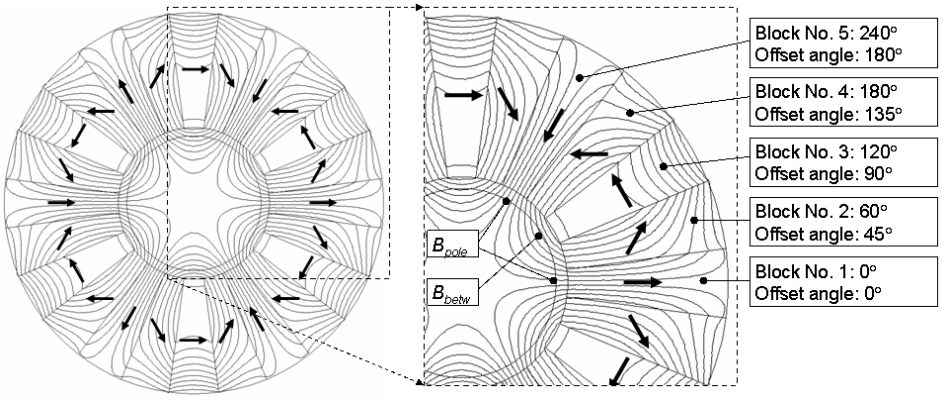

Figure 3.15. Typical design of a 24-segment Halbach-type hexapole.

The *Easy Axis Rotation Theorem* [Hal80] states that by rotating the magnetization vector of each magnet through 22.5°, the magnetic field inside the hexapole is identical to that with un-rotated magnets (see figure 3.16). In this thesis the rotated structure is called an Offset-Halbach (O-HB) structure.

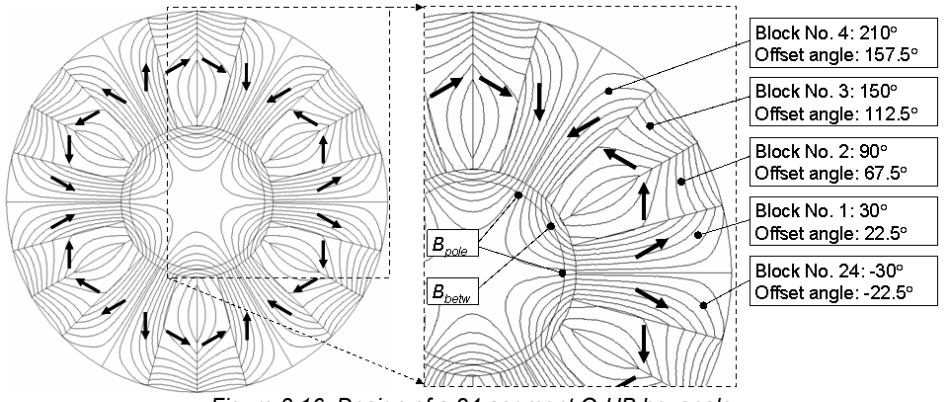

Figure 3.16. Design of a 24-segment O-HB hexapole.

The offset-angle is the angle between the radial (cylindrical coordinate system) and the magnetization vectors. In a typical Halbach structure the offset-angle is 0° (or 180°) for the block at the magnetic pole. From here on the plasma chamber radius, magnet inner radius and the magnet outer radius are noted as R_{pc}, R_{in}, R_{out}, respectively. Definitions for these dimensions and the offset-angle are described in figure 3.17.

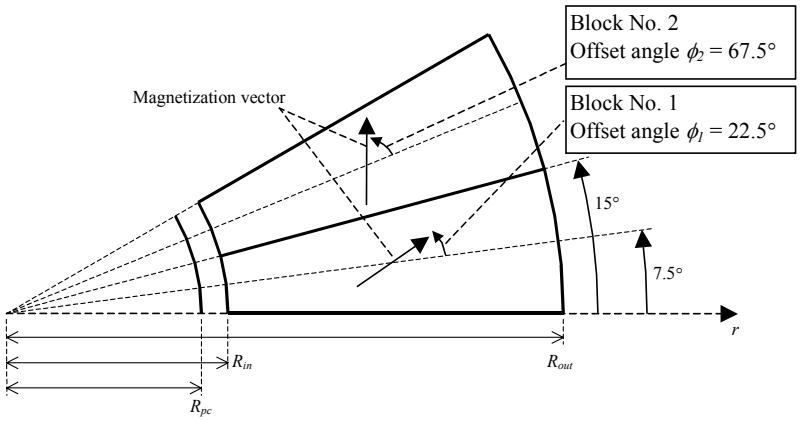

Figure 3.17. Definitions of the offset angles ϕ_1, ϕ_2 and radii R_{pc}, R_{in}, R_{out}. [Suo04].

3.6.3. Hexapole equations; JYFL-HEXE

Based on numerous computer simulations performed in the course of this thesis work, a set of so-called hexapole equations (JYFL-HEXE) were developed (described in more detail in reference [Suo04]). Equation (14) gives the magnetic field strength of a typical 24-segment Halbach structure (see figure 3.15). It includes the values f_{radius} and $B_{remanence}$, which are related to the hexapole dimensions and the permanent magnet material remanence (1.35 T used in the simulations). Equation (15) gives a scaling factor (f_{radius}) for different hexapole dimensions (R_{in}, R_{out}) and plasma chamber radii R_{pc}. The radii should be given in millimeters.

$$B_{pole}^{HB} = 0.985 \cdot f_{radius} \cdot 1.22T \cdot \left(\frac{B_{remanence}}{1.35T} \right) \tag{14}$$

$$f_{radius} = \frac{1.33}{1 + 0.35 \cdot \left(\frac{R_{out}}{R_{in}} - 1 \right)^{-1.23}} \cdot \frac{0.085}{0.053 + \frac{1}{1.24 + R_{in}}} \cdot \frac{R_{pc}^2}{(R_{in} - 5)^2} \cdot \frac{1}{1.22} \tag{15}$$

Equations (16) and (17) are related to the values B_{pole} and B_{betw} of an Offset-Halbach structure (see figures 3.16 and 3.17). These values can be optimized by varying the offset-angles ϕ_1 and ϕ_2 (in degrees).

$$B_{pole}^{O-HB} = f_{radius} \cdot \left(700000 + 7900\phi_1 - 110\phi_1^2 + 9700\phi_2 - 59\phi_2^2\right) \cdot 10^{-6} T \quad (16)$$

$$B_{betw}^{O-HB} = f_{radius} \cdot \left(935000 + 913\phi_1 - 59\phi_1^2 + 11800\phi_2 - 110\phi_2^2\right) \cdot 10^{-6} T \quad (17)$$

Detailed information concerning the $B_{remanence}$ scaling and error limits can be found from [Suo04]. For example the value of B_{pole} in A-PHOENIX was increased by about 10 % [Thu06] after optimizing the offset-angles. At the same time the value of B_{betw} decreased slightly although its value is less critical than the value of B_{pole}. The hexapole equations can be used to get a good estimation of the magnetic field of a 24-segment Halbach-type hexapole. However, in addition a magnetic field simulation program should be used to confirm the values and to ensure that there is no fatal demagnetization of the permanent magnets.

3.6.4. Optimization of the hexapole dimensions

When designing a new hexapole for an ECRIS, its dimensions should be optimized. There are often some external constraints, for example the inner diameter of the solenoids, which must be taken into account. Figure 3.18 shows the simulated magnetic field at the pole as a function of the ratio R_{out} / R_{in}. To produce the data shown in figure 3.18(a), the inner radius of the plasma chamber (R_{pc} = 40 mm) and permanent magnet structure (R_{in}= 45 mm) were kept constant and the outer diameter of the permanent magnet structure (R_{out}) was varied. This behavior was described in [Kur00] and as a consequence, a compromise between the strength of the magnetic field and the size of the plasma chamber has to be made. Structures where the R_{out} / R_{in} -ratio is higher than 3 are not commonly used. The figure also shows that in an Offset-Halbach structure the value of B_{pole} can be optimized to be slightly higher than in a typical Halbach-type hexapole.

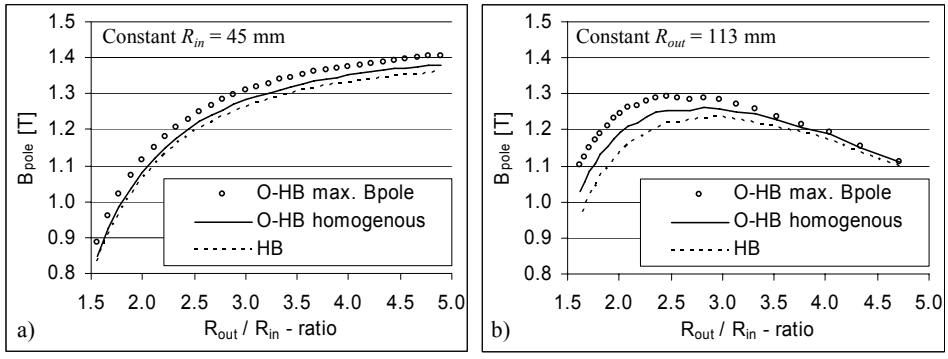

Figure 3.18. Magnet R_{out} / R_{in} – dependence with constant (a) R_{in} = 45 mm and (b) R_{out} = 113 mm [Suo04].

To produce the behavior shown in figure 3.18(b) a different approach has been taken. The outer diameter (R_{out}) and the plasma chamber wall thickness (R_{in} -

R_{pc}) were kept constant. This is due to the fact that an adequate thickness of plasma chamber wall is needed for efficient cooling (to prevent permanent magnet overheating). In addition, the outer diameter of the plasma chamber structure often has to be limited to fit inside the solenoid. As figure 3.18(b) shows, an optimum R_{out} / R_{in} ratio is obtained if the aforementioned boundary conditions have been used. Similar behavior was observed earlier by T. Katayose [Kat95]. The results shown in figure 3.18 can also be found using the JYFL-HEXE hexapole equations.

In some cases it may be possible to take advantage of permanent magnet edge effects. In an ideal hexapole the magnetic field strength increases with r^2. However, close to the magnet the increase is steeper, due to the edge-effect of the magnet. Close to the surface of the magnet, the field is highest at the edge of the magnet, which is consistent with the current loop analogy of permanent magnets.

Figure 3.19(a) shows the magnetic field as a function of azimuthal angle when the distance to the magnet is only 1 mm. Angles of 0° and 60° correspond to the magnetic poles shown in figures 3.15 and 3.16. In a normal Halbach-structure the strongest magnetic field is achieved at the edge of the magnet block (7.5°). This local maximum occurs with a period of 15°, which is the "width" of one magnet block in 24-segment Halbach-hexapole. As a result, the magnetic field at the magnetic pole does not increase as quickly as expected according to the r^2-dependence (see figure 3.19b). This is not the case in an offset-Halbach-structure where the edge of the magnet is on the magnetic pole (see figure 3.16). As a result, the magnetic field close to the magnet increases faster than expected according to r^2-dependence (see 3.19b).

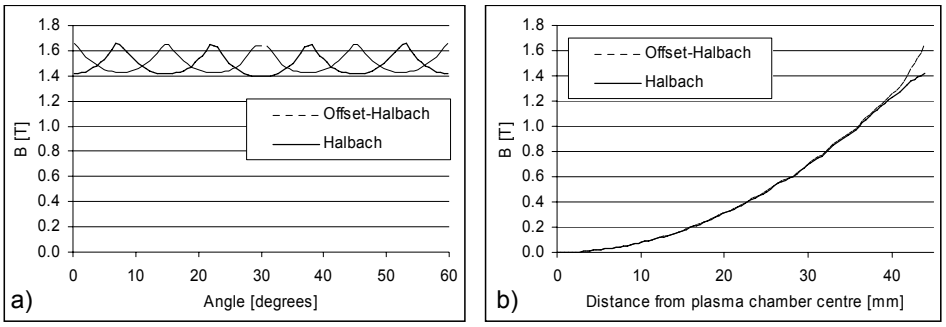

Figure 3.19. Behavior of the magnetic field in the normal Halbach and Offset-Halbach structure (a) at the plasma chamber wall when the distance to the permanent magnet is 1 mm (b) as a function of radius to the direction of the magnetic pole (0°).

Figure 3.20 shows the behavior of the magnetic field as a function of the distance from the permanent magnet surface in the radial direction. Two hexapole structures have been compared: 1) the offset-Halbach structure and 2) the normal Halbach structure. In both cases the comparison between the results obtained by using the POISSON-code, the FEMM-simulation code and the JYFL-HEXE equations has been performed. As can be seen, magnetic field

strengths obtained with the different codes are almost identical as long as the distance from the magnet inner radius is at least 4 mm. The result obtained using the JYFL-HEXE is slightly higher in the case of the typical Halbach-structure and slightly lower in the case of the offset-Halbach-structure. This is due to the deviation from the r^2-dependence described earlier. The results of the POISSON and the FEMM simulation codes are practically identical.

Figure 3.20 also shows that the optimized offset-structure is very effective if the thickness of the plasma chamber wall can be decreased. The optimized offset-structure gives around a 4 % higher magnetic field than the normal Halbach-structure if the thickness of the plasma chamber wall is 5 mm. If a thinner wall can be used, this difference increases as follows: 3 mm → 12 %, 2 mm → 18 % and 1 mm → 28 %.

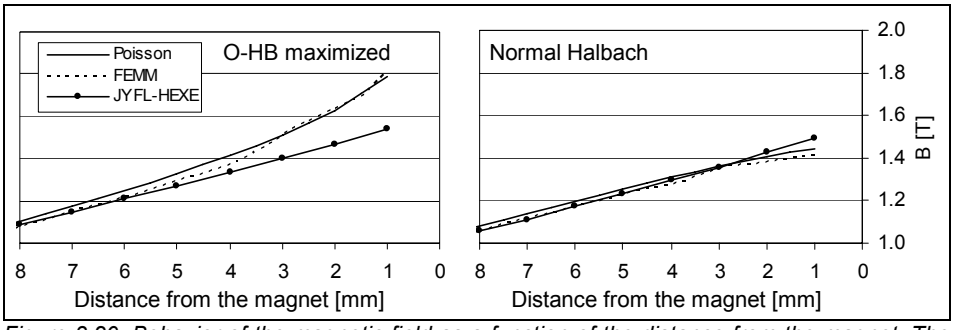

Figure 3.20. Behavior of the magnetic field as a function of the distance from the magnet. The magnetic field has been calculated with the POISSON-code, the FEMM –code and the JYFL-HEXE equations [Suo04].

3.6.5. Permanent magnet material coercive force and temperature dependence

The permanent magnet (PM) material cannot keep its magnetization in a high demagnetizing field. When the opposing magnetic field (with respect to the PM magnetization) is increased the PM material magnetization decreases and finally goes to zero. At that point the PM material is demagnetized and does not recover even after the opposing field is removed. The highest value of the demagnetizing field that the PM can stand is called the coercivity, H_c (or coercive force). Often two different coercivity values are given; H_{cB} is the opposing magnetic field resulting in zero total magnetic field and H_{cJ} the opposing field value resulting in zero magnetization of the permanent magnet material. For example, if VACODYM 677 material is used and the external magnetic field is -915 kA/m, the total magnetic field goes to zero ($B = \mu_0(M + H) = 0 \rightarrow M = -H$). If the external magnetic field is further increased, the total magnetic field becomes negative. The external magnetic field needed to demagnetize VACODYM 677 material is as high as -2465 kA/m. However, in a hexapole design materials which have as high a remanence as possible are preferred. For such materials the coercivity and the difference between H_{cB} and

H_{cJ} are lower. Some examples of permanent magnet material properties are shown in table 3.3.

Table 3.3. Examples of NdFeB-type permanent magnet materials [VAC06].

Product name	Remanence	Coercivity		Energy Density	Temperature coefficient (RT - 100°C)	
	B_r [T]	H_{cB} [kA/m]	H_{cJ} [kA/m]	(BH)max [kJ/m^3]	for (B_r) [%/°C]	for (H_{cJ}) [%/°C]
VACODYM 722 HR	1.47	915	955	415	-0.115	-0.77
VACODYM 745 HR	1.44	1115	1195	400	-0.115	-0.73
VACODYM 510 HR	1.41	980	1035	385	-0.115	-0.79
VACODYM 633 HR	1.35	1040	1430	350	-0.095	-0.65
VACODYM 655 HR	1.28	990	1830	315	-0.090	-0.61
VACODYM 677 HR	1.18	915	2465	270	-0.085	-0.55

In a hexapole, each permanent magnet block is influenced by the other blocks, and a partial demagnetization can occur if the design (dimensions, magnetization angles, PM material) is not made carefully. In an ECRIS the situation is even more complicated due to the presence of a strong solenoid magnetic field, and especially its radial component. In addition these values are temperature dependent, which has to be taken into account in the design. Figure 3.21 shows some typical NdFeB-permanent magnet material demagnetization curves. When the demagnetizing field becomes too high the PM magnetization drops very quickly. At the flat part of the curve the permanent magnet is fully recoverable (reversible process) but close to the "knee-point" it starts to suffer irreversible demagnetization. For example, in a Halbach-type hexapole the opposing magnetic field (a.k.a. permanent magnet load) can easily be -1000 kA/m (even without the ECRIS solenoid field). If the temperature for some reason increases from the typical 20°C to 60°C, the permanent magnet magnetization will be lost. It does not recover when the temperature is decreased back to 20°C. Consequently, it is important to use the correct material parameterization in the magnetic field simulation program. In addition some safety margin for the temperature increase has to be included in the design. Fortunately, if some small areas in the hexapole are demagnetized, the decrease of the hexapole field inside the plasma chamber may not be severe. An example of this is presented in chapter 5.2.3.

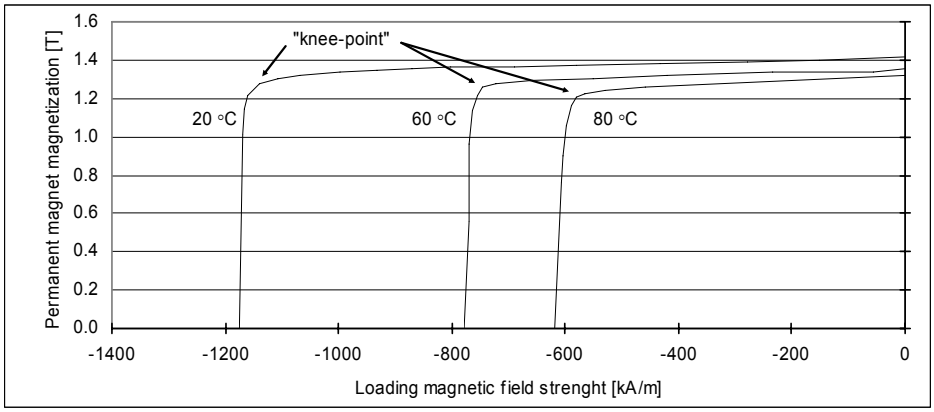

Figure 3.21. Permanent magnet demagnetization curves at 20°C, 60°C and 80°C (NdFeB grade N48 manufactured by China Rare Earth Permanent Magnet Company).

4. Experimental setup

The experimental setup is located at the Accelerator Laboratory, Department of Physics at the University of Jyväskylä (JYFL). Two ECR ion sources are available for heavy ion beam production: the JYFL 14 GHz ECRIS [Koi01] is mainly used for the JYFL K130 cyclotron [Liu92] while the JYFL 6.4 GHz ECRIS [Ärj90] can also be used for ECRIS development work.

4.1. JYFL 6.4 GHz ECRIS

The original JYFL 6.4 GHz ECRIS was a replica of the Michigan State University RT-ECRIS [Ant86]. The design was converted to the metric-system and the source was built in 1990 – 1991 at JYFL. The special features of this ECRIS are a large plasma chamber and vertical alignment (usually ECRISs are placed horizontally). Originally the source was a two-stage ECRIS [Gel96], which was modified [Koi03] in 2002 to a conventional Min-B ECRIS structure ("one-stage") as shown in figure 4.1. The upgrade gave a remarkable increase in the magnetic field maxima, and required full replacement of the iron parts (return yoke, injection and extraction iron plugs). The present iron configuration is shown in figure 4.2 corresponding to the parameters shown in table 4.1.

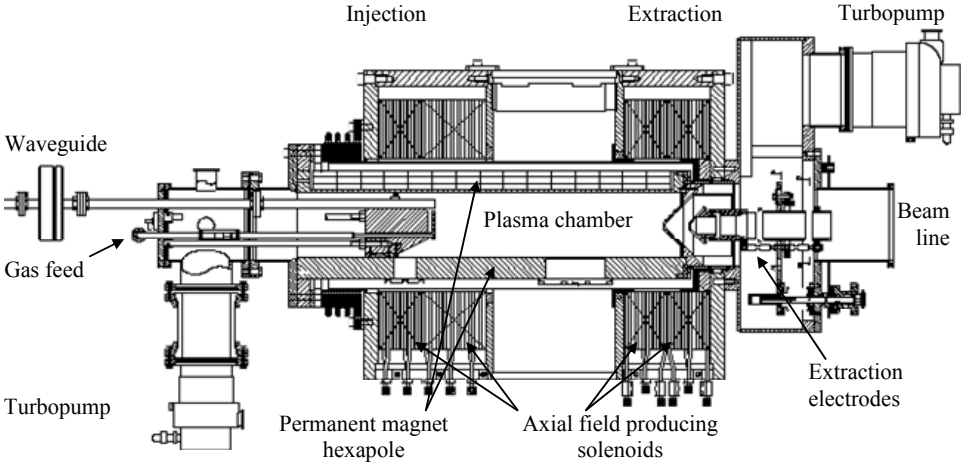

Figure 4.1. Schematic drawing of the JYFL 6.4 GHz ECRIS (figure rotated 90°).

Table 4.1. Main parameters of the JYFL 6.4 GHz ECRIS.

Plasma chamber volume	~7.7 liters
Magnetic field maximum at the injection	1.2 T
Magnetic field maximum at the extraction	0.6 T
Magnetic field minimum (Min-B)	0.2 T
Microwave frequency (Klystron-type amplifier)	6.4 GHz
Maximum RF power (limited by cooling)	1 kW
Maximum acceleration voltage	20 kV

The magnetic field modification was successful. The effect on different oxygen beams is shown in figure 4.3 with the legend: “Axial field upgraded”. In 2003 the hexapole magnetic field was further upgraded by adding an extra iron yoke around the permanent magnet multipole. At that time the hexapole field increased from 0.34 T to 0.37 T (i.e. R_r = 1.49 → 1.62) (see legend: “Hexapole upgraded” in figure 4.3).

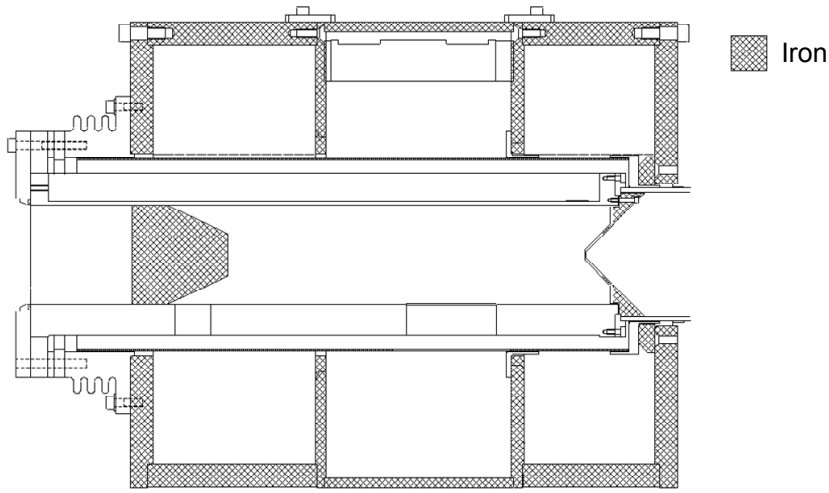

Figure 4.2. Iron configuration of the JYFL 6.4 GHz ECRIS (figure rotated 90°).

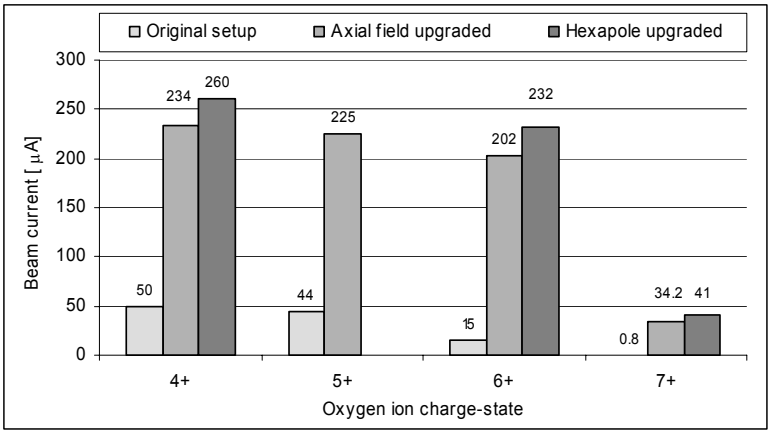

Figure 4.3. Effect of the magnetic field upgrades on the JYFL 6.4 GHz ECRIS performance.

These upgrades clearly showed the importance of magnetic confinement on the ECRIS performance. Good results encouraged the JYFL ion source group to further develop the magnetic confinement. At the International Ion Source Conference 2003 (ICIS'03) at Dubna, Russia, the idea of the Modified MultiPole Structure - MMPS [Koi04] was presented by H. Koivisto. The idea consequently led to this thesis work. The MMPS-technique is described in detail in chapter 5.

4.2. Extraction system and beam line

An extraction electrode system is required to form the ion beam from the plasma. The first electrode, known as the plasma electrode (see figures 3.8 and 4.4), is at the extraction side of the plasma chamber. It is at the same voltage as the plasma chamber. Next electrode is called a puller electrode, which is usually at ground potential. The region between these two electrodes is the most critical in forming the ion beam from the plasma. At JYFL the 6.4 GHz ECRIS beam is focused with an einzel-electrode (the name "einzel" originates from German language and means "one electrode"). The setup is shown in figure 4.4.

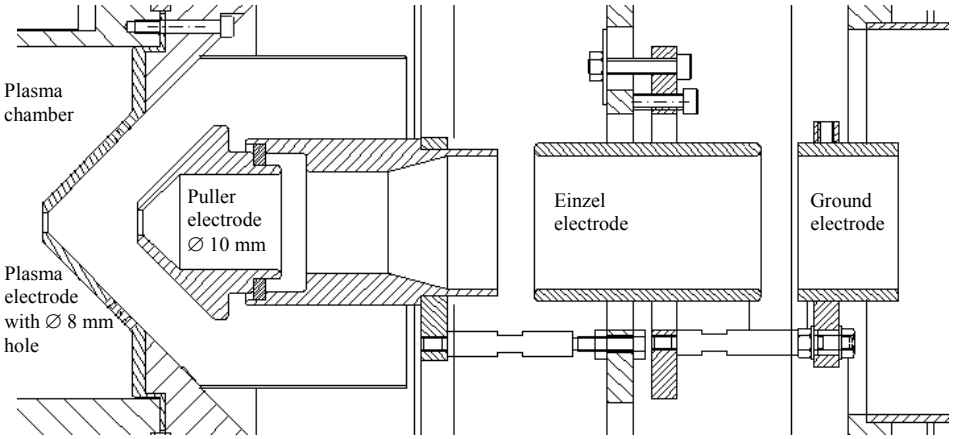

Figure 4.4. The JYFL 6.4 GHz ECRIS extraction system (figure rotated 90°).

The beam line from the JYFL 6.4 GHz ECRIS to the Faraday cup is shown in figure 4.5. The ECRIS extraction system is followed by an XY-magnet, which can be used to steer the beam towards the center axis of the beam line. A solenoid (SOL1) is used to focus the beam through a 30 mm collimator (COL1), which cuts off the outermost (not usable) part of the ion beam (called the beam halo). The ion beam is analyzed with a double-focusing 90 degree bending magnet. The bending radius is 400 mm and the mass resolving power is about 28. Unless mentioned otherwise, the beam current in this work is always measured with the first Faraday cup after the bending magnet (FC1). The Faraday cup has a negatively-biased screening electrode to prevent the escape of secondary electrons.

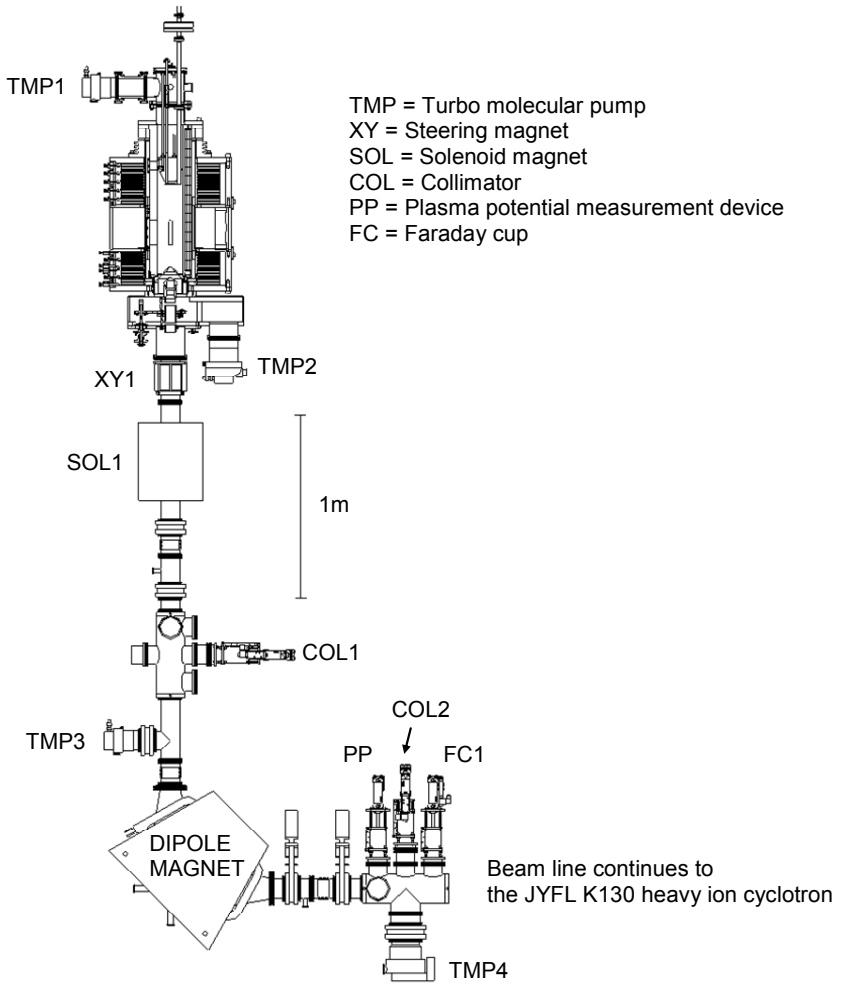

Figure 4.5. Beam line from the JYFL 6.4 GHz ECRIS to the Faraday cup (FC1).

5. Modified multipole structure – MMPS

As discussed earlier the radial magnetic field strength plays an important role in the production of highly charged ion beams with an ECRIS. However, in several ECRISs the radial magnetic field strength is too weak for the optimized production of the highest charge-states. This was observed in several laboratories (for example at JYFL [Koi03] and ANL [Von04]) where the (too weak) permanent magnet hexapoles were upgraded to better satisfy the scaling laws (see chapter 3.4). Unfortunately, today's permanent magnet technology limits the magnetic field of conventional hexapoles to 1.3 T – 1.5 T (the highest reported value can be found from [Thu04]). This is mainly due to the permanent magnet material remanence and coercive force values. Therefore methods to increase the magnetic field strength in permanent magnet hexapoles are very limited.

Experiments done with superconducting ECRISs have shown that the radial mirror ratio (R_r) should be at least 2 for optimized production of highly charged ions. In these experiments the "total" hexapole field was varied meaning that the field was changed everywhere in the plasma chamber (B_{pole}, B_{betw},…). The objective of this thesis work was to study if only a local magnetic field increase at the magnetic poles of the hexapole (i.e. where the plasma intersects the chamber walls) improves the ECRIS performance. As a consequence, the first Modified MultiPole Structure (JYFL-MMPS) prototype was developed and tested.

5.1. Principle of the idea

The principle of the JYFL-MMPS idea is to decrease the loss-cone of the multipole magnetic field by increasing the hexapole field using a material which has high permeability and saturation magnetic field values. An example, where a small cross-section iron block is added to the Halbach-type hexapole, is shown in figure 5.1. The magnetic field at the plasma chamber wall increases from 1.2 to 2 Tesla.

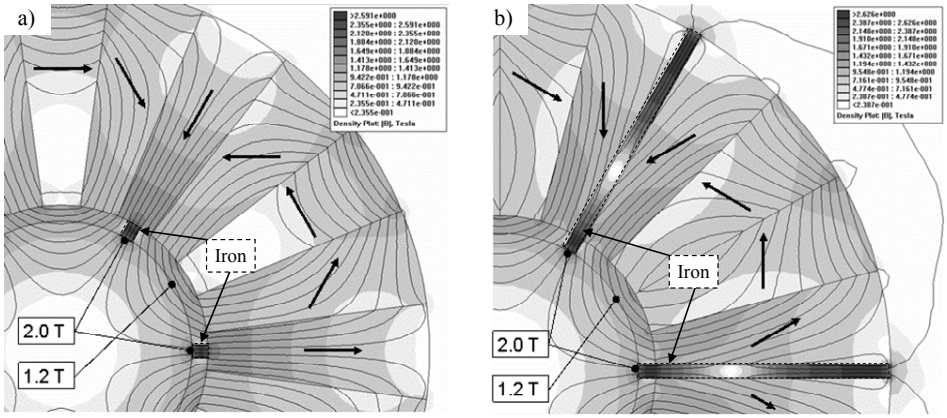

Figure 5.1. An idea of how the MMPS could be implemented in (a) Halbach and (b) Offset-Halbach hexapoles.

The physics basis of the JYFL-MMPS comes from the normal component of the magnetic field ($B_{\perp}$), which is continuous over the boundary between two media. For example, in figure 5.1 a magnetic field of 2 T is induced inside the so-called “iron pole”. The pole goes through the plasma chamber wall and the same magnetic field strength, which is induced inside the pole material, is reached at the inner surface of the plasma chamber wall.

A high permeability material can have a strong magnetic field inside with a relatively low external magnetic field. Comparison between some commercially available high permeability materials (values extracted from the FEMM material database) is shown in figure 5.2. The material called “Mu Metal” has a very high permeability (only 10 A/m can give 0.5 T) but its saturation magnetic field value is relatively low (about 0.71 T). This is the highest field which can be achieved inside the plasma chamber (see figure 5.9). The highest saturation magnetic field values are almost 2.5 T; for example “Vanadium Permedur” can give a field of over 2 T with an external field of only 1000 A/m. However, simulations have shown that the (external) magnetic field at the magnetic pole of a hexapole is very high and good results can be reached by using standard low carbon steels (for example AISI 1010 steel). The price of such steel is low compared to that of special high permeability materials.

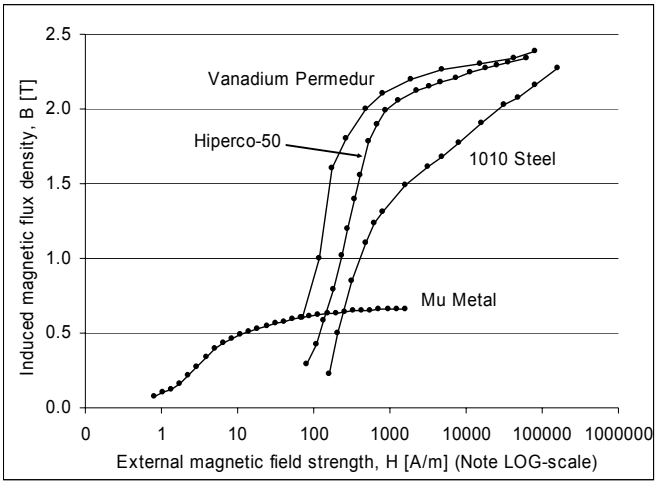

Figure 5.2. Induced magnetic field in some high permeability materials.

In an ECRIS the iron pieces between the permanent magnets are exposed to a relatively high solenoid field (mainly B_z but also B_r). The high field causes non-linear effects, such as the saturation of the iron, which cannot be seen from 2D-simulations. Consequently, 2D-simulations can only be used to get an idea of the highest limit for the radial magnetic field strength. Three dimensional (3D) simulation codes have to be used to obtain more accurate magnetic field values. The permanent magnet load must also be taken into account. In a strong hexapole structure the permanent magnets are exposed to each others magnetic field, which can cause a very high opposite magnetic field. In addition, the load is increased by the radial component of the solenoid magnetic field. If the design is not made carefully this can lead to partial demagnetization of the hexapole. These phenomena can be studied with the magnetic field simulation codes.

In a pure hexapole the radial magnetic field strength (B_r) increases with r^2 from symmetry axis towards the plasma chamber wall (R_{pc}). Figure 5.3 shows an example where the 0.23 T resonance radius (for 6.4 GHz) decreases from 47 mm to 35 mm if the hexapole strength is increased from 0.5 T to 0.9 T. Consequently, in studies performed with superconducting hexapoles the plasma size and shape was changed. The case is different with the MMPS where the magnetic field increases much more steeply in the vicinity of the iron (close to r^{20}). Therefore the magnetic field boost of the MMPS does not affect the plasma volume or shape.

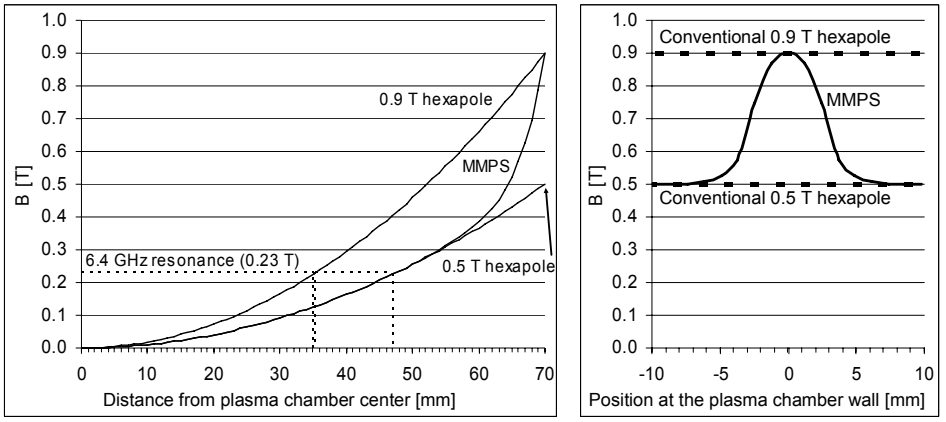

Figure 5.3. Comparison between normal hexapoles and a MMPS-hexapole.

The effect of the iron pole in the azimuthal direction (at the plasma chamber wall) is also local, only a few millimeters wide depending on the shape and the size of the iron pole (a value of 0 mm corresponds to the magnetic pole). Because the collision frequency of warm and hot electrons (T_e > 50 eV) is rather low (compared to ions) they are magnetically confined [Gol95, Tar05]. Consequently, it can be assumed that they follow the magnetic field lines to the magnetic poles of the hexapole. The work described in reference [Tar04b] shows that the ion flux is concentrated in the center of the plasma flux at the plasma chamber wall. This observation supports the afore-mentioned assumption because ions tend to follow electrons in the quasi-neutral plasma flux. Consequently, even a narrow magnetic field peak at the magnetic pole could reflect a remarkable proportion of the electrons back to the plasma.

For this work a hexapole was constructed, but nothing limits the use of the MMPS technique in other order multipoles (quadrupole, octupole or some higher order multipole).

The MMPS idea can be possibly applied in the following cases:

I. An existing multipole is upgraded. In some cases it is relatively easy and cost effective to just add the iron parts needed into the existing structure.
II. A completely new multipole is being built in order to reach the maximum performance; for example in an 18 - 28 GHz ECRIS. In this case it would be necessary to build a Halbach-type hexapole as strong as is possible, i.e. about 1.3 – 1.5 T. With the MMPS the radial magnetic field can be then locally boosted to over 2 T.
III. A very cost effective multipole is needed. For an ECRIS a hexapole with radial mirror ratio (R_r) of about 1.2 to 1.5 could be built and apply the MMPS to increase the radial mirror ratio to over 2.

5.2. MMPS-plasma chamber for the JYFL 6.4 GHz ECRIS

The MMPS plasma chamber prototype was required to include as many variable parameters as possible. Some constraints were listed for the design:

- Aluminum inner surface of the plasma chamber for good secondary electron emission
- Movable iron poles for the adjustable MMPS boost
- Robust construction (minimizing all the risks)
- Possibility to adjust the homogenous hexapole field, i.e. to move the permanent magnets in the radial direction
- Sufficient cooling for 1 kW microwave power
- Possibility to machine all parts in our own workshop (to reduce costs).

In addition the new chamber had to have the same inner diameter (140 mm) as the old plasma chamber, and had to fit into the existing solenoid structure, limiting the outer diameter to 286 mm. The main structure should consist of two parts; the outer part holds the magnets and the inner part is a separate vacuum vessel. The permanent magnet cross-section was required to be rectangular as it makes it possible to have identical magnet blocks, reducing the costs. A 4 mm wide space was reserved for the iron poles between the magnets. As a result of these boundary conditions the magnet blocks had to be placed as shown in figure 5.4. The maximum cross-section for one permanent magnet block was limited to 34 mm x 34 mm. A robust stainless steel cylinder was chosen for the main supporting structure in order to withstand all the forces between the permanent magnets.

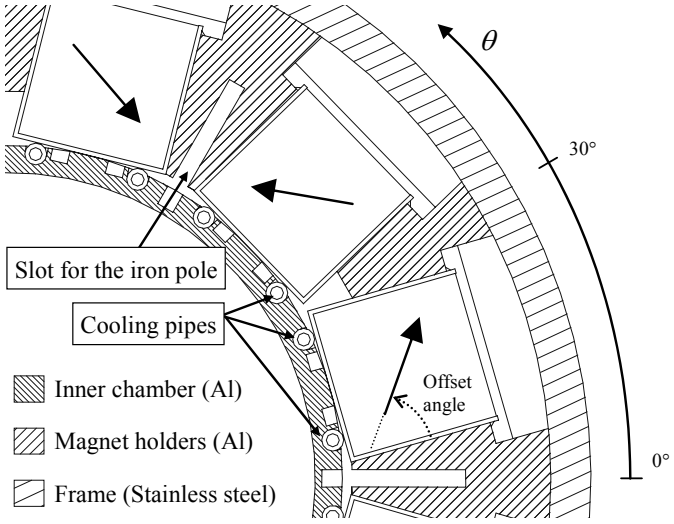

Figure 5.4. A sketch of the new MMPS plasma chamber.

Two-dimensional (2D) simulations were mainly carried out using the Finite Element Method Magnetics software (FEMM), and three-dimensional (3D)

simulations were performed with the RADIA-code. Because the solving time in RADIA increases strongly with the number of objects, a compromise between the accuracy and the number of the objects had to be made. The effects of this compromise are evident in figure 5.14 where the magnetic field is plotted very close to iron. The results are perhaps not as smooth as possible; however, the quality of the pictures is good enough to see the general effect.

Initially, the JYFL 6.4 GHz ECRIS was modeled with the RADIA-code (3D). In order to exclude possible errors in the modeling with a rather complex 3D code every comparable case was solved using both FEMM (2D) and RADIA (for example the magnetic field at the center axis). The results were found to be identical and some of them were also verified with Poisson Superfish (Pandira). The simulations were found to be consistent with the measured field values. The permanent magnet implementation in FEMM and RADIA was carefully studied by P. Frondelius in his master's thesis [Fro05]. In addition, grade N48 permanent magnets were studied in extreme conditions; from liquid nitrogen (LN_2) temperature -196°C up to +50°C. The measured magnetic field and remanence values were consistent with RADIA results.

With a correct permanent magnet material (demagnetization curve) parameterization, RADIA gives very accurate results even in extreme conditions. It was found that in under a high load (as in a Halbach-type hexapole) FEMM can give too optimistic values. This is because the demagnetization curve in FEMM is given with magnetic field flux density (B) instead of magnetization (M), as in many other codes. Strong NdFeB-type permanent magnets can tolerate extremely high external fields when the total B at given point can be negative ($B = \mu_0(H + M)$ = negative external magnetic field + permanent magnet magnetization). However, FEMM cannot calculate negative B values making it possible that the critical "knee-point" (see chapter 3.6.5) is not taken into account.

All dimensions in figures and tables are given in cylindrical coordinates as well as the magnetic field components, i.e. $B_{tot} = \sqrt{B_r^2 + B_t^2 + B_z^2}$. In this notation r, t and z correspond to the radial, azimuthal and axial components of the magnetic field, respectively. The value of z = 0 mm corresponds to the z-value where the solenoid field has only a B_z-component (B_{min}). Consequently, the injection and extraction z-coordinates for the JYFL 6.4 GHz ECRIS are z_{inj} = 250 mm and z_{ext} = -200 mm, respectively. The plasma chamber inner radius is R_{pc} = 70 mm. The notation shown in figure 5.4 is used for the azimuthal coordinates ($\theta = 0^\circ$ at the magnetic pole).

5.2.1. Simulations without iron poles

The next step was to choose a permanent magnet material with sufficient remanence and coercivity for the simulations. It was approximated that the material should have at least 1000 kA/m coercivity (corresponding to ~1.26 T opposite magnetic field). A suitable material would be grade N48 for which

remanence and (H_{cJ}) coercivity values at 20°C are 1.417 T and 1175 kA/m, respectively. The material demagnetization curves at 20°C, 60°C and 80°C are shown in figure 3.21.

Initial simulations were made without iron poles, i.e. according to the sketch shown in figure 5.4. This was done in order to ensure the performance of the ECRIS in the event that the MMPS concept fails. Consequently, the magnetic field profile was required to be as homogenous as possible (i.e. as in a typical hexapole) without the iron poles. Therefore, the offset angle shown in figure 5.4 had to be optimized. Figure 5.5 shows the effect of the offset angle on different components of the hexapole field. The best homogeneity (smallest standard deviation of the total magnetic field at the plasma chamber wall) and highest average field is achieved with an offset angle of 54°. Consequently, permanent magnets with this magnetization angle were chosen. The magnetic field components at the plasma chamber wall (R_{pc} = 70 mm), with a 54° offset-angle but without the MMPS is shown in figure 5.10(a).

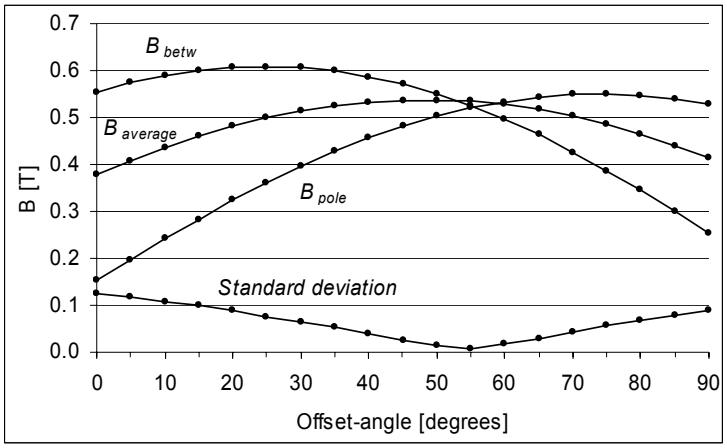

Figure 5.5. Different components of a hexapole field as a function of an offset angle (see figure 5.4). Simulated with FEMM (2D, no solenoid field).

Canning of the permanent magnets and the aluminum holders between them makes it possible to move the permanent magnets 8 mm in the radial direction, i.e. it is possible to change the strength of the homogenous hexapole field (corresponding to radial mirror ratio (R_r) values between 2.3 and 1.7). Consequently, the magnetic field scaling law for the radial field is met at the closest magnet position but not in the furthermost position. The possibility to adjust the magnetic field strength is unique of all ECRIS permanent magnet hexapoles. Figure 5.6 is a 2D FEMM simulation showing how the hexapole field changes with the magnet position (see figure 5.4 where the magnets are at the innermost position).

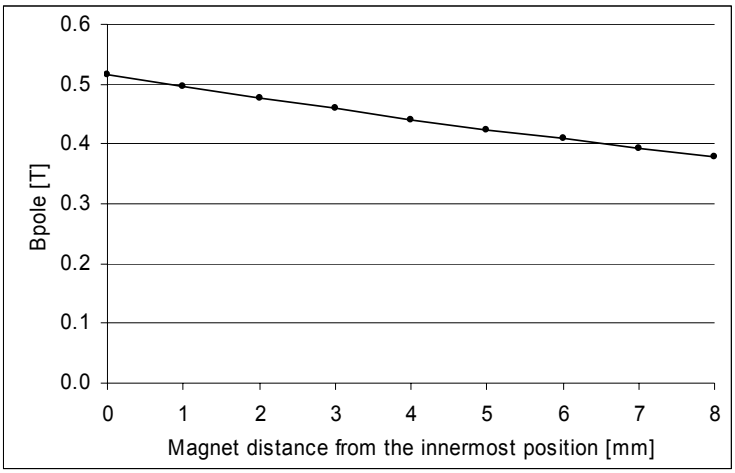

Figure 5.6. Magnetic field at the magnetic pole as a function of permanent magnet block radial position. Simulated with FEMM (2D, no solenoid field).

5.2.2. Optimization of the iron poles

The next step was to include the iron poles in the simulation. Preliminary simulations were carried out in 2D using the FEMM simulation code. Because the maximum available space for the iron poles is 4 mm, the simulations for optimum iron dimensions were done from 1 mm to 4 mm wide iron poles as a function of their length. Figure 5.7 shows the effect of the length and width of the iron pole on the magnetic field at the plasma chamber wall (B_{pole}). According to the results iron poles with a cross-section of 4 mm x 20 mm were chosen for the construction.

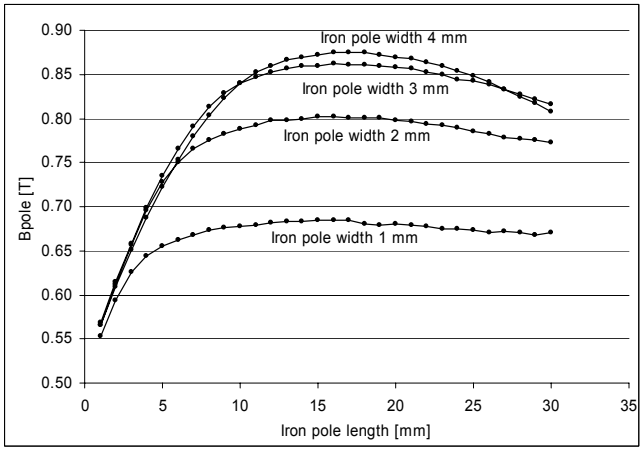

Figure 5.7. The effect of the length and width of the iron pole on the magnetic field at the pole (B_{pole}). Simulated with FEMM (2D, no solenoid field).

Figure 5.8 shows the effect of the iron pole on the magnetic field lines. Part (a) is a 2D plot without the iron poles and part (b) is a corresponding simulation with 4 mm x 20 mm iron poles included. The figure shows that the effect of the iron pole is very local, only some millimeters in length and width. The simulation also shows how the iron concentrates the magnetic field lines at the poles. As the magnetic field lines are guided inside the iron there is a low magnetic field on both sides of the iron pole. For example, in figure 5.8(b) the magnetic field is only 0.1 T, while at the plasma chamber wall it is 0.9 T. Consequently, adding some iron pieces at the inner surface of the plasma chamber can cause a resonance field on both sides of the iron pieces. Possible problems related to this are presented in chapter 7.

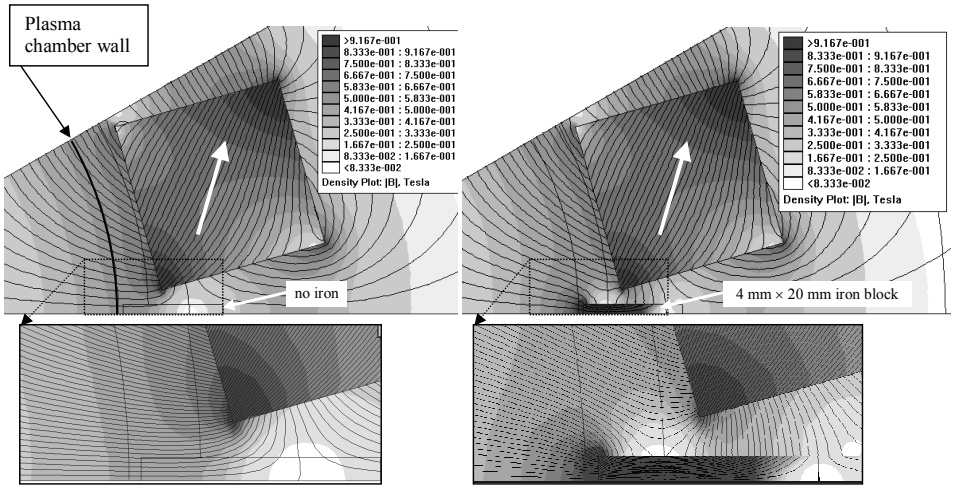

(a) Without iron poles (b) With iron poles

Figure 5.8. Magnetic field simulated with FEMM (2D, no solenoid field). Part (a) shows the typical structure, part (b) shows the MMPS.

Figure 5.9 shows the magnetic field profile at the plasma chamber wall in the azimuthal direction (in mm instead of degrees) with different iron pole materials, a value of 0 mm corresponds to the magnetic pole. The gain of using expensive high permeability material instead of standard low carbon steel is marginal. Consequently, standard AISI 1010 steel was chosen for the iron pole material.

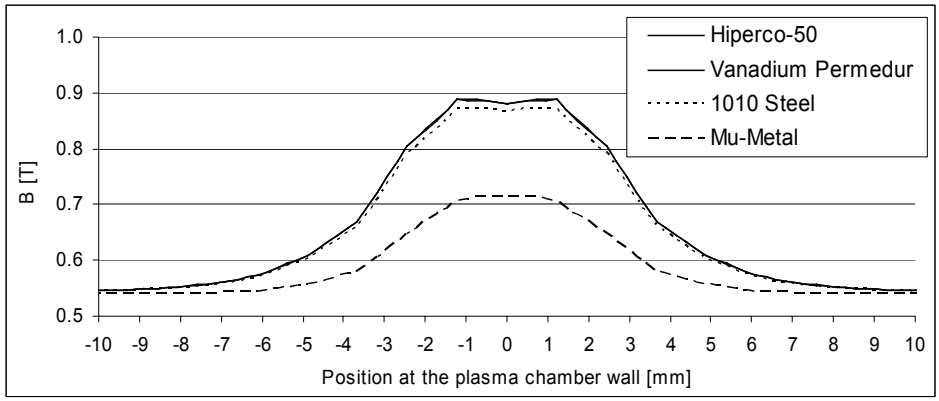

Figure 5.9. The effect of different high permeability materials on the magnetic field at the plasma chamber wall in the azimuthal direction. Simulated with FEMM (2D, no solenoid field).

Figure 5.10(a) shows the magnetic field components at the plasma chamber wall (R_{pc} = 70 mm) without the MMPS. The simulation was made with the 3D RADIA code and it includes constant B_z = 0.2 T, which is achieved with typical solenoid values; 200A / 250A / 230A / 230A (maximum values are 200A / 250A / 250A / 250A). Figure 5.10(b) shows the effect of the MMPS. Note that the MMPS also affects the azimuthal (tangential) component of the magnetic field B_t. However, the effect is not remarkable.

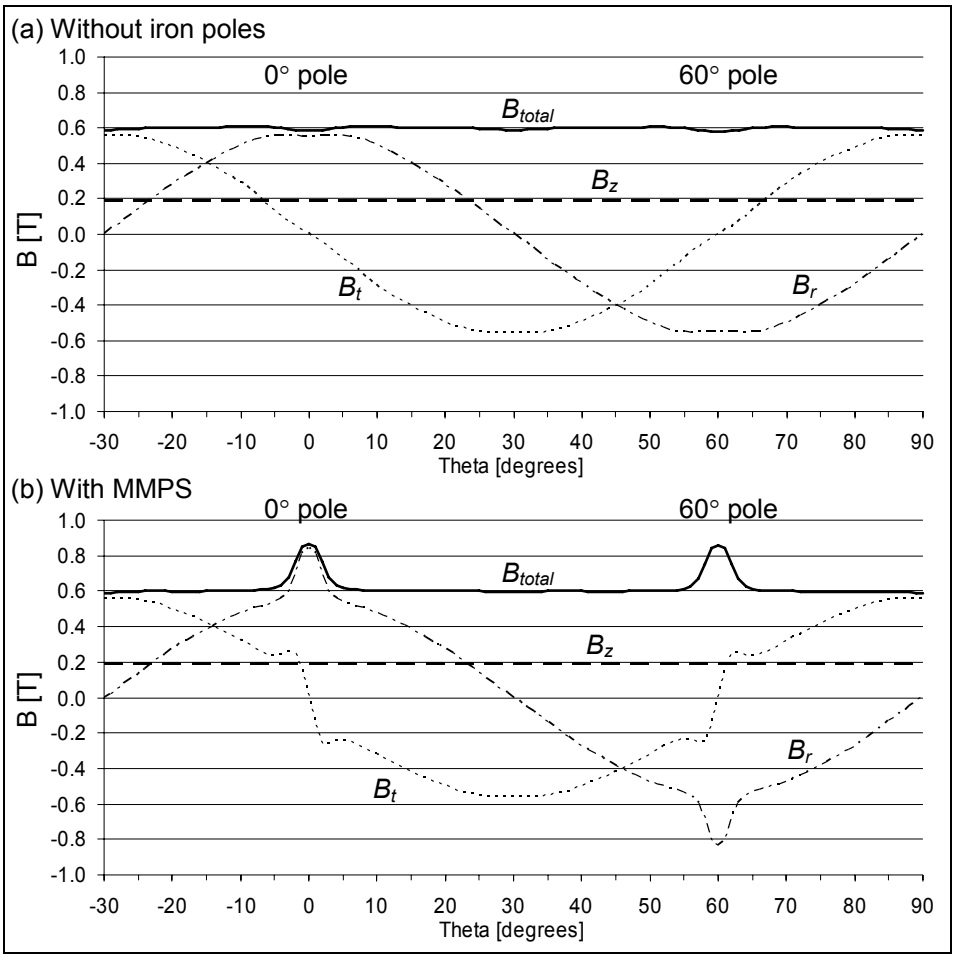

Figure 5.10. Magnetic field at the plasma chamber wall (a) without iron poles (z = 0 mm) and (b) with the MMPS. Simulated with RADIA (3D, with typical solenoid field settings).

Figure 5.11 shows the total magnetic field as a function of radius. The 6.4 GHz electron cyclotron resonance is at a radius of about 27 mm, while the effect of the iron poles starts at a radius of about 55 mm. Therefore the size and the shape of the plasma are not changed by the MMPS.

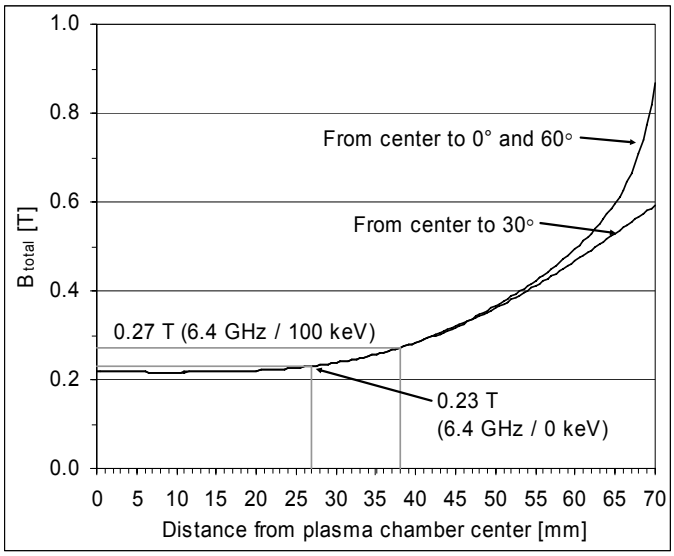

Figure 5.11. Effect of the iron pole on the magnetic field profile (z = 0 mm, θ = 0°) simulated with RADIA (3D, with typical solenoid field settings).

In the new plasma chamber design the radial position of the iron poles can be adjusted so that the distance between the iron and the plasma chamber inner surface is between 1.5 and 13 mm. The thickness of the wall at this location is only 1.5 mm (see figure 5.4). Figure 5.12 shows the influence of the position of the iron block on the magnetic field at the magnetic pole (at the plasma chamber wall). When the distance is about 6.5 mm (5 mm from the innermost position) the magnetic field at the plasma chamber wall is homogenous, i.e. $B_{pole} = B_{betw}$ (= 0.6 T with typical solenoid settings).

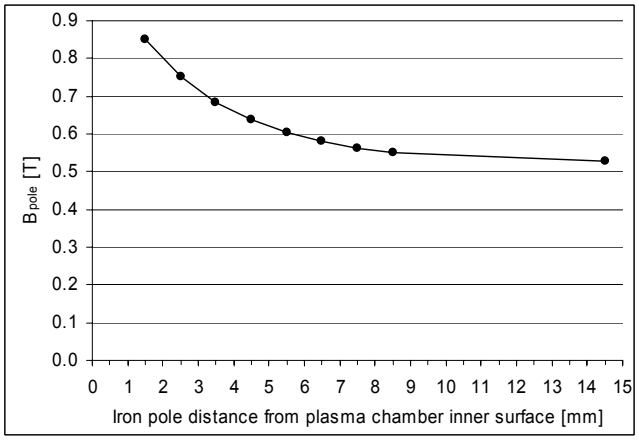

Figure 5.12. Effect of the iron pole position on the magnetic field (r = 70 mm, z = 0 mm, θ = 0°) simulated with RADIA (3D, with typical solenoid field settings).

The effect of the iron pole position on the radial and total magnetic field shape at the plasma chamber wall is plotted in figure 5.13. The full-width at half maximum (FWHM) is only about 5 mm.

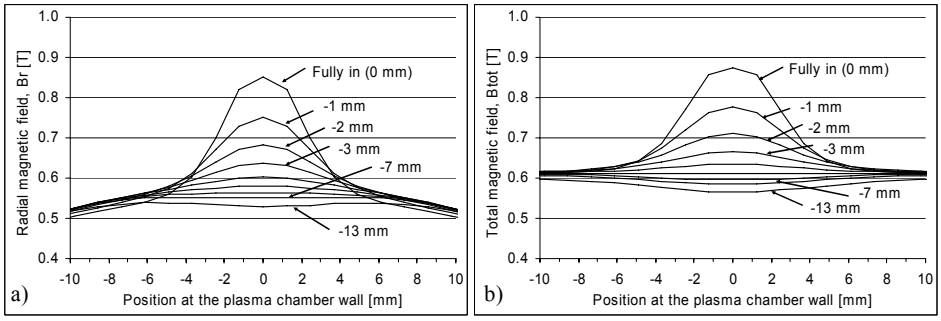

Figure 5.13. The effect of iron pole position on (a) radial and (b) total magnetic field shape at the plasma chamber wall, at the pole (r = 70 mm, z = 0 mm). Simulated with RADIA (3D, with typical solenoid field settings).

The effect of a high solenoid field was studied at the plasma chamber wall in front of the magnetic pole. The effect of the solenoid field strength on B_r and B_{tot} is shown in figure 5.14. Part (a) shows the radial magnetic field profile at the plasma chamber wall when different solenoid field strengths are used. In the JYFL 6.4 GHz ECRIS, the current in the solenoids is usually about 95 % of the maximum. At the 0°, 120° and 240° poles the effect of the solenoid field is most apparent at the injection (z > 0) where the radial component of the solenoid field is strongest and reduces the total B_r magnetic field (multipolar + solenoid B_r component). Providing the iron is not saturated, B_r should increase at the extraction side because the radial component of the solenoid field has an opposite direction compared to the injection side. In fact the B_z component (caused by solenoids) is over 2 T inside the iron pole, the iron is saturated and B_r stays unchanged at the extraction side. Figure 5.14(b) is a comparable simulation showing how the strong solenoid field affects the total magnetic field at the plasma chamber wall. The dashed line shows the case without iron poles. The effect is opposite on the poles at 60°, 180° and 300° (measurements shown in figures 5.23 and 5.24).

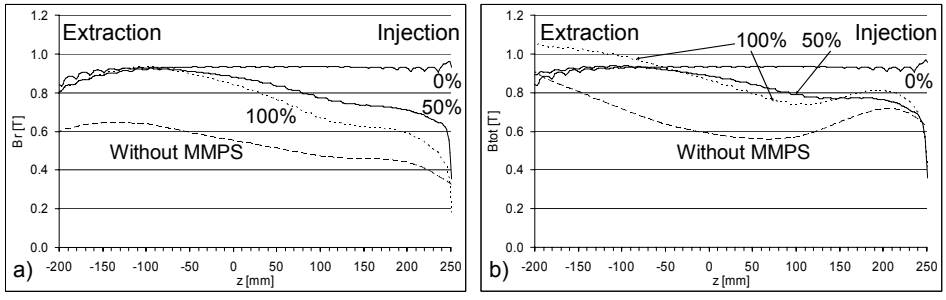

Figure 5.14. Effect of the solenoid field (with currents 0 %, 50 % and 100 %) on (a) the radial and (b) the total magnetic field at the plasma chamber wall at the front of the magnetic pole (r = 70 mm, θ = 0°). Simulated in 3D with RADIA.

The general effect of the iron poles can be seen from figure 5.15 where the total magnetic field B_{tot} and the radial magnetic field B_r are plotted with and without the iron poles at the plasma chamber wall (at the magnetic pole) as a function of the z-coordinate. The axial component B_z is also plotted and is the same in both cases.

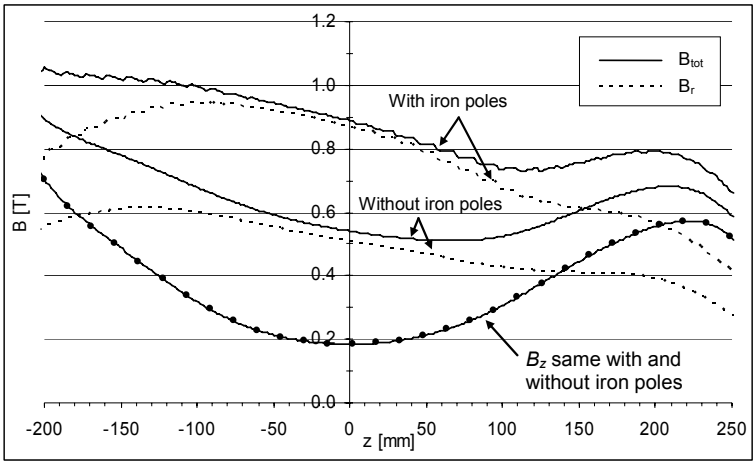

Figure 5.15. Effect of the iron pole on the different magnetic field components at the plasma chamber wall in front of the magnetic pole (r = 70 mm, θ = 0°). Simulated with RADIA (3D, with typical solenoid field settings).

The simulation shows that the shape of the magnetic field is maintained and the positive effect of the iron poles is very clear along the plasma chamber wall. The average increase of the radial magnetic field B_r is 56 %. Results presented in reference [Suo04b] show that the impact spots of the plasma flux are clearest at the height where the value of B_{tot} is a minimum (in figure 5.15: z = 70 mm without iron poles and z = 120 mm with iron poles). This indicates that the strength of the total magnetic field minimum at the plasma chamber wall is an important parameter in ECRIS design. Using the MMPS technique the minimum B_{tot} at the plasma chamber wall increases 43 % (from 0.51 T to 0.73 T) and the radial mirror ratio (B_{rad} / B_{ecr}) increases 73 % (from 2.2 to 3.8) at z = 0 mm.

5.2.3. Permanent magnet load and temperature effects

As was mentioned earlier, the temperature dependence of the permanent magnet properties is an important factor, which has to be taken into account in hexapole design. The load distribution in the permanent magnet material was studied with 3D simulations. It is especially important to define the most critical locations and the maximum safe operating temperature of the new hexapole. Simulations had to be done in 3D due to the presence of the solenoid field. For this, the temperature dependence of N48 grade magnets was parameterized for RADIA. Figure 5.16 shows the decrease of the permanent magnet

magnetization at different locations indicating the highest load. The most critical points in this design are at the corners of the permanent magnet block, due to the fact that the field lines tend to follow the shortest closed loop. The value of "demagnetized area" indicates the percentage of the area where permanent magnet magnetization has decreased below the "knee-point" (about 1.2 T in figure 3.21).

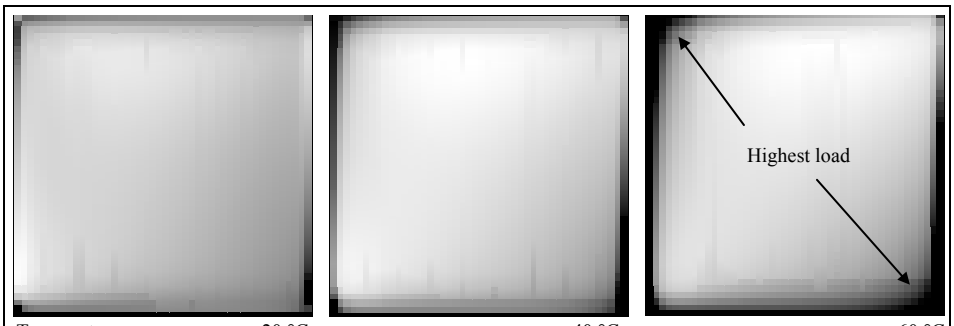

Temperature	20 °C	40 °C	60 °C
Magnetization (max)	1.401 T	1.375 T	1.346 T
(min)	1.283 T	0.857 T	0.408 T
Demagnetized area	0 %	1.3 %	4.3 %

Figure 5.16. The decrease of the permanent magnet magnetization at temperatures of 20°C, 40°C and 60°C. Simulated with Radia (3D, with typical solenoid field settings).

In the ECRIS hexapole the demagnetized area changes from injection to extraction (as a function of the z-coordinate). The percentage of irreversibly demagnetized area (where magnetization is below 1.2 T) is presented in figure 5.17. The most interesting (and critical) z values are ±130 mm. The right-hand part of figure 5.17 shows the percentage of the demagnetized area at these z-values and also at z = 0 as a function of temperature.

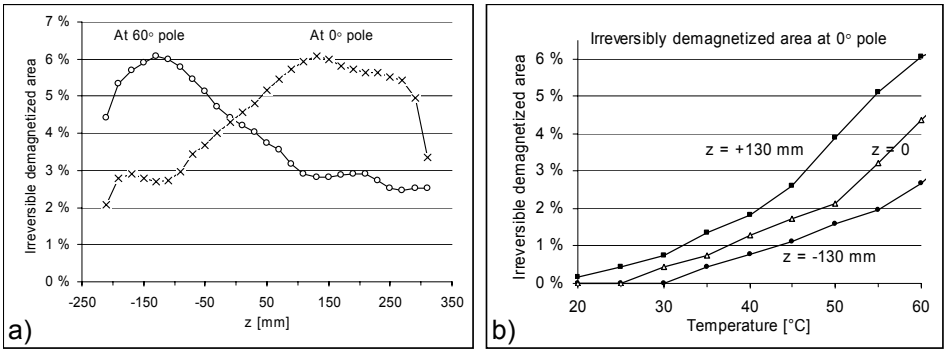

Figure 5.17. The effect of temperature on the demagnetized area in the hexapole; (a) at a constant temperature of 60°C and (b) at critical z-values for the 0° pole as a function of temperature. Simulated with Radia (3D, with typical solenoid field settings).

The simulation indicates that the demagnetization begins at room temperature. However, it occurs in such a small volume that the effect on the magnetic field is not remarkable. This was studied by FEMM simulations where demagnetized areas at the corners (see figure 5.16) were omitted. The magnetic field inside

the plasma chamber was almost identical with and without the demagnetized parts. Consequently, the partial demagnetization here is negligible. Figure 5.18 shows how the increased temperature affects the hexapolar magnetic field. The value of B_{pole} decreases from 0.55 T to 0.51 T, i.e. about 7%, when temperature increases from 20°C to 60°C. The decrease is mainly due to the decreased permanent magnet remanence - not the demagnetization. Figure 5.18 also shows the measured value of 0.52 T, which was measured at a radius of about 68.5 mm (R_{pc} = 70 mm, the active area of the probe is about 1.5 mm from the probe surface). The measured value agrees well with the simulations. Demagnetization simulations were performed with and without iron poles and the results were found to be almost identical. The small difference shows that the permanent magnet load decreases when the magnetic flux goes through the iron poles.

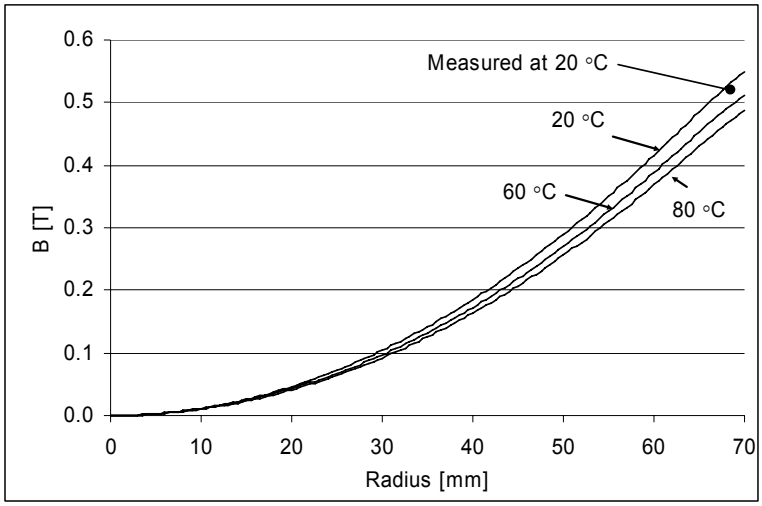

Figure 5.18. The hexapolar magnetic field at different temperatures. Simulated with FEMM (2D, no solenoid field).

5.2.4. Final MMPS plasma chamber design and construction

It was confirmed by the simulations that the material used is suitable and safe to use in the conditions of the JYFL 6.4 GHz ECRIS. Consequently, grade N48 magnets were ordered. The final construction of the new MMPS plasma chamber, based on the simulation studies, is shown in figure 5.19 (see 5.4 for a close-up). Figure 5.19(b) shows the magnet array without the inner plasma chamber. There are 7 identical permanent magnets in the z-direction because the manufacturer had a limit of 80 mm for the maximum dimension of one permanent magnet block. To make assembly easier (and safer) the permanent magnets were glued into stainless steel cans. These cans are located between aluminum holders, which also prevent the magnets from sliding towards a smaller radius. At the magnetic poles these aluminum holders have a slot for the iron poles.

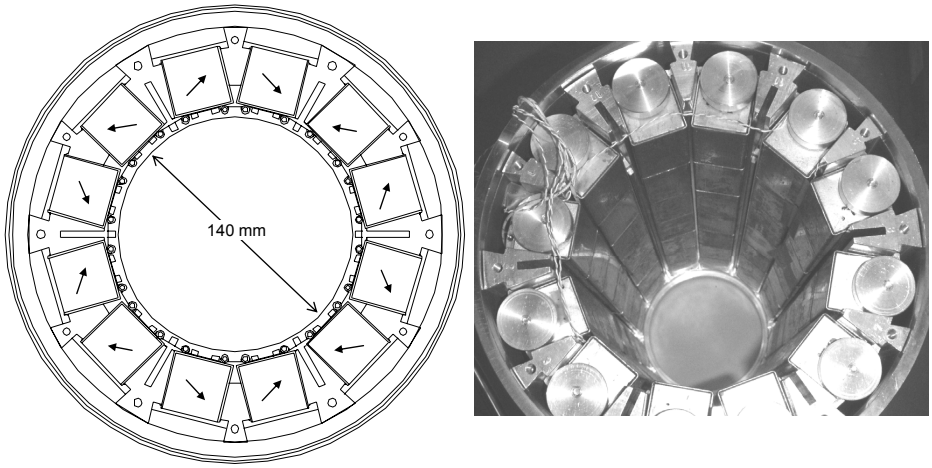

Figure 5.19. (a) final design and (b) picture of the new MMPS plasma chamber.

Figure 5.20(a) shows the inner part of the new construction. It is made of aluminum pipe, which has a 140 mm bore as in the original plasma chamber (made of copper). The wall thickness is mainly 6 mm but at the location of the iron poles it is only 1.5 mm. Due to the plasma flux, almost the whole heat load is concentrated at the magnetic poles. Cooling is arranged with twelve cooling pipes, which are embedded in the inner part of the chamber. However, to decrease the number of connectors two consecutive cooling circuits were connected in series. According to 2D heat transfer simulations performed with FEMLAB [FEML], the cooling pipe close to the iron pole is so efficient that the temperature of the outer surface of the inner part rises only a few degrees. The temperature is monitored with five K-type thermo-elements added at different locations inside the hexapole. According to the simulations, there should not be a need for separate cooling of the magnet array. However, simulations showed that if the iron pole is in contact with inner chamber, heat conduction through the iron pole could heat up the magnet holders and damage the magnets. In experiments performed later it was found that the maximum temperature inside the structure is about 30°C. In fact the temperature rise is highest at the outside of the plasma chamber. This is because of the heat flux coming from the axial field producing solenoids. Figure 5.20(b) shows the complete structure ready to be installed into the JYFL 6.4 GHz ECRIS.

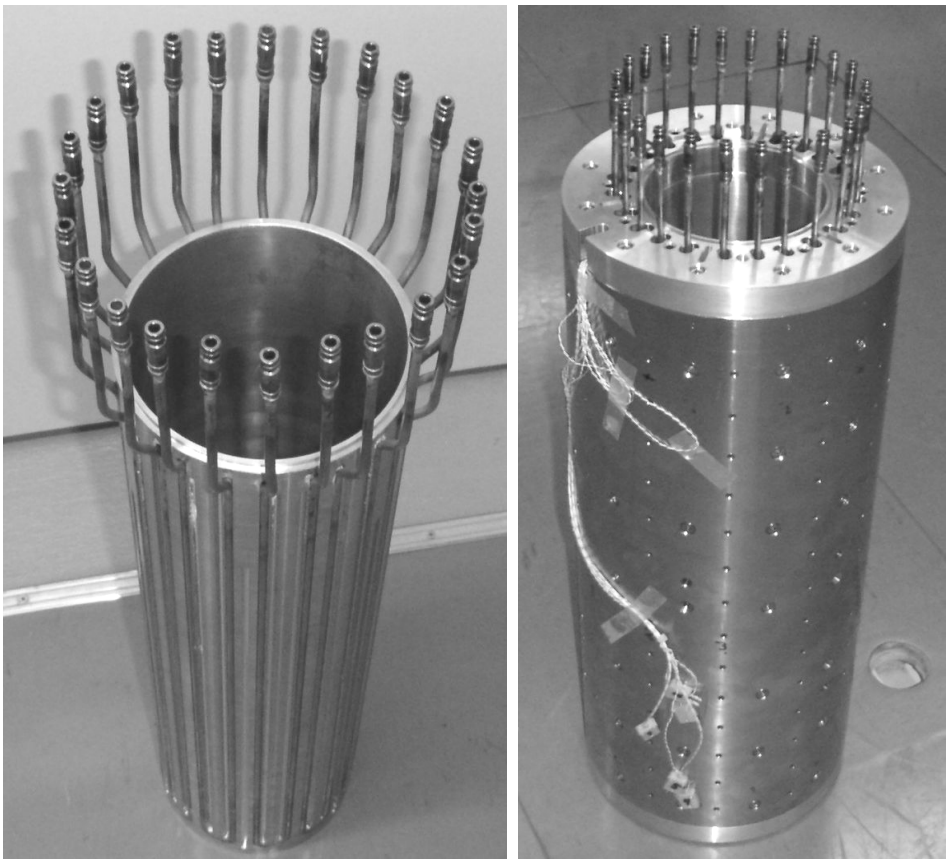

Figure 5.20. (a) Inner part of the plasma chamber and (b) the new MMPS plasma chamber assembly completed.

Figure 5.21(a) shows the iron pole adjustment mechanism. The iron poles are connected to screws making it possible to adjust their location outside the source. One screw turn (360°) corresponds to 1 mm movement. Each pole has two screws, which have to be adjusted simultaneously to avoid tilting of the iron pole. The “calibrated” zero-position is obtained by moving the iron poles to the innermost position (as close to the plasma chamber wall as possible). Figure 5.21(b) shows the iron pole at the innermost position.

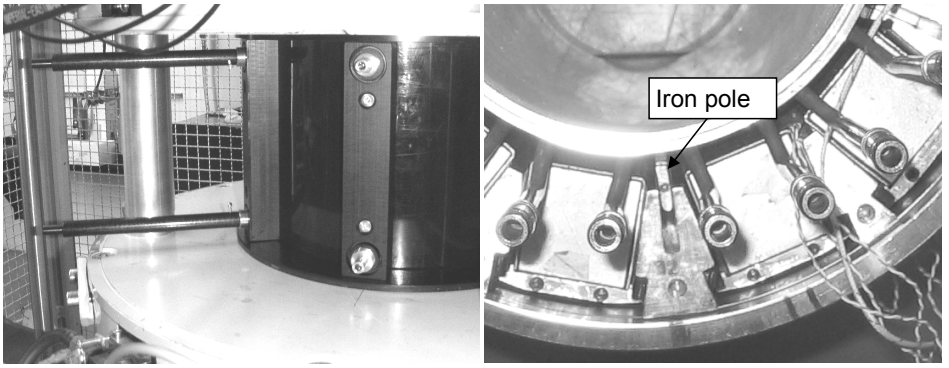

Figure 5.21. Pictures showing (a) iron pole adjustment mechanism and (b) iron pole at the innermost position.

5.2.5. Magnetic field measurements

In the magnetic field measurements two different setups were used. The more accurate setup had a resolution of 1 μT (Group3 teslameter). However, most of the measurements were performed with a holder where seven Hall-sensors (LakeShore HGT-2100) were attached. A Hall-current of 1 mA was driven through the sensors while the Hall-voltage was measured using a data acquisition card connected to a PC. The resolution of this homemade system is only 1 mT and the absolute error about 5 %. However, the system of seven sensors is a fast tool for mapping the whole magnetic field inside the plasma chamber.

Measurements were begun before the new MMPS plasma chamber was installed into the JYFL 6.4 GHz ECRIS. A summary of the measurements performed with the more accurate Hall-sensor are shown in table 5.1. Due to the size of the magnetic field probe it can be positioned approximately 1.5 mm from the plasma chamber wall. At this radius (68.5 mm) the simulated magnetic field is 0.534 T without the iron poles and 0.774 T with the iron poles (corresponding to the values of 0.551 T and 0.936 T at the plasma chamber wall, R_{pc} = 70 mm). The measured values can be seen to agree well with the simulations.

Table 5.1. Measured hexapole average magnetic field values at the plasma chamber wall.

Pole	Radial magnetic field at r = 68.5 mm	
	Iron poles fully out	Iron poles fully in
0°	0.527 T (simulated 0.534 T)	0.740 T (simulated 0.774 T)
60°	0.533 T	0.735 T
120°	0.532 T	Not measured
180°	0.528 T	Not measured
240°	0.524 T	Not measured
300°	0.536 T	Not measured

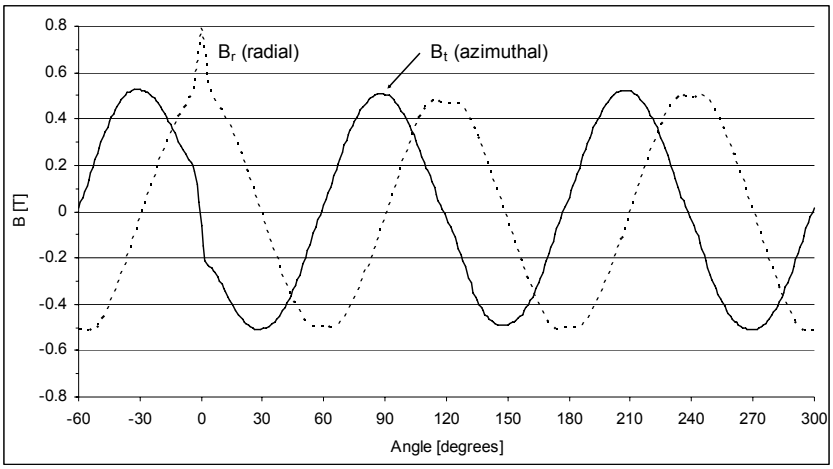

Figure 5.22. Measured radial and azimuthal magnetic field at the plasma chamber wall when solenoids are not powered. The iron pole is fully in at the angle of 0°.

Figure 5.22 shows the measured radial and azimuthal magnetic field around the plasma chamber. In this measurement the sensor array was rotated by a step of one degree at approximately z = 0 mm (to avoid distortions from hexapole end effects).

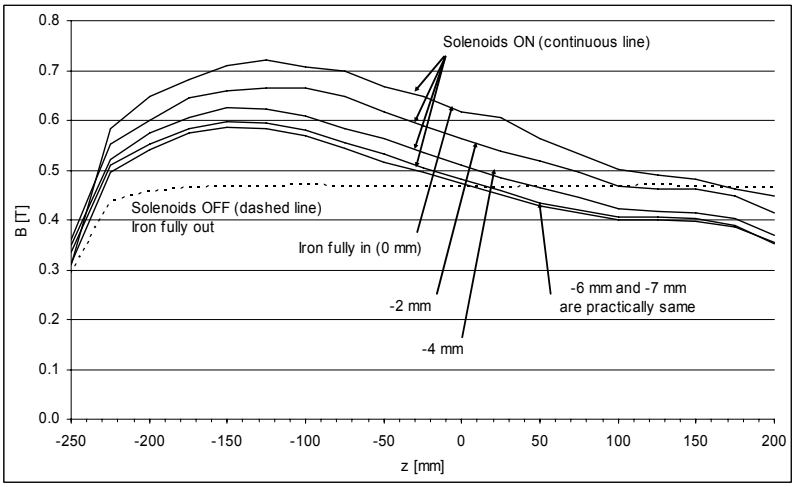

Figure 5.23. Measured radial magnetic field at the plasma chamber wall (0° pole) with and without solenoids and different iron pole positions.

Figure 5.23 shows the radial magnetic field at the plasma chamber wall (0° pole). The positioning of the probe was somewhat difficult which led to irregularities in the curve. The step size in this measurement was 25 mm in z-direction. However, the shape corresponds well, for example, to the curves shown in figure 5.15. The measured values are again slightly smaller due to the

finite size of the Hall-probe. Similar measurements carried out at the 60° pole are shown in figure 5.24.

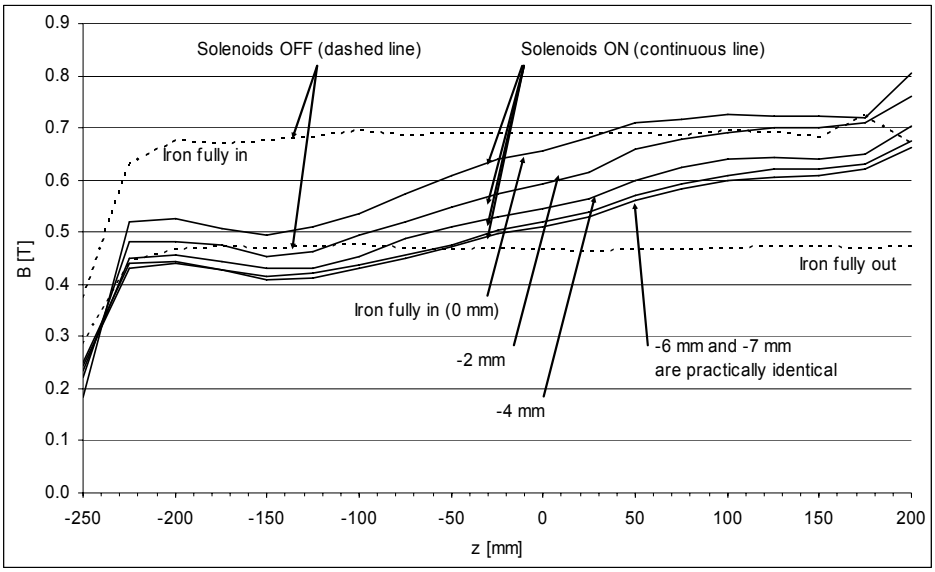

Figure 5.24. Measured radial magnetic field in front of the 60° pole with and without solenoids and different iron pole positions.

Finally, the iron pole effect on B_r was measured with a smaller step size and with different iron pole positions. The results obtained are shown in figure 5.25. Note that the horizontal axis here is in millimeters along the plasma chamber wall. A maximum boost of 0.3 T is achieved when the iron poles are as close to the plasma chamber wall as possible, i.e. “fully in”. The full-width at half maximum of the magnetic field “boost” is only about 6 mm, which agrees well with the simulations shown in figure 5.13. The measured hexapole field agrees well with the 3D simulations performed with RADIA. At the locations where the magnetic field cannot be measured, one can trust the values obtained from simulations.

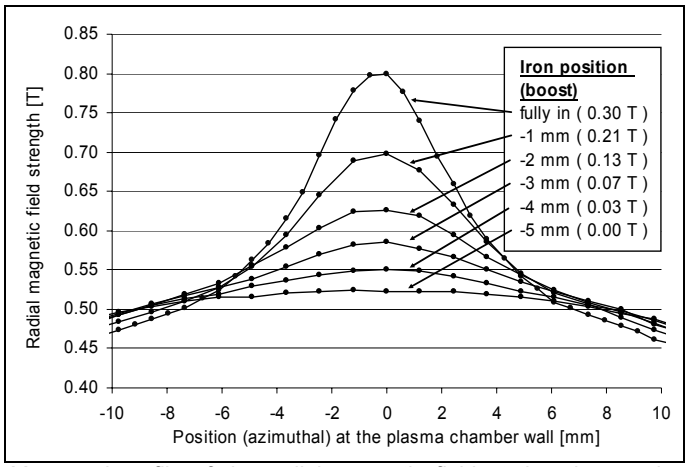

Figure 5.25. Measured profile of the radial magnetic field at the plasma chamber wall for different iron pole positions (z = 0 mm, solenoids are not powered) [Suo06].

6. Experiments with the MMPS plasma chamber

The experiments were initiated by replacing the old conventional plasma chamber with the new MMPS plasma chamber. Their performances were first compared without using the MMPS as in the upgrade the plasma chamber wall material was changed from copper to aluminum and the homogenous hexapole strength at the plasma chamber wall increased from 0.37 T to 0.53 T. Consequently, the radial mirror ratio increased from 1.6 to 2.3, which now meets the scaling law for the radial magnetic field. The performance was increased significantly; for highly charged argon ions the intensity at least doubled (for example Ar^{12+}: 3.4 μA → 15 μA). However, most of the measurements were performed with more stable settings where the intensities are not close to the records. Close to the optimum settings, the ECRIS plasma is sensitive to all parameters and even a small adjustment can cause a sudden intensity drop. Tuning must be restarted and it may be difficult to reach the previous conditions. The measurements were therefore carried out with the settings such that the intensity remained stable.

Most of the experiments were carried out with argon plasmas where oxygen was used as a mixing gas. A typical JYFL 6.4 GHz ECRIS charge-state distribution (using the MMPS) of an argon-oxygen plasma is shown in figure 6.1. In this example, the charge-state distribution is peaked at Ar^{11+}, but the highest ion currents were measured for oxygen, which was used as a mixing gas. Figure 6.2 shows the distribution of the highest charge-states (mass number / charge-state, m/q-ratios from 2 to 7).

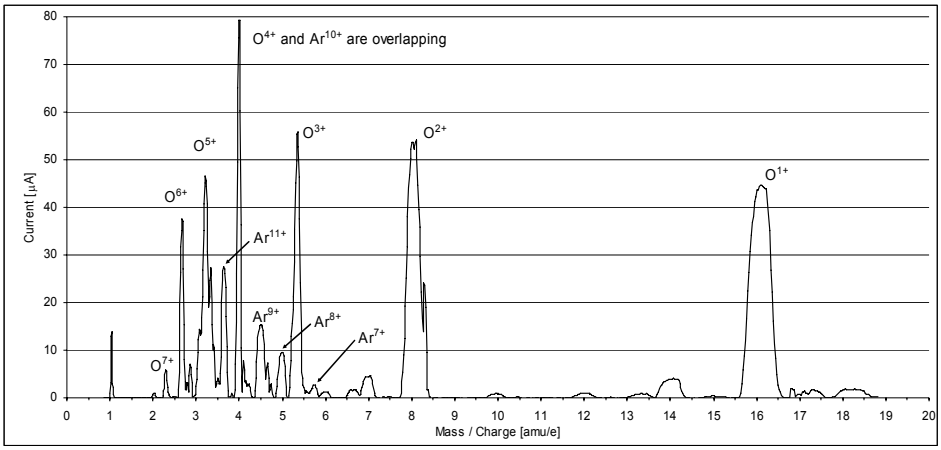

Figure 6.1. Typical charge-state distribution of an argon-oxygen plasma when the JYFL 6.4 GHz ECRIS has been tuned for high charge-states and the MMPS is applied.

The ion beam contains several other species in addition to the injected argon and oxygen. Some carbon contamination and a small amount of nitrogen are often present. There can also be contamination from previous plasmas (for example silicon (Si), sulfur (S) and fluorine (F)). Figure 6.2 gives an idea of the

mass scan resolution, which includes 1000 steps on the m/q-axis. In the spectrum shown, Ar^{13+} and O^{5+} are the most difficult (interesting) peaks to separate and measure, due to the partial overlapping of the peaks. The theoretical mass resolving power ($m/\Delta m$) of the system is about 28.

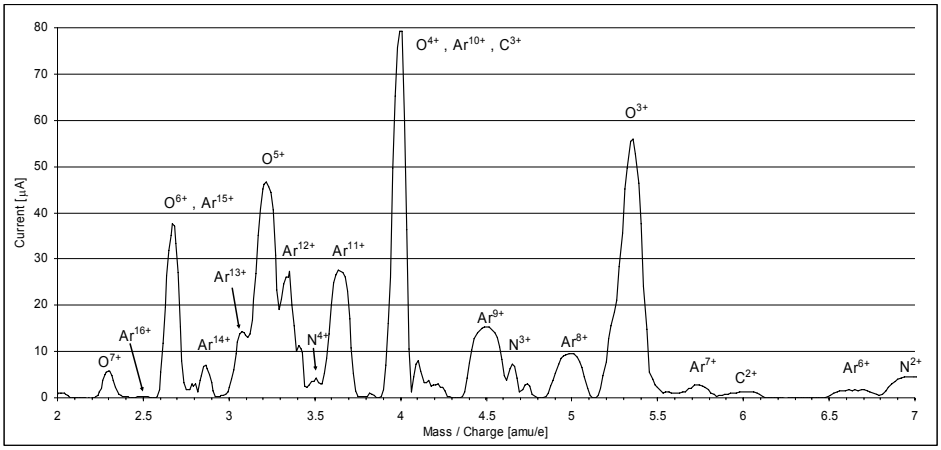

Figure 6.2. A spectrum showing m/q-ratios from 2 to 7.

6.1. MMPS measurements with 6.4 GHz microwaves

At the start of the MMPS measurements the iron poles were moved as close to the plasma chamber wall as possible. This was done in order to calibrate the "zero position". At this point the iron pole distance is 1.5 mm from the plasma chamber inner surface corresponding to a 0.3 T magnetic field boost on the magnetic pole (0.53 T → 0.83 T). During the measurements the iron poles were moved outwards in 1 mm steps. Usually the poles were moved to the position where the MMPS hexapole field is as homogenous as possible (5 mm from the innermost position). However, in some measurements the poles were moved even further (7 mm) where B_{pole} decreases below the most homogenous case (see figure 5.12). All measurements were performed using an acceleration voltage of 10 kV. Some magnetic field and plasma parameters are listed in table 6.1, showing that the JYFL 6.4 GHz ECRIS fully meets all the magnetic field scaling laws (see chapter 3.4).

Table 6.1. Parameters related to the 6.4 GHz experiments.

		Magnetic field, B	Mirror ratio, R
Resonance	B_{ECR}	0.23 T	
Injection	B_{inj}	1.20 T	5.3
Minimum	B_{min}	0.20 T	$0.88 \times B_{ECR}$
Extraction	B_{ext}	0.60 T	2.6
Radial	No MMPS	0.53 T	2.3
	With MMPS	0.83 T	3.6
Resonance zone	Length	59 mm	
	Radius	26 mm	
	Volume (ellipsoid)	0.083 liters	

6.1.1. Improvement of the ion beam intensities

In the initial measurements all possible settings (gas feed, solenoid currents, microwave power) were optimized for each MMPS boost. However, this is time consuming and gives almost the same relative intensity increase as adjusting only the MMPS boost (iron pole position). Consequently, the measurements were performed as follows; first the source was optimized with the iron poles at 0 mm position (full boost) and then the iron poles were moved while all other parameters were kept constant. Measurements were double-checked by tuning the source at the 5 mm position (homogenous case, no boost) and then moving the iron pole to increase the MMPS boost. Figure 6.3 shows the typical effect of the MMPS for different argon charge-states. Measurements were performed with constant gas feed rate, solenoid currents and microwave power, i.e. only MMPS was adjusted in one measurement series. The value of 100 % is normalized to the most homogenous case, i.e. where the iron poles are moved 5 mm from the innermost location (0 mT boost). The ion beam intensities shown in the figure legend correspond to this case.

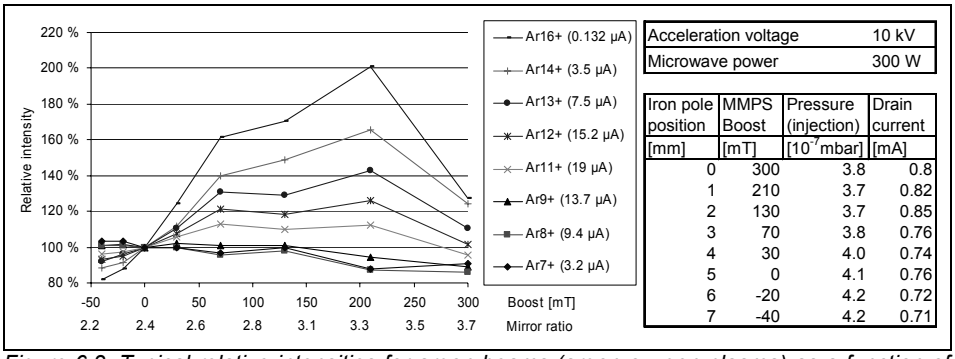

Acceleration voltage	10 kV
Microwave power	300 W

Iron pole position [mm]	MMPS Boost [mT]	Pressure (injection) [10^{-7} mbar]	Drain current [mA]
0	300	3.8	0.8
1	210	3.7	0.82
2	130	3.7	0.85
3	70	3.8	0.76
4	30	4.0	0.74
5	0	4.1	0.76
6	-20	4.2	0.72
7	-40	4.2	0.71

Figure 6.3. Typical relative intensities for argon beams (argon-oxygen plasma) as a function of the MMPS boost [Suo06].

Various argon ion beam charge-states were measured from Ar^{7+} to Ar^{16+} (excluding Ar^{15+}, which overlaps with O^{6+}). The best performance was reached with a high radial mirror ratio (R_r) of about 3.3. At the higher values the intensities usually decrease. A possible explanation is the decrease of the secondary electron emission from the plasma chamber wall. It was found that the positive effect increases with charge-state and for low charge-states the MMPS effect can even be negative. The intensity of the highest charge-states was quite low (Ar^{16+} being 100 – 400 nA). However, for an ECRIS operating with 6.4 GHz this is quite a good result. The Ar^{16+} ion current record for the conventional plasma chamber was of the order of nanoamperes.

Figure 6.4 shows the argon intensities for different MMPS boosts as a function of charge-state. The charge-state distribution (CSD) stays almost constant (slightly improves) while the intensity value changes. The CSD was peaked at Ar^{11+} for every MMPS boost, although the intensities of Ar^{11+} and Ar^{12+} were almost the same for the highest boost (300 mT).

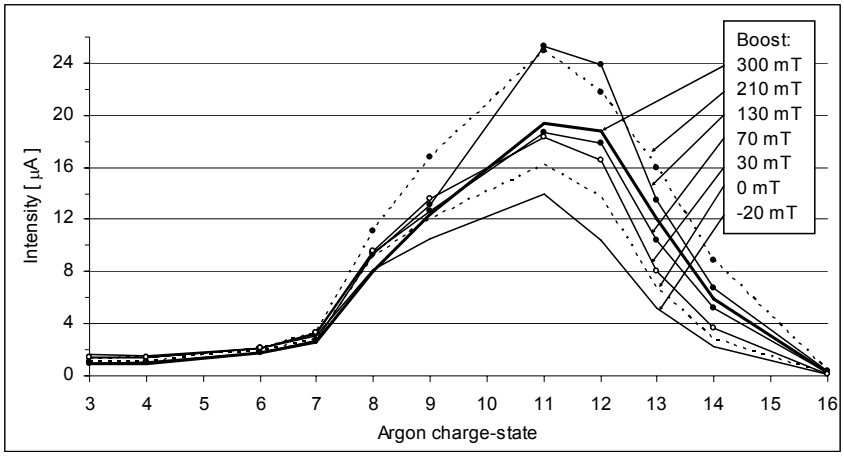

Figure 6.4. Argon charge-state distribution for different MMPS boosts.

It seems that the positive effect of the MMPS increases with charge-state. Consequently, the experiments were continued by measuring even higher charge-states with a krypton-oxygen plasma. The results of these measurements are summarized in figure 6.5.

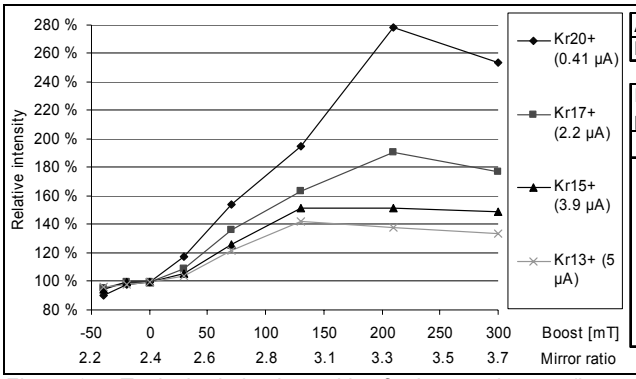

Acceleration voltage	10 kV
Microwave power	350 W

Iron pole position	MMPS Boost	Pressure (injection)	Drain current
[mm]	[mT]	[10^{-7}mbar]	[mA]
0	300	4.2	0.54
1	210	4.2	0.54
2	130	4.1	0.54
3	70	4.2	0.52
4	30	4.4	0.52
5	0	4.4	0.51
6	-20	4.4	0.50
7	-40	4.5	0.50

Figure 6.5. Typical relative intensities for krypton beams (krypton-oxygen plasma) as a function of the MMPS boost [Suo06].

As expected, the most significant improvement was again obtained for the highest charge-states. The optimum MMPS boost was same; around 200 mT (corresponding to a radial mirror ratio of about 3.3).

In the MMPS measurements the highest ion currents were usually obtained with a radial mirror ratio (R_r) of 2.8 – 3.3. The observed behavior is in good agreement with the measurements performed using the SC-ECRIS (6.4 GHz) at MSU, where the optimized radial mirror ratio was measured to be about 2.9 [Ant94]. When applying the MMPS the pressure seems to drop by about 5 - 10 %, i.e. there are fewer neutrals in the plasma chamber. Because the gas feed was kept constant this indicates that the MMPS increases the total ionization efficiency. Also the total ionic current (high voltage power supply current) increases by about 5 - 10 % with the MMPS boost. Calculations, based on the previously shown intensities, showed that the MMPS slightly increases both the average ion charge-state of the plasma and the number of extracted particles.

6.1.2. X-Ray spectrum

An ECRIS produces a large number of X-rays when the electrons collide with the plasma chamber wall. In order to understand more deeply the processes caused by the MMPS the X-ray energy distribution was measured with a high-quality germanium-detector borrowed from the JYFL in-beam spectroscopy group. The setup allowed the measurement of photon energies between 40 keV and 1 MeV (1024 channels). The detector was not collimated and it was located between the poles at about one meter from the ECRIS. At this location the X-ray flux was found to be proper for the detector and data acquisition hardware. In all measurements, the data collection time was 60 seconds (“dead time” being less than 10 %). The X-ray spectrum measurements were performed using a 5.85 – 6.65 GHz traveling wave tube amplifier (TWTA) in collaboration with the Oak Ridge National Laboratory, Tennessee, USA. Due to a tight schedule the measurements were not extensive. However, they clearly showed that the MMPS affects the electron energy distribution in the plasma. An example of the MMPS effect on the X-ray spectrum is shown in figure 6.6,

where it can be seen that when the MMPS boost is applied the ECRIS produces less X-rays in the energy range from 60 keV to 170 keV. This behavior is expected because the MMPS improves the confinement of the high energy electrons (decreasing their contribution to the X-ray spectrum).

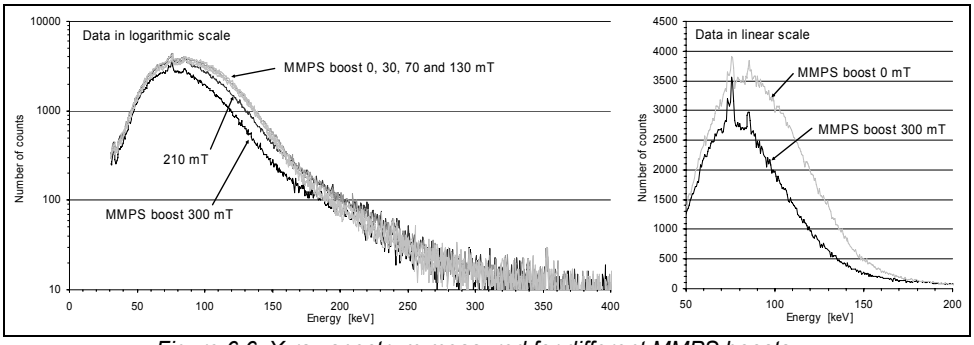

Figure 6.6. X-ray spectrum measured for different MMPS boosts.

However, the main purpose of these X-ray experiments was to study the difference between narrow and broadband plasma heating using the same central frequency of 6.4 GHz. It is proposed that the electron confinement in the plasma improves because of the extended resonance volume. Figure 6.7(a) shows a picture taken from a spectrum analyzer screen when a narrowband oscillator (1.5 MHz) was used with the TWTA. The signal was measured using a biased disk as a microwave probe. A corresponding picture, but here using a 200 MHz bandwidth White-Noise Generator (WNG), is show in figure 6.7(b). Here the spectrum is not perfectly flat-topped because certain microwave modes are better coupled (with waveguide, chamber and plasma). The shape of the TWTA output signal was wide and flat (marked with a dashed line). The results of the white-noise heated plasma experiments are published in [Kaw06].

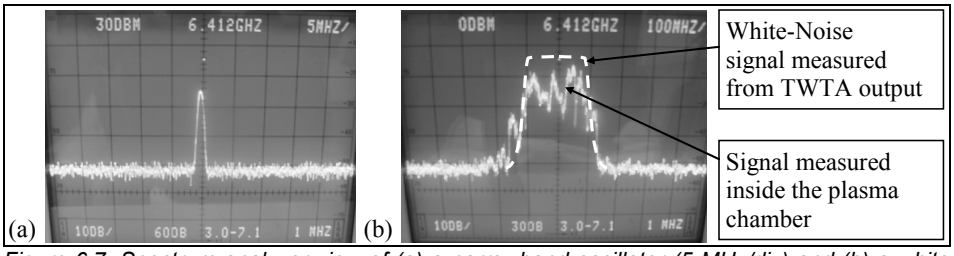

Figure 6.7. Spectrum analyzer view of (a) a narrowband oscillator (5 MHz/div) and (b) a white noise generator (100 MHz/div) [Kaw06].

It was found that the broadband heating with the same total microwave power was more efficient, especially for highly-charged ion production. It seems that the electron confinement improves by both MMPS and broadband heating. This is evidenced in the X-ray spectrum of figure 6.8 where the effect of the MMPS boost together with white-noise heating is not as clear as in figure 6.6. In addition, the effect of the MMPS is now in a more narrow range; from 80 keV to 140 keV. In this measurement the beam intensities were also measured as a

function of the MMPS. However, the performance of the source was poor (less than 400 nA of Ar^{13+}) and no improvement together with the MMPS and WNG was seen. No satisfactory explanation for the behavior was found.

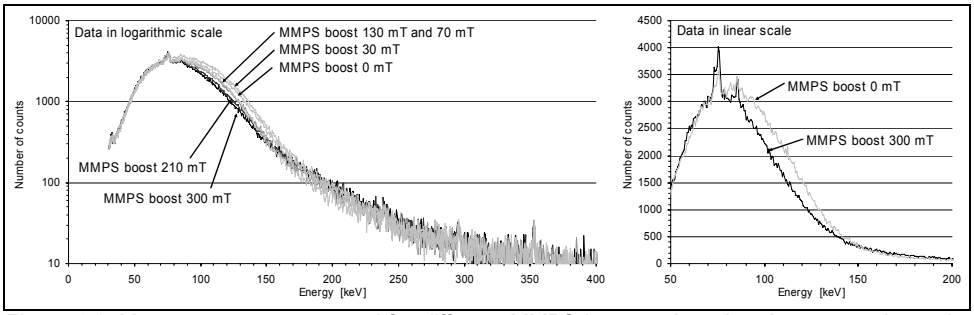

Figure 6.8. X-ray spectrum measured for different MMPS boosts when the plasma was heated with white-noise.

6.1.3. Radial plasma impact patterns

In some cases a 0.5 – 1 mm thick aluminum sheet (liner) is used inside the ECRIS. Its purpose is to protect the surface of the chamber against contamination. For example, carbon contamination which occurs when using MIVOC-method. After the contaminating experiment the liner can be taken out and opened for a closer look. Figure 6.9 shows liners used in the JYFL 6.4 GHz ECRIS, JYFL 14 GHz ECRIS and Argonne National Laboratory (ANL) ECRIS2 (14 GHz). All these represent the typical shape of ECRIS radial plasma flux impact areas (see chapter 3.3). In part (c) the microwave power used was too high and overheated the hexapole, which was then partially demagnetized. The plasma flux was increased at this point and melted a hole in the liner. It is located exactly where the total magnetic field (B_{tot}) has a minimum at the plasma chamber wall. This clearly indicates that this location is a potential place of demagnetization and the magnetic field here is an important parameter to be taken into account when designing ECRIS hexapoles.

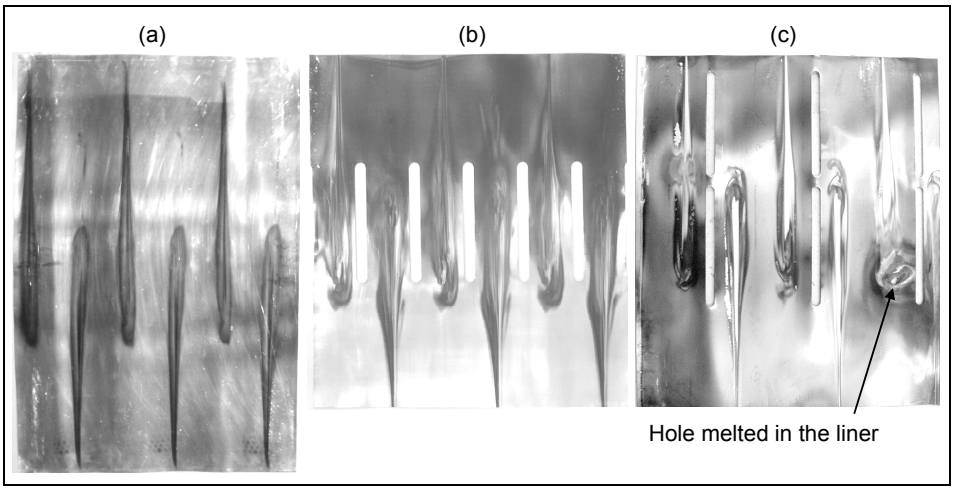

Figure 6.9. Aluminum liners used in the (a) JYFL 6.4 GHz ECRIS, (b) JYFL 14 GHz ECRIS and (c) Argonne National Laboratory: ANL ECRIS2 (14 GHz). Note that the pictures are not to scale.

Figure 6.10 is a close-up picture of two aluminum liners, which were placed inside the JYFL 6.4 GHz ECRIS during a one-week contaminating run. The upper part (a) shows the flux without the MMPS boost and lower part (b) the case with the full MMPS boost. Although the MMPS boost is very narrow it clearly makes the plasma impact areas smaller. The dark area in the figure is formed when carbon ions impact and remain on the liner surface. A more detailed study including the spatial distribution of the ions can be found in reference [Tar04b]. The figure shows that not only the electron flux but also the ion flux is changed by the MMPS.

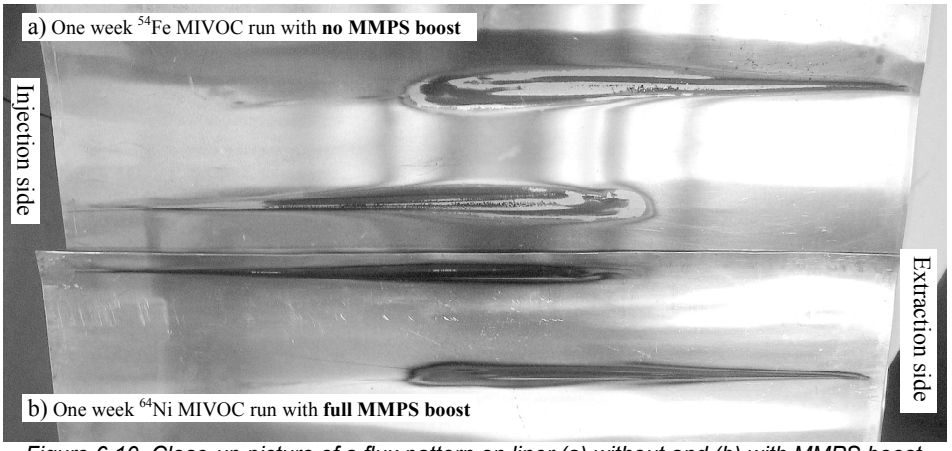

Figure 6.10. Close-up picture of a flux pattern on liner (a) without and (b) with MMPS boost.

6.1.4. Plasma potential

Because the mobility of electrons is much higher than that of the ions they can escape more easily from the magnetic bottle. Consequently, when the plasma is ignited the electron losses are higher and the potential of the plasma starts to increase (positive voltage with respect to the plasma chamber walls). However, the increasing positive plasma potential reduces electron losses. Finally the plasma potential finds stable conditions, where the losses of positive and negative charges are the same. The plasma potential has been found to be about 10 – 100 V. Some preliminary plasma potential measurements were done as a function of the MMPS boost using a device developed at JYFL [Tar04]. The results are summarized in figure 6.11.

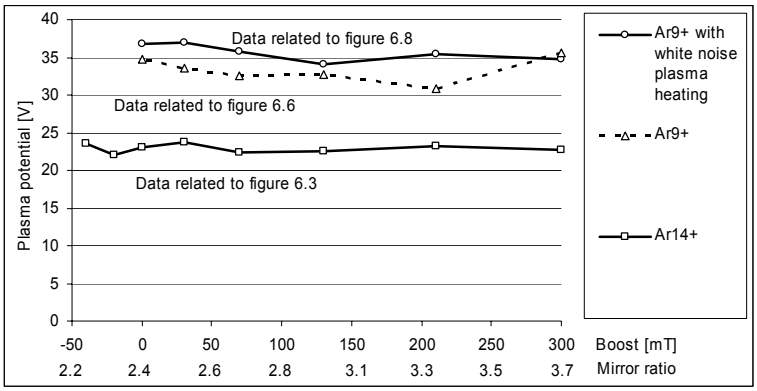

Figure 6.11. Plasma potential as a function of the MMPS boost.

The plasma potential measured with Ar^{14+} ions (see figure 6.3) was (23 $\pm$ 1) V as a function of the MMPS boost. The plasma potential being almost constant was unexpected, as according to the X-ray measurements one could expect the plasma electron density to increase and plasma potential to decrease. However, the measurements described in [Tar04] also showed no remarkable change in the plasma potential when the axial mirror ratio was changed. This may be because the plasma potential is mainly formed by low energy electrons, whose movement is dominated by collisions [Dre03, Tar05], not by the magnetic field. In addition, the measurements shown in the previous chapter showed that the MMPS also decreases the ion flux towards the plasma chamber walls. Consequently, the number of positive charges in the plasma increases and the plasma potential remains almost unchanged. The increased ion density can also be seen from the increased intensity of the extracted ion beam.

The plasma potential values measured with Ar^{9+} also stayed practically constant as a function of the MMPS boost. However, the measured values are higher than in other experiment measured for Ar^{14+}, as for the Ar^{9+} measurements the ECRIS was not well conditioned (previously described TWTA / WNG / X-ray –measurements). It has been found that the plasma

potential is lower when the ECRIS has a good performance and is well conditioned [Dre03].

6.2. MMPS measurements with 10.75 GHz microwaves

In the previous measurements the radial mirror ratio was at least 2.2, which is considered to be sufficient for efficient ECRIS operation (see chapter 3.4 about the magnetic field scaling laws). The next step was to study if the MMPS could be used when the radial mirror ratio is not sufficient without the MMPS boost. For these measurements an extra waveguide for a 10.75 GHz TWTA was connected to the JYFL 6.4 GHz ECRIS. Some magnetic field and plasma parameters related to 10.75 GHz plasma heating are listed in table 6.2.

Table 6.2. Parameters related to the 10.75 GHz experiments.

		Magnetic field, B	Mirror ratio, R
Resonance	B_{ECR}	0.38 T	
Injection	B_{inj}	1.20 T	3.1
Minimum	B_{min}	0.22 T	$0.57 \times B_{ECR}$
Extraction	B_{ext}	0.60 T	1.6
Radial	No MMPS	0.55 T	1.4
	With MMPS	0.85 T	2.2
Resonance zone	Length	246 mm	
	Radius	53 mm	
	Volume (ellipsoid)	1.448 liters	

In this experiment the axial field producing coils were set at full power but the magnetic field was still too weak. Consequently, the mirror ratios given by the “scaling laws” were not fully satisfied. Experiments (see for example [Gam99] and [Gam01]) have shown that the injection and extraction mirror ratios here are almost high enough and no severe intensity drop should be caused by these values. However, the values of minimum and radial magnetic field are so low that a remarkable intensity drop is expected. The radial magnetic field can be boosted with the MMPS but the B-minimum being only $0.57 \times B_{ecr}$ caused the plasma size to be large and the power density low. Consequently, the measured beam intensities in this experiment were quite low. However, the effect of the MMPS on the relative intensities of various charge-states is clear, as noted in figure 6.12.

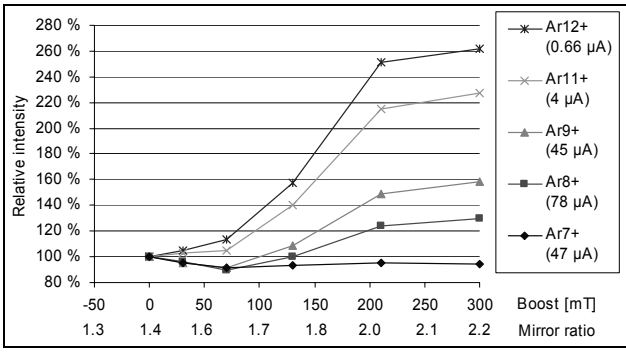

Acceleration voltage	10 kV
Microwave power	220 W

Iron pole position	MMPS Boost	Pressure (injection)	Drain current
[mm]	[mT]	[10^{-7} mbar]	[mA]
0	300	6.4	1.42
1	210	6.9	1.26
2	130	6.9	1.24
3	70	6.8	1.22
4	30	6.9	1.19
5	0	6.9	1.19

Figure 6.12. Typical relative intensities for argon beams (argon-oxygen plasma) as a function of the MMPS boost [Suo06].

In this measurement the optimum MMPS boost was not obtained as the maximum radial mirror ratio was only 2.2. It seems that the increase in intensity was significant in gain from 1.7 to 2.0, but after that the current starts to saturate. Similar results have been measured with a fully superconducting ECRIS using 14 GHz and 18 GHz frequencies (see for example [Gam01]). The result indicates that the MMPS can also give a beneficial effect in ECRIS's using higher frequencies (> 14 GHz).

6.3. MMPS effect as a function of ion charge-state

It seems clear that the MMPS has the strongest effect on the highest charge-states. To study this behavior in more detail the highest relative argon ion beam intensities were taken from figure 6.3 (210 mT boost) and figure 6.12 (300 mT boost) and plotted in figure 6.13 as a function of the charge-state.

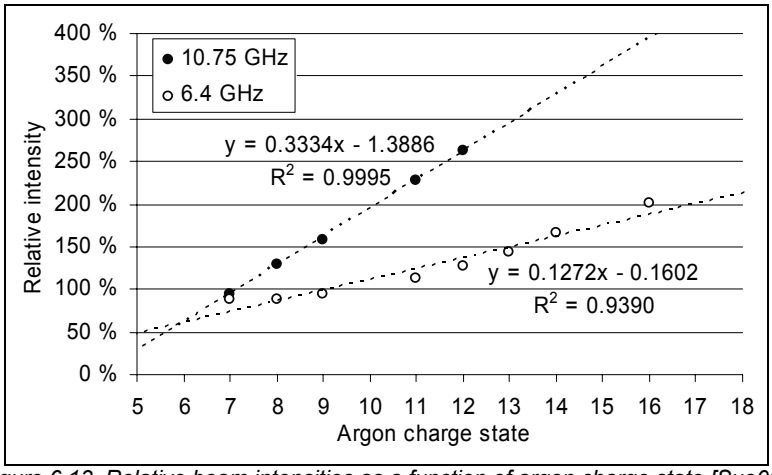

Figure 6.13. Relative beam intensities as a function of argon charge state [Suo06].

The increase of the relative ion beam intensity is almost linear as a function of the ion charge-state. This was unexpected, but an excellent result since the

highest charge-state ions are always the most difficult to produce. The intensity of low charge-state ions decreases when the MMPS is applied. This is also beneficial in the case of the space-charge and extraction problems caused by a high total beam current (extracted from ECRIS).

At 10.75 GHz the radial mirror ratio was increased from 1.4 to 2.2 by the MMPS. The expected relative intensity for Ar^{16+} in this case is as high as 400%. A new hybrid-ECRIS called A-PHOENIX has a comparable case when the MMPS is used in it. According to the presented measurements, the improvement of the highly charged ion production should be remarkable.

To study why the improvement is linear as a function of charge-state, a new plot was made using relative **particle** current values instead of relative **ion** currents (i.e. each ion current value was divided by the ion charge-state). However, by doing this the relative values are the same and the graph does not change. In figure 6.14 the data of figure 6.3 is "transposed", i.e. plotted as a function charge-state while the different boost values are shown in separate series. It was found that the charge-state dependence is almost linear for every MMPS boost, not only for the "best" ones shown in figure 6.13.

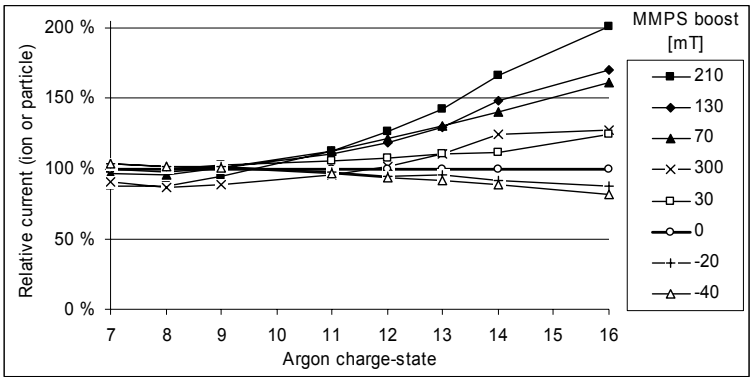

Figure 6.14. Relative currents for different MMPS boosts as a function of argon charge-state (see figure 6.3 for a comparison).

The reason for the linear behavior was also investigated using theoretical equations derived for ECRIS plasma physics. However, that and several discussions with ECRIS plasma physics experts resulted in no solid explanation for this interesting phenomenon.

7. Summary and future prospects

The performance of ion sources must develop due to the increasing demands of applications. Usually this means higher intensity and higher charge-states. According to the semi-experimental scaling “laws”, proposed by the ECRIS inventor R. Geller, the ion beam intensity increase is proportional to the square of the microwave frequency ($\propto f^2$). Consequently, the most straightforward way to improve ECRIS performance is to use higher microwave frequency. However, this requires sufficient magnetic confinement of the plasma. Such confinement is a big technological challenge, especially for permanent magnet hexapoles. With currently available technology the highest permanent magnet hexapole strength is about 1.5 T. The value is mainly limited by the properties of the permanent magnet material (NdFeB). The highest performance modern (superconducting) ECRISs use 28 GHz microwave frequency. For optimum ECRIS performance this means that the hexapole field at the plasma chamber wall should be at least 2 T.

In the first part of this thesis, optimization of the permanent magnet hexapole was studied extensively. Numerous simulations were performed in order to learn the dependence of the different parameters (permanent magnet dimensions and magnetization angles) in the hexapole. It was found that an Offset-Halbach -type hexapole is often a good solution rather than the “conventional” Halbach hexapole. In addition, very useful equations, called JYFL-HEXE, were derived for the hexapole design. These equations are a fast and easy tool when the permanent magnet hexapole has to be optimized for different needs. The results are quite accurate but it is recommended that the solution is double-checked with a magnetic field simulation code. This is also needed to consider the permanent magnet demagnetization effects, especially when designing strong hexapoles.

It was found that even with a careful optimization it is not possible to reach a hexapole field of over 2 T. The problem had to be overcome with another solution. The idea of using iron as a magnetic field booster is not new, but has not been used before in a hexapole. This may be because in the hexapoles used in the particle accelerators, a homogenous field is required to ensure as high beam quality as possible. However, in plasma ion sources the magnetic field homogeneity is not needed. Rather, good magnetic confinement and proper electron cyclotron resonance are necessary. For an ECRIS hexapole this means that the magnetic field has to be high at the location where plasma tries to leak out from the magnetic bottle. Because the plasma follows closely the magnetic field lines, the field has to be high at the location where the magnetic field lines go through the plasma chamber wall. These positions are located at the magnetic poles of the hexapole. Consequently, some iron was added here to boost the magnetic field locally only at the magnetic poles. The new concept was given the name Modified MultiPole Structure (JYFL-MMPS).

At first the idea of MMPS was studied with 2D magnetic field simulation codes. The first results were outstanding; the magnetic field of over 2.3 T was reached at the plasma chamber wall. However, it was not fully understood what happens when the axial field producing solenoids are powered and that time a 3D-code was not available to check it. Instead a simple experiment was done. Six small iron bars (semicircular, 4 mm in width) were added inside the old plasma chamber. The hexapole field ensured their location exactly at the magnetic pole and the magnetic field increased from 0.37 T to 0.5 T (35 %). The plasma was stable and the performance looked promising but in a first mass scan some iron was found. The source was opened and it was found that one of the six iron bars was partly melted. The plasma flux melted the iron even when the microwave power was low and the strong hexapole field ensured a good contact between the (cooled) plasma chamber wall and the iron bars. A closer look at the 2D simulations revealed that there was a resonance on the both sides of the iron bar. The resonance was due to the fact that the iron guides the magnetic field lines to go through the iron decreasing the magnetic field flux density on the both sides of the iron. At this point two options were available: to add cooling for the iron poles or perform more accurate 3D-magnetic field simulations taking also the solenoid field into account. It was decided to proceed with the more realistic 3D-simulations.

In the first 3D-simulations the iron cross-section was too large and when the solenoids were turned on the radial field at the plasma chamber wall decreased significantly. When the cross-section was optimized it was found that a remarkable improvement could still be achieved by using iron poles. It was found that the 3D simulations are necessary because of the non-linear effects in the iron. The 2D simulations can be used only in a few special cases, as in most cases they give somewhat too optimistic results. For example, figure 5.14 shows that by increasing the solenoid field from zero to maximum, the value of B_r decreases from 0.93 T to 0.84 T at z = 0. This effect cannot be seen from 2D-simulations, which always give the highest value.

Some simulations were made also for 14 GHz and 28 GHz ECRISs. In a typical ECRIS solenoid construction the value of B_z at the plasma chamber wall (same z-value with B_{min}) was found to be about 90 % of B_{min}, i.e. $B_{z@\text{wall}} \approx 0.9 \times B_{min}$. For example in a 28 GHz ECRIS B_{min} should be about 0.8 T resulting $B_{z@\text{wall}} \approx$ 0.7 T. If the hexapole strength without iron poles is B_r = 1.3 T the total magnetic field will be $B_{tot@\text{wall}} \approx \sqrt{(B_{z@wall})^2 + (B_r)^2}$ = 1.5 T. Now it can be calculated that the radial magnetic field at the wall is about 88 % of the total magnetic field. This ratio will remain when the iron poles are added into the structure. The external magnetic field will boost the iron to its saturation magnetic field value (2.3 T) and the radial magnetic field with MMPS will be about $B_{MMPS} \approx 0.88 \times$ 2.3 T = 2 T. It was found that similar calculation can be considered as a “rule of thumb” in the MMPS design.

After the extensive 3D-simulations it seemed that the MMPS could be used to remarkably improve the hexapole strength. However, as with all new ideas,

some unknown factors were also present in this case. It was not known how the high gradient of the magnetic field at the magnetic pole affects the plasma and the performance of the ion source. This gradient causes a so-called gradB-drift, whose direction is mainly parallel with the main axis of the plasma chamber. To study these phenomena a new MMPS plasma chamber was designed for the JYFL 6.4 GHz ECRIS. The MMPS prototype was required to be as versatile as possible and its performance should also improve if the MMPS-idea fails. The design included for the first time a possibility to adjust the homogenous part of the permanent magnet hexapole field. However, even more important was the possibility to adjust the MMPS boost online. The new MMPS plasma chamber enabled several new types of measurements to be performed. One of the most interesting was to find how the local magnetic field boost affects the production of highly-charged heavy ions.

Before the plasma was ignited the magnetic field of the new MMPS plasma chamber was measured carefully in order to check the validity of the 3D-magnetic field simulations. Everything seemed to be correct and the next step was to study how the new chamber worked without using the MMPS. Finally, the MMPS measurements were begun with oxygen but only a small increase was measured for the highest charge-states. However, the measurements revealed that the MMPS performance improves as a function of charge-state. Consequently, measurements were continued by measuring higher charge-states using argon and krypton. The highest measured relative intensity was about 300 % (for krypton).

Measurements were also done by injecting 10.75 GHz microwaves into the JYFL 6.4 GHz ECRIS. Here the radial mirror ratio was very low (1.4) without the MMPS. The idea of this experiment was to study how the MMPS works in the case where the homogenous hexapole magnetic field is too low. Again, remarkable intensity improvements were obtained by using the MMPS. It looked promising to use the idea in two cases. The first one is to build a relatively low-cost hexapole and boost the magnetic field with the MMPS in order to meet the magnetic field scaling “laws”. This could be applied for example for 14 GHz and 18 GHz ECRISs. In the second case a strong hexapole (i.e. 1.4 – 1.6 T) could be built and then the MMPS could be used to boost the field up to 2 T in order to meet the requirements for over 20 GHz operation. Simulations have shown that this is possible. During this thesis work a new permanent magnet hexapole for an ECRIS, called A-PHOENIX, was designed in collaboration with LPSC-Grenoble (France) ion source group. The radial magnetic field (B_{pole}) in this hexapole will be 2.3 T, higher than ever before in an ECRIS permanent magnet hexapole. In A-PHOENIX the MMPS cannot be used under the superconducting solenoids (see figure 3.11) because the axial magnetic field there is extremely high and saturates the iron. However, using an optimized Offset-Halbach structure (part of this thesis work) a 10 % magnetic field increase was gained under the solenoids. The ultimate performance of the JYFL-MMPS using a frequency of 28 GHz will be seen when the source is in operation (scheduled time is in 2007).

Altogether, this thesis work was the first step in the development of a new MMPS-technique. There is still a lot of work to be done. For example, the most important ion beam quality parameter, emittance, was not measured as a function of the MMPS boost. However, there are reasons to believe that the MMPS does not have a remarkable effect on the emittance. The results presented in [Spä05] show that the emittance is strongly dependent on the multipolar magnetic field at the extraction region, which is not affected by the MMPS. In addition, the results in [Tar06] state that the emittance increases in the dispersive magnetic components (such as dipole) because of the beam energy distribution caused by the plasma potential. The measurements presented in this thesis show that the MMPS does not affect the plasma potential. In the emittance measurements [Suo02] performed with the old plasma chamber (same extraction system) it was found that the emittance is beyond the acceptance of the JYFL K130 cyclotron (100 π mm mrad). On several occasions when the beam was delivered to the cyclotron, the beam intensity was increased with the MMPS and about the same relative increase was measured before and after the cyclotron. This also gives reason to assume that the emittance was not remarkably changed by the MMPS.

The primary aim for this thesis work was to design, construct and perform “proof-of-principle” measurements with the first MMPS plasma chamber. The set goal was fully covered; however it was not possible to include all the interesting measurements in one thesis. The theory and physics behind the linear increase of the intensities as a function of charge-state are interesting topics for future work. In addition, several interesting measurements can be performed with the existing setup. For example, the ionization efficiency could be measured as a function of the MMPS to get a better idea of what happens when the MMPS is applied. Does the number of neutral ions in the plasma chamber decrease (increasing the ionization efficiency) or is the efficiency about the same but ions are ionized to higher charge-states? One of the most interesting future experiments could be to build water-cooled iron bars and add them inside the 14 GHz AECR-type hexapole (the resonance at the sides of the iron bars must be prevented), which may reveal an extremely cost-effective way to improve the existing ECRIS performances. In the ECRISs where closed Halbach-type hexapoles are used (for example Grenoble Test Source; GTS) the “inner plasma chamber” is often detachable (as the plasma chamber designed in this thesis). It would not be much of an effort to build a new inner chamber utilizing the idea of the MMPS. In addition it would be interesting to use the MMPS in other order multipoles than a hexapole. It should also be studied if the MMPS could be used in other plasma ion sources than an ECRIS or other applications where charged particles have to be confined in the magnetic field.

References

[Ant86] T.A. Antaya and Z.Q. Xie, Contributed Papers of the 7th International Workshop on ECR Ion Sources, ISSN 0344-5798, Jülich, Germany, (1986) 72

[Ant94] T.A. Antaya, S. Gammino, Rev. Sci. Instr. 65 (1994) 1723

[Bro89] I. G. Brown, The Physics and Technology of Ion Sources, John Wiley & Sons, USA, 1989, ISBN 0 471 85708 4

[Cas94] Proceedings of CERN Accelerator School – Fifth general accelerator course, CERN 94-01, ISBN 92-9083-057-3

[Cav04] M. Cavenago, T. Kulevoy, and S. Petrenko, Rev. Sci. Instrum. 75 (2004) 4934

[Cia94] G. Ciavola, S. Gammino, P. Briand, G. Melin, and P. Seyfert, Rev. Sci. Instrum. 65 (1994) 1057

[Cia96] G. Ciavola, S. Gammino, Nucl. Instrum. Methods Phys. Res. A, 382 (1996) 267

[Cia06] G. Ciavola, et al., Rev. Sci. Instrum. 77 (2006) 03A303

[Cla89] D.J. Clark and C.M. Lyneis, The Physics of Multiply Charged Ions and E.C.R. Ion Sources, Grenoble, France, Journal de Physique, (1989) C1-759

[Dre85] A. G. Drentje, Nucl. Instrum. Methods Phys. Res. B 9 (1985) 526

[Dre03] A. G. Drentje, Rev. Sci. Instrum. 74 (2003) 2631

[Dup90] C. Dupont, Y. Jongen, K. Arakawa, W. Yokota, T. Satoh, and T. Tachikawa, Rev. Sci. Instrum. 61 (1990) 265

[FEML] FEMLAB, The COMSOL Group, Version 2.3 <http://www.comsol.com/products/femlab>

[Fro05] P. Frodelius, Master's thesis (in Finnish), Department of Physics, University of Jyväskylä, 2005

[Gam96] S. Gammino, G. Ciavola, T. Antaya and K. Harrison, Rev. Sci. Instrum. 67 (1996) 155

[Gam99] S. Gammino, G. Ciavola, L. Celona, M. Castro, F. Chines, and S. Marletta, Rev. Sci. Instrum. 70 (1999) 3577

[Gam00] S. Gammino and G. Ciavola, Rev. Sci. Instrum. 71 (2000) 631

[Gam01] S. Gammino, G. Ciavola, L. Celona, D. Hitz, A. Girard, and G. Melin, Rev. Sci. Instrum. 72 (2001) 4090

[Gel86] R. Geller and B. Jacquot, Contributed Papers of the 7th International Workshop on ECR Ion Sources, ISSN 0344-5798, Jülich, Germany, (1986) 31

[Gel87] R. Geller, F. Bourg, P. Briand, J. Debernardi, M. Delaunay, B. Jacquot, P. Ludwig, R. Pauthenet, M. Pontonnier, P. Sortais, International Conference on ECR Ion Sources and their Applications, East Lansing, USA, (1987) 1

[Gel96] R. Geller, Electron Cyclotron Resonance Ion Sources and ECR Plasmas, Institute of Physics Publishing, London, (1996), ISBN 0 7403 0107 4

[Gol95] R.J. Goldston, Introduction to Plasma Physics, Institute of Physics Publishing, London, (1995), ISBN 0-7503-0183-X

[Hal80] K. Halbach, Nuclear Instruments and Methods 196 (1980) 1

[Har94] R. Harkewicz, J. Stacy, J. Greene, and R. C. Pardo, Rev. Sci. Instrum. 65 (1994) 1104

[Har95] R. Harkewicz, P. J. Billquist, J. P. Greene, J. A. Nolen, Jr., and R. C. Pardo, Rev. Sci. Instrum. 66 (1995) 2883

[Hit93] D. Hitz, G. Melin, M. Pontonnier and T. K. NGuyen, Proc. of the 11th Int. Workshop on ECRIS, Groningen, Netherlands, (1993) 91

[Hit02] D. Hitz, A. Girard, G. Melin, S. Gammino, G. Giavola, L. Celona, Rev. Sci. Instrum. 73 (2002) 509

[Hit02b] D. Hitz, D. Cormier, and J. M. Mathonnet, 8th European Particle Accelerator Conference, Paris, France, (2002) 1718

[Hit04] D. Hitz, A. Girard, K. Serebrennikov, G. Melin, D. Cormier, J. M. Mathonnet, J. Chartier, L. Sun, J. P. Briand, and M. Benhachoum, Rev. Sci. Instrum. 75 (2004) 1403

[Hit05] D. Hitz, M. Delaunay, A. Girard, L. Guillemet, J. M. Mathonnet, J. Chartier, and F. W. Meyer, AIP Conference Proceedings, (2005) Volume 749, Issue 1, p. 123

[Kat95] T. Katayose, T. Hattori, S. Yamada, K. Kitagawa, and M. Sekiguchi, Proceedings of the 12th International Workshop on ECR Ion Sources, Riken, Japan, (1995) 281

[Kaw06] Y. Kawai, G. D. Alton, O. Tarvainen, P. Suominen, and H. Koivisto, Rev. Sci. Instrum. 77 (2006) 03A331

[Knu81] H. Knudsen, H.K. Haugen and P. Hvelplund, Phys. Rev. A, Vol 23, Number 2, (1981) 597

[Koi94] H. Koivisto, J. Ärje, and M. Nurmia, Nucl. Instrum. Methods Phys. Res. B 94 (1994) 291

[Koi01] H. Koivisto et al., Nucl. Instrum. Methods Phys. Res. B 174 (2001) 379

[Koi03] Koivisto H, Moisio M, Nieminen V, Suominen P and Liukkonen E, Nukleonika, vol. 48, supplement 2, (2003) 81

[Koi04] H. Koivisto, P. Suominen, O. Tarvainen, and D. Hitz, Rev. Sci. Instrum. 75 (2004) 1479

[Kur00] T. Kurita, T. Nakagawa, T. Kawaguchi, and S.-M. Lee, Rev. Sci. Instrum. 71 (2000) 909

[Lan02] R. Lang, J. Bossler, R. Iannucci, K. Tinschert, Proc. of the 15th Int. Workshop on Electron Cyclotron Resonance Ion Sources, Jyväskylä, Finland, (2002) 180

[Lei99] M.A. Leitner, S. A. Lundgren, C.M. Lyneis, C.E. Taylor, D. Wutte, Proceedings of 14th international workshop on ECRIS, CERN, Geneva, Switzerland, (1999) 66

[Lei05] D. Leitner, C.M. Lyneis, S.R. Abbott, D. Collins, R.D. Dwinell, M.L. Galloway, M. Leitner, D.S. Todd, Nucl. Instrum. Methods Phys. Res. B 235 (2005) 486

[Lei06] D. Leitner, C. M. Lyneis, T. Loew, D. S. Todd, S. Virostek, and O. Tarvainen, Rev. Sci. Instrum. 77 (2006) 03A302

[Liu92] E. Liukkonen, 13th International Conference on Cyclotrons, Vancouver, Canada, (1992) 22

[Lud98] P. Ludwig et al., Rev. Sci. Instrum. 69 (1998) 653

[Lyn87] C. M. Lyneis, Proceedings of International Conference on ECRIS and their applications, East Lansing, USA, (1987) 42

[Lyn04] C.M. Lyneis, D.Leitner, S.R. Abbot, R.D. Dwinell, M. Lietner, C.S. Silver, and C. Taylor, Rev. Sci. Instrum., 75 (2004) 1389

[Nak90] T.Nakagawa, T.Kageyama, E.Ikezawa, M.Hemmi, and Y.Miyazawa, Proceedings of 10th Workshop on ECRIS, Oak Ridge National Laboratory, Knoxville, USA, (1990) 163

[Nak00] T. Nakagawa and Y. Yano, Rev. Sci. Instrum. 71 (2000) 637

[Nak02] T. Nakagawa et al., Rev. Sci. Instrum. 73 (2002) 513

[Nak04] T. Nakagawa, Y. Higurashi, M. Kidera, T. Aihara, M. Kase and Y. Yano, Nucl. Instr. and Meth. B 226/3 (2004) 392

[Nak06] T. Nakagawa, Y. Higurashi, M. Kidera, T. Aihara, M. Kase, A. Goto, and Y. Yano, Rev. Sci. Instrum. 77 (2006) 03A304

[Sor95] P. Sortais et al., Proceedings of the 12th International Workshop on ECRIS, Riken, Japan, September 1995, INS-J-182

[Spä05] P. Spädtke, K. Tinschert, R. Lang, and R. Iannucci, AIP Conference Proceedings, (2005) Volume 749, Issue 1, p. 47

[Sri96] A. K. Srivastava and T. A. Antaya, Rev. Sci. Instrum. 67 (1996) 1618

[Suo02] P. Suominen, O. Tarvainen, H. Koivisto, A. Lassila, P. Heikkinen and E. Liukkonen, Proceedings of the 15th International Workshop on ECRIS, Jyväskylä, Finland (2002) 161

[Suo04] P. Suominen, O. Tarvainen, H. Koivisto and D. Hitz, Rev. Sci. Instr. 75 (2004) 59

[Suo04b] P. Suominen, O. Tarvainen, H. Koivisto, Nucl. Instr. and Meth. B 225/4 (2004) 572

[Suo06] P. Suominen, O. Tarvainen, and H. Koivisto, Rev. Sci. Instrum. 77 (2006) 03A332

[Tar04] O. Tarvainen, P. Suominen, and H. Koivisto, Rev. Sci. Instrum. 75 (2004) 3138

[Tar04b] O. Tarvainen, P. Suominen, H. Koivisto, I. Pitkänen, Rev. Sci. Instrum. 75 (2004) 1523

[Tar05] O. Tarvainen, PhD. thesis, Department of Physics, University of Jyväskylä, JYFL Reseach Report No. 8/2005, ISBN 951-39-2339-8

[Tar06] O. Tarvainen, P. Suominen, T. Ropponen, and H. Koivisto, Rev. Sci. Instrum. 77 (2006) 03A309

[Taw87] H. Tawara, T. Kato, Atomic Data and Nuclear Data Tables, Vol 36, No 2 (1987)

[Thu04] T. Thuillier, J.-C. Curdy, T. Lamy, P. Sole, P. Sortais, J.-L. Vieux-Rochaz, and D. Voulot , Rev. Sci. instrum. 75 (2004) 1526

[Thu06] T. Thuillier, T. Lamy, P. Sortais, P. Suominen, O. Tarvainen, and H. Koivisto, Rev. Sci. Instrum. 77 (2006) 03A323

[VAC06] Vacuumschmelze GmbH & Co. <http://www.vacuumschmelze.de> (21.3.2006)

[Von02] R. C. Vondrasek, R. H. Scott, R. C. Pardo, and D. Edgell, Rev. Sci. Instrum. 73 (2002) 548

[Von04] R. C. Vondrasek, R. Scott, and R. C. Pardo, Rev. Sci. Instrum. 75 (2004) 1532

[Xie97] Z.Q. Xie, C.M. Lyneis, Proceedings of the 13th International Workshop on ECR Ion Sources, Texas A&M University, Texas, USA, (1997) 16

[Zav06] P. A. Zavodszky et al., Rev. Sci. Instrum. 77 (2006) 03A334

[Zha04] H. W. Zhao et al., Rev. Sci. Instrum. 75 (2004) 1410

[Ärj90] J. Ärje, V. Nieminen, J. Choinski and T.A. Antaya, Proc. of the 10th Int. Workshop on ECR Ion Sources, Oak Ridge National Laboratory, Knoxville, USA, (1990) 343